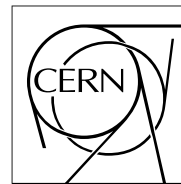


The Compact Muon Solenoid Experiment
Analysis Note

The content of this note is intended for CMS internal use and distribution only



16 September 2010 (v8, 11 January 2011)

A First Search for General Gauge Mediated Supersymmetry

A. Askew,

Florida State University, Tallahassee, FA.

S. Arora, Y. Gershtein, S. Thomas,

Rutgers University, Piscataway, NJ.

G. Hanson, R. Stringer,

University of California, Riverside, CA.

W. Flanagan, B. Heyburn, U. Nauenberg, S. L. Zang,

University of Colorado, Boulder, CO.

R. Nandi,

Imperial College, London, UK

D. Elvira, D. Mason,

Fermi National Accelerator Laboratory, IL

M. Balazs, B. Cox, B. Francis, A. Ledovskoy, R. Yohay,

University of Virginia, Charlottesville, VA.

Abstract

This paper describes the search for General Gauge Mediated Supersymmetry Breaking (GGM) production of SUSY in $\sqrt{s} = 7$ TeV proton-proton interactions. Events that contain two photons and missing transverse energy (MET) plus multiple jet production are expected to result from strong production of pairs of supersymmetric particles that, through their decays, result in a pair of neutralinos, each of which decay into a gravitino, the lowest mass supersymmetric particle (LSP) in this scenario, and a photon. The search is done using a data sample with integrated luminosity of 35.5 ± 3.9 pb $^{-1}$. We observe a single $\gamma\gamma$ event in our data sample with $MET \geq 50$ GeV. We expect 1.2 ± 0.8 events from Standard Model backgrounds due to QCD and EW sources in the $MET \geq 50$ GeV region. An upper limit of 0.44 pb is obtained for this measurement choosing a squark-gluino-neutralino mass point of 800, 1920, and 150 GeV/c 2 respectively which has an acceptance times efficiency of 26.8%. We present in the paper upper limit calculations and exclusion regions for the gluino and squark mass ranges 400-2000 GeV/c 2 and several neutralino masses.

35 **Contents**

36	1 Introduction	2
37	2 Datasets, Trigger, and Event Selection	2
38	2.1 Datasets	2
39	2.2 Trigger	3
40	2.3 Event Selection	3
41	2.3.1 Photon and Electron Identification	3
42	2.3.2 Fake Photons	4
43	2.3.3 The Fake-Fake and $\gamma\gamma$ Data Sets	5
44	2.3.4 Jet Selection	5
45	3 Tag and Probe Study	5
46	3.1 Photon Identification Efficiency	5
47	3.1.1 Determination of the Photon Efficiency Scale Factor $\epsilon_e^{data}/\epsilon_e^{MC}$	6
48	3.1.2 Dependence of ϵ_e^{data} on Pileup	6
49	3.1.3 Comparison between MC Truth and Tag and Probe Efficiencies	8
50	3.1.4 Check that $\epsilon_\gamma^{data}/\epsilon_\gamma^{MC} = \epsilon_e^{data}/\epsilon_e^{MC}$	8
51	3.1.5 Comparison of ϵ_{MC} for γ +Jet and ϵ_{MC} for the GGM Signal	8
52	3.1.6 GGM Signal Photon Isolation	12
53	3.2 Electron Misidentification	13
54	3.2.1 Determination of the Electron Misidentification Fraction	13
55	3.2.2 Fitting the ee, e γ , and $\gamma\gamma$ Spectra	14
56	4 Estimation of MET Backgrounds	14
57	4.1 Fake-Fake and $Z \rightarrow ee$ QCD Background Estimates	14
58	4.1.1 Correcting Differences Between $\gamma\gamma$ and ff and $Z \rightarrow ee$ Background diEM Spectra	14
59	4.1.2 The QCD Background Estimate using fake-fake Sample	16
60	4.1.3 The QCD Background Estimate using the $Z \rightarrow ee$ Sample	16
61	4.2 Electroweak Background	16
62	4.3 Total Background Prediction with $MET \geq 50$ GeV	16
63	5 The Wγ EW Contribution to the MET Background	17
64	6 Table of Backgrounds	20
65	7 Table of Uncertainties	22
66	8 Estimation of Upper Limit Contours for the GGM SUSY	22
67	8.1 Upper Limits Using the Bayesian Method	22
68	8.2 Example of an Upper Limit Calculation	23

69	8.2.1 GGM Example Calculations	23
70	8.3 Construction of GGM Exclusion Regions	25
71	9 Summary	25
72	A Breakdown of Various Effects on Signal Acceptance	29
73	B Effect of Loosening the Tight Photon Analysis Requirement	31
74	C Study of ΔR Criterion for Proximity of Isolated Jets to γ Candidates	33
75	D Effect of Number of Jets on Acceptances	35
76	E Comparison of TcMET and PfMET	38
77	F Pixel Seed Veto Systematics	38
78	G Comparison of Lead Jet η Distributions for $\gamma\gamma, Z \rightarrow ee$, QCD fake-fake, and GGM Event Samples	39
79	H Use of TCjets vs. PFjets	39
80	I Comparison of QCD MET Spectra from ff and $Z \rightarrow ee$ Events	41
81	J Check of Effects of Use of Corrected Jets in TcMET	42
82	K Effect of Overcleaning on the GGM Signal	42
83	L Effect of Variation of p_T Cuts on Jet and Photon Transverse Momenta	44
84	M Kinematic Plots with No Jet and ≥ 1 Jet Requirements	45

85 List of Figures

86	1 Sketch illustrating the isolation cones for the ECAL and HCAL E_T deposits.	4
87	2 $\epsilon_e^{data}/\epsilon_e^{MC}$ Top left: vs. p_T ; Top Right vs. η ; Bottom Left: vs. $\Delta R_{\gamma-jet}$; Bottom Right: vs. N_{jets}	7
88	3 Electron efficiency ϵ_e^{data} determined by the tag criteria on $Z \rightarrow ee$ events vs. number of reconstructed primary vertices N_{PV}	8
90	4 Efficiency ϵ_e^{MC} determined by the tag and probe method using reconstructed $Z \rightarrow ee$ MC events minus the MC truth for the same eventsVs. Top left: ΔR ; Top right: η ; Bottom left: N_{jets} ; Bottom right: p_T	9
93	5 Ratio of electron distribution to photon MC distribution for the five photon ID variables: Top left: ECAL Isolation ; Top right: HCAL Isolation; Botton left: H/E; Bottom right $\sigma_{in\eta}$; Bottom Center: Track Isolation.	10
96	6 Ratio of the GGM signal photon efficiency to MC $\gamma+jet$ photon efficiency Top Left - $\Delta R_{\gamma-jet}$; Top Right - η ; Bottom Left - jet p_T ; Bottom Right - N_{jets}	11
98	7 Correlation between $\Delta R_{RECO\gamma-RECOjet}$ and $\Delta R_{GEN\gamma-GENjet}$	12
99	8 Energy deposits inside and outside the $\Delta R = 0.9$ isolation cones for reconstructed photons that are matched to generated neutralino decay photons for: Left - ECAL isolation energy; Right HCAL Isolation energy	12

102	9	GGM signal photon ID efficiency as a function of $\Delta R_{GEN\gamma-GENjet}$	13
103	10	The invariant mass of two electron candidates; the Z peak is fit using a Crystal Ball function and a linear background.	14
104	11	The invariant mass of electron and photon candidates; The $e\gamma$ distribution is fit with a Crystal Ball function plus a linear background.	15
105	12	Invariant mass of two photon candidates fit using a Breit-Wigner convoluted with a Gaussian plus a linear background.	15
106	13	Top left: The diEM p_T spectrum for $\gamma\gamma$ and fake-fake events (histogram) with no jet requirement; Top right: The diEM p_T spectrum for $\gamma\gamma$ and fake-fake events (histogram) with ≥ 1 jet requirement; Bottom Left: The diEM p_T spectrum for $\gamma\gamma$ and $Z \rightarrow ee$ events (histogram) with no jet requirement; Bottom right: The diEM p_T spectrum for $\gamma\gamma$ and $Z \rightarrow ee$ events (histogram) with ≥ 1 jet requirement. We also show in all cases the expected diEM spectrum produced by the GGM1 SUSY model.	17
107	14	Top left: The $\gamma\gamma$ diEM/ff diEM ratio vs. diEM p_T for $\gamma\gamma$ and fake-fake events with no jet requirement; Top right: The $\gamma\gamma$ diEM/ff diEM vs. diEM p_T for $\gamma\gamma$ and fake-fake events with ≥ 1 jet requirement; Bottom Left: The $\gamma\gamma$ diEM/ee diEM vs. diEM p_T for $\gamma\gamma$ and $Z \rightarrow ee$ events with no jet requirement; Bottom right: The $\gamma\gamma$ diEM/ee diEM vs. diEM p_T for $\gamma\gamma$ and $Z \rightarrow ee$ events with ≥ 1 jet requirement.	18
108	15	Top Left: The fake-fake events prediction of the QCD MET background is compared to the $\gamma\gamma$ spectrum (no jet requirement); Top Right: The same except requiring one or more jets; Bottom Left: The $Z \rightarrow ee$ events prediction of the QCD MET background (no jet requirement); Bottom Right: The same except with one or more jet requirement; The prediction of the GGM1 SUSY model (discussed in section 8.2) is shown in each plot. In addition, the yellow error bars and their red extensions represent respectively statistical errors (yellow) and extensions (red) of the statistical error when ratio scaling errors and renormalization errors (due to both ff and $e\gamma$) are added in quadrature.	19
109	16	Top Left: The fake-fake events prediction of the QCD MET background compared to the $\gamma\gamma$ spectrum with one isolated jet requirement and diEM reweighting; Top Right: The same except without the diEM reweighting.	19
110	17	The MET of the $e\gamma$ candidates (no jet requirement) compared to the QCD expectation for this spectrum plus a Monte Carlo of $W\gamma$ production (boosted by a K factor of 1.8 to take into account next to leading order production). The prediction of the QCD background is estimated using the $Z \rightarrow ee$ MET spectrum. The contribution of the $W\gamma$ and Wjet MET backgrounds to the overall MET spectrum of $e\gamma$ events is displayed. Here the Wjet contribution occurs when the jet is misidentified as a photon.	20
111	18	Top Left: the 3D event display of the one observed $MET \geq 50$ GeV event; Top Right: the lego event display of the event; Bottom Left: The rz display of the event; Bottom Right: the xy display of the event.	21
112	19	95% CL upper limits for the squark-gluino mass plane and for Top plot: 50, Middle plot: 150, and Bottom Plot: $500 \text{ GeV}/c^2$ neutralino masses; The units are pb.	24
113	20	K factor ratio as a function of squark-gluino masses	25
114	21	Top: PDF uncertainties as a function of squark-gluino masses; Bottom: Acceptance uncertainties	26
115	22	Cross sections for GGM production as a function of squark and gluino masses with a neutralino mass of Top: $50 \text{ GeV}/c^2$, Bottom: $150 \text{ GeV}/c^2$; The units are pb.	27
116	23	Exclusion contours in the squark-gluino mass plane for 50, 150, and $500 \text{ GeV}/c^2$ neutralino masses for GGM SUSY: Left: without K factors; Right: with K factors.	28
117	24	Breakdown of factors in determining the acceptance for $\gamma\gamma$ events due to SUSY	29
118	25	Distribution of E_T for the lead and trail photons from 50 and $150 \text{ GeV}/c^2$ neutralinos from squark-gluino mass states of 880 and 560 GeV/c^2 respectively	30

151	26	η distributions for photons from 50 and 500 GeV/c^2 neutralino decays	30
152	27	Left: $\sigma_{inj\eta}$ plot of lead vs. trail electron for the $Z \rightarrow ee$ sample; Right: same for the fake-fake QCD sample.	31
153	28	$\sigma_{inj\eta}$ plot of lead vs. trail γ candidate for the $\gamma\gamma$ candidate sample.	31
154	29	Scatterplot of ΔR between jets and the leading photon vs. the ΔR between the jets and the trailing photon for $\gamma\gamma$ data events before applying the ΔR criteria.	33
155	30	In each plot the black histogram is the efficiency, the blue solid histogram is the fraction of events as a function of ΔR of the closest jet, and the red histogram is the plot of the distance of the most distant jet from the lead photon. Each plot is made for events with different numbers of jets; 1st Row Left: $N_{jets}=1$; 1st Row Right: $N_{jets}=2$; 2nd Row Left: $N_{jets}=3$; 2nd Row Right: $N_{jets}=4$; 3rd Row Left: $N_{jets}=5$; 3rd Row Right: $N_{jets}=6$	34
156	31	Left: Acceptance for GGM singal events with and without the ΔR requirement of at least one jet with $\Delta R \geq 0.9$ as a function of the number of jets in the events; Right: Ratio of acceptances without to the acceptances with the $\Delta R \geq 0.9$ requirement. The GGM point used is squark mass = 640 GeV/c^2 , gluino mass = 640 GeV/c^2 , and neutralino mass = 150 GeV/c^2	35
157	32	Number of jets in the event vs. squark-gluino masses for Top: 50, Middle: 150, and Bottom: 500 GeV/c^2 neutralino masses.	36
158	33	Acceptance times efficiency vs. squark-gluino mass with Top plot: 50, Middle plot: 150, and Bottom plot: 500 GeV neutralino masses.	37
159	34	TcMET vs. PfMET for $\gamma\gamma$ data events.	38
160	35	Track corrected MET for $\gamma\gamma$ events with a 30 GeV JPT jet required (shown in black); Track corrected MET for $\gamma\gamma$ events with a 30 GeV particle flow jet selected (shown in blue); particle flow MET for $\gamma\gamma$ events with a 30 GeV particle flow jet selected (shown in red).	39
161	36	Top left: Lead jet η for QCD events; Top right: lead jet η for Z events; Bottom left Lead jet η for $\gamma\gamma$ events; Bottom right: Lead jet η for GGM example point.	40
162	37	Left: The fake-fake and $Z \rightarrow ee$ MET distributions normalized to each other for comparison; Right: Ratio of QCD MET distribution from $Z \rightarrow ee$ data to QCD MET from fake-fake events.	41
163	38	TcMET in $\gamma\gamma$ events with uncorrected jets (histogram) compared to $\gamma\gamma$ TcMET using corrected jets (dots). The bands are the 10% uncertainties due to JEC uncertainties.	42
164	39	1st row left: GGM MET spectra normal and cleaned - gluino,squark,neutralino masses 640,1840,500 resp.; 1st row right: GGM MET spectra normal and cleaned - gluino,squark,neutralino masses 640,640,50 resp.; 2nd row left: GGM MET spectra normal and cleaned - gluino,squark,neutralino masses 1840,640,50 resp.; 2nd row right: GGM MET spectra normal and cleaned - gluino,squark,neutralino masses 1840,640,500 resp.; 3rd row left: GGM MET spectra normal and cleaned - gluino,squark,neutralino masses 2000,2000,1500 resp.; 3rd row right: GGM MET spectra normal and cleaned - gluino,squark,neutralino masses 2000,2000,150 resp.	43
165	40	All plots in this figure show the sum of the QCD plus EW MET background compared to the MET from our sample of $\gamma\gamma$ events. They differ by whether the QCD background is determined from fake-fake events or $Z \rightarrow ee$ events: 1st Row Left : ff MET with lead jet $p_T \geq 35$ GeV; 1st Row Right: ff MET with lead jet $p_T \geq 25$ GeV; 2nd Row Left : ee MET with lead jet $p_T \geq 35$ GeV; 2nd Row Right: ee MET with lead jet $p_T \geq 25$ GeV; 3rd Row Left : ff MET with trail photon $p_T \geq 20$ GeV; 3rd Row Right: ee MET with trail photon $p_T \geq 20$ GeV.	44
166	41	left plots: leading electron vs. trailing electron with no jet requirement for E_T , η , and ϕ respectively; right plots: leading electron vs. trailing electron with ≥ 1 jet for E_T , η , and ϕ respectively .	45
167	42	left plots: leading photon vs. trailing photon with no jet requirement for E_T , η , and ϕ respectively; right plots: leading photon vs. trailing photon with ≥ 1 jet for E_T , η , and ϕ respectively .	46
168	43	left plots: leading or electron photon vs. trailing photon or electron with no jet requirement for E_T , η , and ϕ respectively; right plots: leading photon or electron vs. trailing photon or electron with ≥ 1 jet for E_T , η , and ϕ respectively; these plots are made for e γ events	47

200	44	left plots: leading fake vs. trailing fake with no jet requirement for E_T , η , and ϕ respectively for fake fake events; right plots: leading fake vs. trailing fake with ≥ 1 jet for E_T , η , and ϕ respectively for fake fake	48
203	45	left plots: leading electron vs. trailing electron with no jet requirement for $\sigma_{\eta\eta}$, Time, and Energy respectively for ee events; right plots: leading electron vs. trailing electron with ≥ 1 jet for $\sigma_{\eta\eta}$, Time, and Energy respectively for ee events	49
206	46	left plots: leading photon vs. trailing photon with no jet requirement for $\sigma_{\eta\eta}$, Time, and Energy respectively for $\gamma\gamma$ events; right plots: leading photon vs. trailing photon with ≥ 1 jet for $\sigma_{\eta\eta}$, Time, and Energy respectively for $\gamma\gamma$ events	50
209	47	left plots: leading electron or photon vs. trailing electron or photon with no jet requirement for $\sigma_{\eta\eta}$, Time, and Energy respectively for $e\gamma$ events; right plots: leading electron or photon vs. trailing electron or photon with ≥ 1 jet for $\sigma_{\eta\eta}$, Time, and Energy respectively for $e\gamma$ events	51
212	48	left plots: leading fake vs. trailing fake with no jet requirement for $\sigma_{\eta\eta}$, Time, and Energy respectively; right plots: leading fake vs. trailing fake with ≥ 1 jet for $\sigma_{\eta\eta}$, Time, and Energy respectively	52
214	49	1st row left plot: ee events leading photon with no jet requirement ECAL iso; right plots: same except ≥ 1 jet requirement; 2nd row left plot: $e\gamma$ events leading photon with no jet requirement ECAL iso; right plots: same except with ≥ 1 jet requirement; 3rd row left plot: ff events leading photon with no jet requirement ECAL iso; right plots: same except with ≥ 1 jet requirement; 4th row left plot: $\gamma\gamma$ events leading photon with no jet requirement ECAL iso; right plots: same except with ≥ 1 jet requirement; 5th row left plot: GGM events leading photon with no jet requirement ECAL iso; right plots: same except with ≥ 1 jet requirement;	53
221	50	1st row left plot: ee events leading photon with no jet requirement HCAL iso; right plots: same except ≥ 1 jet requirement; 2nd row left plot: $e\gamma$ events leading photon with no jet requirement HCAL iso; right plots: same except with ≥ 1 jet requirement; 3rd row left plot: ff events leading photon with no jet requirement HCAL iso; right plots: same except with ≥ 1 jet requirement; 4th row left plot: $\gamma\gamma$ events leading photon with no jet requirement HCAL iso; right plots: same except with ≥ 1 jet requirement; 5th row left plot: GGM events leading photon with no jet requirement HCAL iso; right plots: same except with ≥ 1 jet requirement;	54
228	51	1st row left plot: ee events leading photon with no jet requirement Track iso; right plots: same except ≥ 1 jet requirement; 2nd row left plot: $e\gamma$ events leading photon with no jet requirement Track iso; right plots: same except with ≥ 1 jet requirement; 3rd row left plot: ff events leading photon with no jet requirement Track iso; right plots: same except with ≥ 1 jet requirement; 4th row left plot: $\gamma\gamma$ events leading photon with no jet requirement Track iso; right plots: same except with ≥ 1 jet requirement; 5th row left plot: GGM events leading photon with no jet requirement Track iso; right plots: same except with ≥ 1 jet requirement;	55
235	52	1st row left plot: ee events leading photon with no jet requirement Sum iso; right plots: same except ≥ 1 jet requirement; 2nd row left plot: $e\gamma$ events leading photon with no jet requirement Sum iso; right plots: same except with ≥ 1 jet requirement; 3rd row left plot: ff events leading photon with no jet requirement Sum iso; right plots: same except with ≥ 1 jet requirement; 4th row left plot: $\gamma\gamma$ events leading photon with no jet requirement Sum iso; right plots: same except with ≥ 1 jet requirement; 5th row left plot: GGM events leading photon with no jet requirement Sum iso; right plots: same except with ≥ 1 jet requirement;	56
242	53	1st row left plot: ee events Time leading photon with no jet requirement; right plots: same except ≥ 1 jet requirement; 2nd row left plot: $e\gamma$ events Time leading photon with no jet requirement; right plots: same except with ≥ 1 jet requirement; 3rd row left plot: ff events Time leading photon with no jet requirement; right plots: same except with ≥ 1 jet requirement; 4th row left plot: $\gamma\gamma$ events Time leading photon with no jet requirement; right plots: same except with ≥ 1 jet requirement; 5th row left plot: GGM events Time leading photon with no jet requirement; right plots: same except with ≥ 1 jet requirement	57

249	54	1st row left plot: ee events $\sigma_{inj\eta}$ leading photon with no jet requirement; right plots: same except ≥ 1 jet requirement; 2nd row left plot: $e\gamma$ events $\sigma_{inj\eta}$ leading photon with no jet requirement; right plots: same except with ≥ 1 jet requirement; 3rd row left plot: ff events $\sigma_{inj\eta}$ leading photon with no jet requirement; right plots: same except with ≥ 1 jet requirement; 4th row left plot: $\gamma\gamma$ events $\sigma_{inj\eta}$ leading photon with no jet requirement; right plots: same except with ≥ 1 jet requirement; 5th row left plot: GGM events $\sigma_{inj\eta}$ leading photon with no jet requirement; right plots: same except with ≥ 1 jet requirement	58
256	55	1st row left plot: ee events calomet with no jet requirement; right plots: same except ≥ 1 jet requirement; 2nd row left plot: $e\gamma$ events calomet with no jet requirement; right plots: same except with ≥ 1 jet requirement; 3rd row left plot: ff events calomet with no jet requirement; right plots: same except with ≥ 1 jet requirement; 4th row left plot: $\gamma\gamma$ events calomet with no jet requirement; right plots: same except with ≥ 1 jet requirement; 5th row left plot: GGM events calomet with no jet requirement; right plots: same except with ≥ 1 jet requirement	59
262	56	1st row left plot: ee events tcmet with no jet requirement; right plots: same except ≥ 1 jet requirement; 2nd row left plot: $e\gamma$ events tcmet with no jet requirement; right plots: same except with ≥ 1 jet requirement; 3rd row left plot: ff events tcmet with no jet requirement; right plots: same except with ≥ 1 jet requirement; 4th row left plot: $\gamma\gamma$ events tcmet with no jet requirement; right plots: same except with ≥ 1 jet requirement; 5th row left plot: GGM events tcmet with no jet requirement; right plots: same except with ≥ 1 jet requirement;	60
268	57	1st row-left plot: ee events-number of vertices with no jet requirement; right plot: same except with ≥ 1 jet requirement; 2nd row-left plot: $e\gamma$ events-number of vertices with no jet requirement; right plot: same except with ≥ 1 jet requirement; 3rd row-left plot: ff events-number of vertices with no jet requirement; right plot: same except with ≥ 1 jet requirement; 4th row-left plot: $\gamma\gamma$ events-number of vertices with no jet requirement; right plot: same except with ≥ 1 jet requirement; 5th row-left plot: GGM events-number of vertices with no jet requirement; right plot: same except with ≥ 1 jet requirement	61
275	58	left plots: masses for ee, $e\gamma$, ff, $\gamma\gamma$ and GGM events with no jet requirement; right plots: same sequence except with ≥ 1 jet requirement	62
277	59	left plots: deltaeta for ee, $e\gamma$, ff, $\gamma\gamma$ and GGM events with no jet requirement; right plots: same sequence except with ≥ 1 jet requirement	63
279	60	left plots: deltaphi for ee, $e\gamma$, ff, $\gamma\gamma$ and GGM events with no jet requirement; right plots: same sequence except with ≥ 1 jet requirement	64
281	61	left plots: deltaphi between leading jet and MET for ee, $e\gamma$, ff, $\gamma\gamma$ and GGM events with no jet requirement; right plots: same sequence except with ≥ 1 jet requirement	65
283	62	left plots: delta phi between leading photon and MET for ee, $e\gamma$, ff, $\gamma\gamma$ and GGM events with no jet requirement; right plots: same sequence except with ≥ 1 jet requirement	66
285	63	left plots: delta R for ee, $e\gamma$, ff, $\gamma\gamma$ and GGM events with no jet requirement; right plots: same sequence except with ≥ 1 jet requirement	67
287	64	left plots: diEmPt for ee, $e\gamma$, ff, $\gamma\gamma$ and GGM events with no jet requirement; right plots: same sequence except with ≥ 1 jet requirement	68
289	65	left plots: pt of the leading jet for ee, $e\gamma$, ff, $\gamma\gamma$ and GGM events with no jet requirement; right plots: same sequence except with ≥ 1 jet requirement	69
291	66	left plots: jet HT sum for ee, $e\gamma$, ff, $\gamma\gamma$ and GGM events with no jet requirement; right plots: same sequence except with ≥ 1 jet requirement	70
293	67	1st row-left plot: ee events- number of jets with no jet requirement; right plot: same except with ≥ 1 jet requirement; 2nd row-left plot: $e\gamma$ events- number of jets with no jet requirement; right plot: same except with ≥ 1 jet requirement; 3rd row-left plot: ff events- number of jets with no jet requirement; right plot: same except with ≥ 1 jet requirement; 4th row-left plot: $\gamma\gamma$ events-number of jets with no jet requirement; right plot: same except with ≥ 1 jet requirement; 5th row-left plot: GGM events-number of jets with no jet requirement; right plot: same except with ≥ 1 jet requirement	71

300	68	1st row-left plot: ee events jet η with no jet requirement; right plot: same except with ≥ 1 jet requirement; 2nd row-left plot: $e\gamma$ events jet η with no jet requirement; right plot: same except with ≥ 1 jet requirement; 3rd row-left plot: ff events jet η with no jet requirement; right plot: same except with ≥ 1 jet requirement; 4th row-left plot: $\gamma\gamma$ events jet η with no jet requirement; right plot: same except with ≥ 1 jet requirement; 5th row-left plot: GGM events jet η with no jet requirement; right plot: same except with ≥ 1 jet requirement	73
306	69	1st row-left plot: ee events jet ϕ with no jet requirement; right plot: same except with ≥ 1 jet requirement; 2nd row-left plot: $e\gamma$ events jet ϕ with no jet requirement; right plot: same except with ≥ 1 jet requirement; 3rd row-left plot: ff events jet ϕ with no jet requirement; right plot: same except with ≥ 1 jet requirement; 4th row-left plot: $\gamma\gamma$ events jet ϕ with no jet requirement; right plot: same except with ≥ 1 jet requirement; 5th row-left plot: GGM events jet ϕ with no jet requirement; right plot: same except with ≥ 1 jet requirement	74

312 List of Tables

313	1	List of datasets and raw triggers in the 35.5 pb^{-1} data sample.	3
314	2	List of triggers used to accumulate the events in the 35.5 pb^{-1} data sample.	3
315	3	Comparison between the number of integrated observed events above a given MET and the number expected due to QCD and $W\gamma$ and Wjet event where the jet is misidentified as a photon	20
317	4	The number of events with $MET \geq 50 \text{ GeV}$ from $\gamma\gamma$, fake-fake, and $Z \rightarrow ee$ as well as the total number of background events with $MET \geq 50 \text{ GeV}$ using either the fake-fake events or the $Z \rightarrow ee$ data. The final line gives the number of events or our GGM example predicted for $MET \geq 50 \text{ GeV}$ without or with a K factor of 1.66. We give the numbers with both no jet requirement and a ≥ 1 jet requirement. We display in the final three columns the contributions to the errors of the statistics, the error due to the scaling technique, and the error due to the normalization. The components of the error are quoted for the ≥ 1 jet data sample.	21
324	5	Critical parameters and errors for determination of SUSY cross sections	22
325	6	Upper limits for fake-fake and $Z \rightarrow ee$ of QCD backgrounds and background uncertainty distributions	23
327	7	Composition of $N_{\gamma\gamma}$ candidates for loose and tight photon cuts	32
328	8	Comparison of TCjet and PFjet Content of Event with $MET \geq 50 \text{ GeV}$	40

329 1 Introduction

330 The final state of two high transverse momentum (E_T) photons and large MET can harbor new physics signals in
331 a variety of theoretical scenarios, most notably from GGM Supersymmetry Breaking [1]. In this paper, we use a
332 data-driven strategy [2, 3] to obtain the MET distribution for events that contain two high E_T photons and large
333 MET in an early search for GGM induced SUSY signals. Observation of an excess of events over extremely small
334 SM backgrounds at high MET will be a signature of new physics, in particular, SUSY.

335 The GGM SUSY signals can have a wide range of cross sections depending on the exact parameters used as input
336 to the model. Certain general statements can be made about GGM, the most important of which is that GGM
337 SUSY production is expected to proceed at the LHC via strong interactions and can have large production cross
338 sections for low mass gluino or squarks. Therefore, GGM is a particularly appropriate SUSY scenario to search for
339 new physics in CMS where the higher center of mass energy of LHC gives CMS a decided advantage compared to
340 Fermilab experiments [4]. In the GGM process searched for in this paper, the neutralino is the next to lowest mass
341 SUSY particle (NLSP) and the gravitino is the lowest mass SUSY particle (LSP). The GGM event topology that is
342 being searched for in this paper contains high E_T diphotons and large MET . These diphoton events are expected
343 to also have multiple jet activity. Therefore, the results are presented with either no jets requirement or requiring
344 one or more jets. The results of this paper are couched in terms of an exclusion region in the space of the GGM
345 gluino and squark masses.

346 The di-photon plus MET signature of SUSY signal events can be mimicked in other ways. QCD processes with
347 no true MET , such as direct di-photon, photon plus jets, and multijet production produce events with the same
348 topology as the GGM SUSY signal. In the latter two cases one or both signals reconstructed as photons may
349 really be electromagnetically rich jets misidentified as photons. The MET comes from poorly measured hadronic
350 activity in the event. The MET resolution for the QCD background is much poorer than the resolution of the total
351 E_T of the di-photon (diEM) and is determined by the resolution of the hadronic energy in the event. The strategy
352 for determining the shape of the MET distribution for the QCD background is, therefore, to find a control sample
353 that reproduces the hadronic activity in the candidate sample while having no significant real MET . Two such
354 samples have been used to determine the QCD background. The first is a sample of events with electromagnetically
355 rich di-jets that are characterized as fake photons referred to as the fake-fake or ff sample. The second sample are
356 $Z \rightarrow ee$ events where the electrons are used as diEM proxies for the di-photon. The di-EM distribution in these
357 samples is scaled to accurately model the hadronic activity of the candidate sample. This background is referred
358 to as the **QCD background**.

359 The second background comes from events with real MET . This background is dominated by $W\gamma$ and Wj
360 production where the W decays into an electron plus a neutrino and the electron is misidentified as a photon.
361 We determine these backgrounds in the following way: since the photon is expected to have almost identical
362 distributions as electrons in the electromagnetic calorimeter, electrons can be mistaken as photons except that
363 electrons should have a matching pixel in the tracker pixel detector (pixel seed). We have measured the electron-
364 photon misidentification rate, $f_{e \rightarrow \gamma}$, using $Z \rightarrow ee$ decays where sometimes one or both of the electrons are
365 misidentified as a photon. We then estimate the contribution of the second background using the resulting $e\gamma$
366 sample. The contribution of this background to the GGM signal region is accomplished by scaling the MET
367 distribution in the $e\gamma$ sample by this misidentification rate. Drell-Yan events can also contribute a background if
368 both electrons are misidentified as photons. While the Drell-Yan process does not have true MET , it can have
369 false MET due to resolution in the accompanying hadronic activity. Fortunately, given the high expected electron
370 pixel match efficiency, the contribution from this background is negligible. These backgrounds are referred to as
371 the **Electroweak backgrounds**.

372 Other processes with true MET that have di-photons in their final states are quite small. The physics backgrounds
373 with true MET include $Z\gamma\gamma \rightarrow \nu\nu\gamma\gamma$, $W\gamma\gamma \rightarrow \ell\nu\gamma\gamma$, $t\bar{t}\gamma\gamma$, or $Z\gamma\gamma$ events where the $Z \rightarrow \tau\tau$ is followed by
374 the τ decays such as $\tau \rightarrow \pi\nu$ or $\tau \rightarrow e(\mu)\nu\nu$. Finally, $Z \rightarrow ee\gamma$ involves electron-photon misidentification, and
375 therefore is partially accounted for in the EWK background. It also has no true MET, so any residual contribution
376 from it will be accounted for by our QCD background normalization.

377 2 Datasets, Trigger, and Event Selection

378 2.1 Datasets

379 The datasets used in this analysis are listed in Table 1.

380 The 3,850,570 skimmed events were reconstructed with CMSSW 3.8.3. The CMSSW 3.8.3 reconstruction process

Table 1: List of datasets and raw triggers in the 35.5 pb^{-1} data sample.

Dataset	Raw Triggers	Skimmed Events
Photon-Run2010B-PromptReco-v2-RECO	16592333	2750303
EG-Run2010A-Sep17Reco-v2-RECO	52257480	1100267

Table 2: List of triggers used to accumulate the events in the 35.5 pb^{-1} data sample.

Triggers
HLT-Photon30-L1R
HLT-Photon30-Cleaned-L1R
HLT-Photon30-L1R-8E29
HLT-Photon30-Isol-EBOnly-Cleaned-L1R-V1
HLT-Photon22-SC22HE-L1R-V1

381 includes “spike-cleaning” in the barrel. The ECAL barrel suffers from energy ”spikes” due to dE/dx deposits in
 382 the APDs that can fake high E_T photons. The standard ECAL RecHit cleaning process is applied. The removal
 383 of these spikes from the ECAL RecHit collection is accomplished by applying the “Swiss Cross” topological test
 384 in which the energy of the four nearest neighbor crystals (two in the η direction and two in the ϕ direction) to
 385 the central seed crystal are compared to the energy of the seed RecHit. If the ratio of the sum of the signals
 386 of the neighbor crystals to the seed crystal is less than 5%, the shower is designated a spike and rejected. See
 387 <http://cmssw.cvs.cern.ch/cgi-bin/cmssw.cgi/UserCode/EGamma/EGammaSkims/> for more details.

388 2.2 Trigger

389 These datasets are accumulated using the OR of the triggers in Table 2.

390 All these triggers require a leading photon with $E_T \geq 30 \text{ GeV}$ except HLT-Photon22-SC22HE-L1R-V1 which re-
 391 quires a single photon with $E_T \geq 22 \text{ GeV}$ that matches an ECAL supercluster. All triggers are cleaned of anomalous
 392 signals (the spikes mentioned above). Some of the later triggers in Table 2 have a photon isolation requirement
 393 that the photon have no track within a given radius $R \leq 0.4$ (where $R = \sqrt{(\phi_{\text{track}} - \phi_{\text{photon}})^2 + (\eta_{\text{track}} - \eta_{\text{photon}})^2}$)
 394 of the photon. Although the analysis cuts discussed below are performed with an $E_T \geq 30 \text{ GeV}$ cut on the leading
 395 and trailing photon, the effect of the threshold turn on of the trigger efficiency on the signal efficiency is minimal.
 396 When the analysis cut on the leading photon E_T is raised to 35 GeV , the loss of signal over the entire signal grid
 397 from 400 to 2000 GeV in the squark and gluino masses with the majority of the grid points changed and the bulk
 398 of the rest showing less than 1.0% drop in efficiency. Only six grid points out of 821 show a change greater than
 399 1.0% and five of those have changes less than 2%.

400 2.3 Event Selection

401 The events of interest to us contain large $MET \geq 50 \text{ GeV}$ and two high E_T photons, each with $E_T \geq 30 \text{ GeV}$. The
 402 criteria for the selection of photons is defined in section 2.3.1 below. In addition, as mentioned above, in SUSY
 403 GGM events, we expect multiple jets to be present. So we have examined the data with either no jet requirement
 404 or requiring one or more jets. For our final signal sample we require the events to have at least one jet isolated
 405 from the lead and trail photons in the event as described in section 2.3.4 below. This requirement suppresses beam
 406 halo backgrounds and eliminates the need for a timing cut on the photons in the event.

407 2.3.1 Photon and Electron Identification

408 The photon selection criteria require two photon objects in the ECAL barrel with $p_T \geq 30 \text{ GeV}/c$. If these objects
 409 satisfy the following standard photon criteria, they are selected as good photons in the ECAL barrel (where the
 410 ECAL barrel region is defined to be where the seed shower crystal is not within $\Delta\eta=0.1$ (≈ 6 crystals) of the edge
 411 of the barrel at $\eta=1.479$). The photons are required to be isolated with no electromagnetic or hadronic activity (as
 412 specified below) within a radius $R = 0.4$ of the photon. The isolation cones that are used in this analysis are shown
 413 in Fig. 1. The track isolation cone differs from the ECAL isolation cone by the width of the η strip (0.03) and the
 414 radius of the central hole (0.04).

- 415 • ECAL $E_T > 30$ GeV;
- 416 • ECAL E_T in the ECAL isolation cone $< 0.006 * E_T + 4.2$ GeV;
- 417 • HCAL E_T in HCAL isolation cone $< 0.0025 * E_T + 2.2$ GeV;
- 418 • H/E < 0.05 (here H/E is the ratio of hadronic energy in the tower directly behind the ECAL supercluster
419 divided by the ECAL supercluster energy) The H/E ratio is determined using the E_T in the ECAL and HCAL
420 cones shown in Fig. 1;
- 421 • E_T of the tracks in the track isolation cone $< 0.001 * E_T + 2.0$ GeV;
- 422 • $\sigma_{in\eta} < 0.013$;
- 423 • $e2/e9 \leq 0.95$ (where $e2/e9$ is the ratio of the energy of the highest two crystal energies in the 3x3 crystal core
424 of the supercluster to the total energy of the 3x3 core);
- 425 • the time of the signal from the seed crystal must be within $\pm 3ns$ of the interaction time if no jet requirement
426 is imposed to reduce the non-beam backgrounds; if a ≥ 1 jet requirement is imposed, the timing cut is
427 dropped.

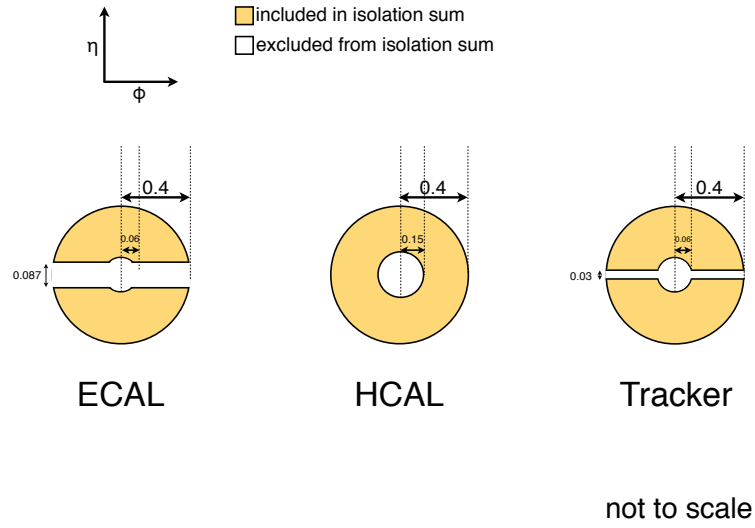


Figure 1: Sketch illustrating the isolation cones for the ECAL and HCAL E_T deposits.

428 We classify the selected objects as photons if they have no pixel match. Otherwise they are designated as electrons.
429 Note that the electron and photon definitions are orthogonal, and are designed so that the efficiency for passing all
430 cuts except the pixel seed should be similar for isolated electrons and isolated photons. This will eventually allow
431 us to use a tag-and-probe method on Z decays to determine the photon selection efficiency. $\sigma_{in\eta}$ is the log energy
432 weighed width (σ) of the extent of the shower in the η dimension based on the core 5x5 matrix of crystals of the
433 supercluster.

434 2.3.2 Fake Photons

435 We select fake photon-like signals with a definition identical to that of photons except that the track isolation or
436 the $\sigma_{in\eta}$ criteria given below are *not* satisfied:

- 437 • The E_T of the tracks be in the track isolation cone $\leq 0.001 * E_T + 2.0$ GeV;
- 438 • $\sigma_{in\eta} < 0.013$;

439 Note that the definition of the fake photon is very similar to that of the good photon definition. The energy
 440 resolution of the fake photons is similar to that of the good photons. So this set of criteria selects very special jets,
 441 those which are mainly electromagnetic, with little to no other indication of hadronic activity in the vicinity (other
 442 than the tracks which cause it to fail the track isolation criteria).

443 2.3.3 The Fake-Fake and $\gamma\gamma$ Data Sets

444 Using the above definitions, we define the following two data sets.

- 445 • $\gamma\gamma$ candidate sample, containing events with at least two objects satisfying the photon criteria;
- 446 • fake-fake (ff) control sample - with at least two objects satisfying the fake photon criteria;
- 447 • for both the $\gamma\gamma$ and ff samples, the two objects must be separated by $\Delta R \geq 0.8$;
- 448 • for the no jet requirement data sample, $\Delta\phi \geq 0.05$;

449 2.3.4 Jet Selection

450 We also require jets in the GGM SUSY analysis. The jets are formed using the JPT (jets plus track) algorithm with
 451 L1, L2, and L3 corrections for E and E_T . They must also satisfy the requirements given below:

- 452 • Jet $p_T \geq 30$ GeV/c;
- 453 • $\eta \leq 2.6$ (no forward hadron calorimeter (HF) jets);
- 454 • fHPD ≤ 0.98 (fHPD is the fraction of energy contributed by the highest energy hybrid photodetector readout);
- 455 • N90 ≥ 2 (N90 is the minimum number of ECAL and HCAL cells required to contain 90% of the jet energy);
- 456 • EMF ≥ 0.01 (EMF is the electromagnetic fraction of the jet);

457 For events to be retained in the signal sample, at least one of the jets defined by the criteria above must be isolated
 458 from the lead and trail photons in the event by a $dR \geq 0.9$;

459 3 Tag and Probe Study

460 3.1 Photon Identification Efficiency

461 We must determine photon efficiencies for our analysis in order to determine cross sections for any signal we
 462 might see. In order to determine the photon efficiencies, since there is no large clean sample of photons in the data,
 463 we rely on similarities between the detector response to electrons and photons to extract the photon efficiency, as
 464 verified with MC simulation. A scale factor to correct the MC photon efficiency to the photon efficiency for the
 465 data is obtained from the ratio of the electron efficiency from the data to the electron efficiency from the MC.

466 The criteria imposed for photon identification variables - ECAL isolation, HCAL isolation, track isolation, H/E,
 467 and $\sigma_{inj\eta}$ - are chosen so that their distributions for isolated electrons and photons are similar. Using a tag and probe
 468 method with $Z \rightarrow ee$ data events, we determine the data-driven correction to the Monte Carlo photon identification
 469 efficiency using the isolation cuts for electrons. The efficiency for photons is calculated as follows:

$$\epsilon_\gamma = \epsilon_\gamma^{MC} \times \frac{\epsilon_e^{data}}{\epsilon_e^{MC}} \quad (1)$$

470 where

- 471 • ϵ_γ is the estimated efficiency for photons in the data;
- 472 • ϵ_γ^{MC} is the efficiency for MC photons;

473 • ϵ_e^{data} is the electron efficiency obtained using the $Z \rightarrow ee$ electrons in the data that satisfy the photon id
474 cuts;

475 • ϵ_e^{MC} is the electron efficiency obtained using the $Z \rightarrow ee$ electrons in the MC that satisfy the photon id cuts.

476 The ratio $\epsilon_e^{data}/\epsilon_e^{MC}$ is defined as the scale factor with which the photon MC efficiency must be adjusted to equal
477 the efficiency of photons in the data. Explicitly, the photon id requirements are the ECAL and HCAL isolation,
478 H/E and $\sigma_{inj\eta}$ criteria, as described in section 2.3.1. Both the tag and probe objects are required to be spike-cleaned
479 as described above in section 2.1.

480 The electron efficiency in the data is determined using the tag and probe method with $Z \rightarrow ee$ events. The
481 following selection of the tag electron is made:

- 482 • the tag must have $E_T > 30$ GeV;
483 • the tag must be matched to a track with $p_T > 15$ GeV/c within $\Delta R = 0.04$ computed using the position
484 vector of the track at its closest approach to the primary vertex, with the track in the barrel fiducial region
485 (“track” here refers to a `reco::Track` “generalTracks” object);
486 • the tag must have showered in the ECAL barrel region as defined above;
487 • the tag must have $\sigma_{inj\eta} < 0.009$;
488 • the tag must be matched to a hit in the silicon pixel detector;
489 • the tag must have a ratio of hadronic energy (in the tower directly behind the ECAL supercluster) divided by
490 the ECAL supercluster energy ≤ 0.05 ;
491 • the probe must be separated from the nearest jet by $\Delta R \geq 0.9$.

492 The probe requirements were:

- 493 • the probe must have $p_T > 30$ GeV/c;
494 • the probe must be in the ECAL barrel as defined above;
495 • the probe must be loosely matched (within $\Delta R < 0.1$) to a track with $p_T \geq 30$ GeV/c. “Track” here refers to
496 a `reco::Track` “generalTracks” object;
497 • the probe must have a loose H/E ratio < 0.5 .

498 Two samples of tag-probe pairs are then formed: those in which the probe passes the photon ID selection in
499 section 2.3.1, and those where the probe fails the selection. The two distributions of tag-probe pair invariant mass
500 ($m_{tag-pass}$ and $m_{tag-fail}$) are fitted simultaneously using an extended likelihood method to extract the efficiency
501 ϵ_e^{data} . For both samples the signal shape is assumed to be a Breit-Wigner convoluted with a Gaussian distribution.
502 Exponential background shapes are assumed for each sample and they are allowed to be different.

503 3.1.1 Determination of the Photon Efficiency Scale Factor $\epsilon_e^{data}/\epsilon_e^{MC}$

504 Fig. 2 shows the dependence of the photon efficiency scale factor $\epsilon_e^{data}/\epsilon_e^{MC}$ on p_T , η , $\Delta R_{\gamma-jet}$, and N_{jets} . Note
505 that in the plot of $\epsilon_e^{data}/\epsilon_e^{MC}$ vs. $\Delta R_{\gamma-jet}$ only events with ≥ 1 jet are included. Since the dependence is flat in
506 p_T , η , $\Delta R_{\gamma-jet}$, and N_{jets} , we use the combined all bins for a more precise determination of a global scale factor.
507 The scale factor thus obtained is $1.002 \pm 0.005(\text{stat}) \pm 0.001(\text{syst})$.

508 3.1.2 Dependence of ϵ_e^{data} on Pileup

509 The dependence of ϵ_e^{data} on pileup is also studied. Fig. 3 shows ϵ_e^{data} vs. the number of reconstructed primary
510 vertices per event (N_{PV}). The data fit well to a constant value of 0.88 ± 0.01 , which agrees with the efficiency
511 of 0.89 ± 0.02 obtained from a sample of tag-probe pairs with $N_{PV} = 1$. We compute the scale factor $\epsilon_e^{data}/\epsilon_e^{MC}$
512 first using all data for which $N_{PV} > 0$, and a second time using only data for which $N_{PV} = 1$, and found $0.98 \pm$
513 0.01 for all data vs. 0.99 ± 0.02 for data with $N_{PV} = 1$. We take the difference of 0.01 as a systematic error on the
514 scale factor.

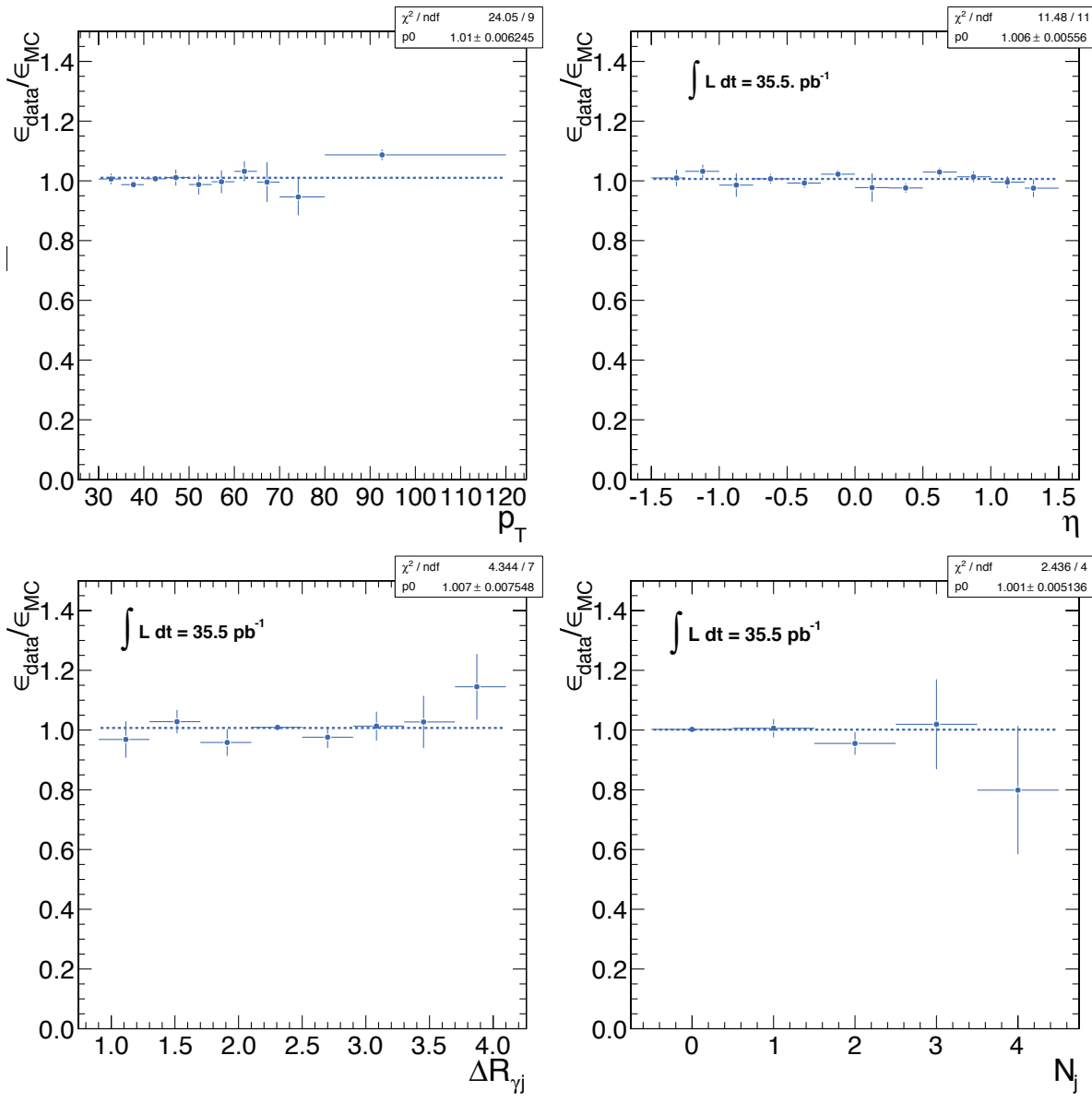


Figure 2: $\epsilon_e^{\text{data}}/\epsilon_e^{\text{MC}}$ Top left: vs. p_T ; Top Right: vs. η ; Bottom Left: vs. $\Delta R_{\gamma\text{-jet}}$; Bottom Right: vs. N_{jets}

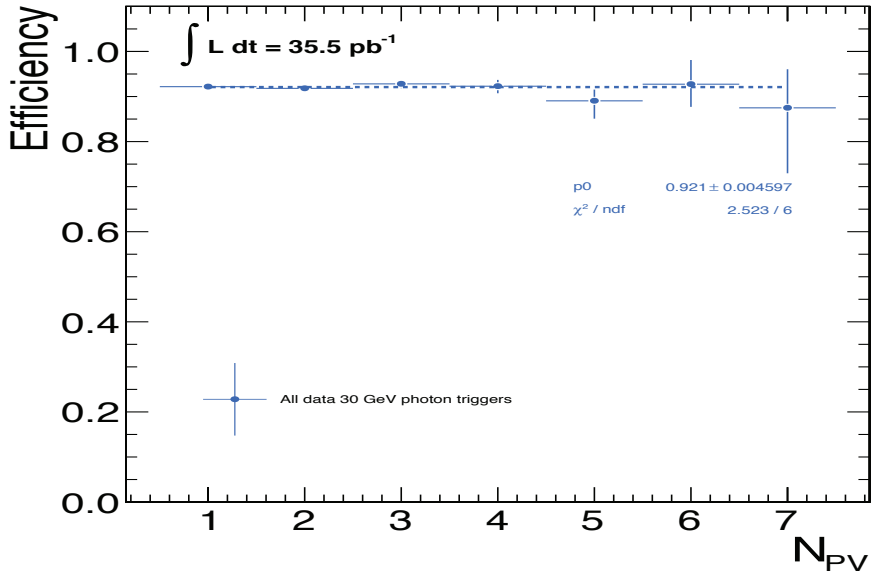


Figure 3: Electron efficiency ϵ_e^{data} determined by the tag criteria on $Z \rightarrow ee$ events vs. number of reconstructed primary vertices N_{PV} .

515 3.1.3 Comparison between MC Truth and Tag and Probe Efficiencies

516 We also checked the agreement between the MC $Z \rightarrow ee$ electron efficiency ϵ_e^{MC} as determined by tag and probe
517 on reconstructed events and the same efficiency as determined by using the MC truth information. Fig. 4 shows
518 the difference between the MC truth and tag and probe methods divided by the tag and probe efficiency. This
519 difference is independent of p_T , η , $\Delta R_{\gamma-jet}$ and N_{jets} , and fits well to a constant value of approximately 0.1%,
520 which we take as a systematic error on the scale factor.

521 3.1.4 Check that $\epsilon_\gamma^{\text{data}}/\epsilon_\gamma^{MC} = \epsilon_e^{\text{data}}/\epsilon_e^{MC}$

522 The assumption that $\epsilon_\gamma^{\text{data}}/\epsilon_\gamma^{MC} = \epsilon_e^{\text{data}}/\epsilon_e^{MC}$ – i.e., that the source of differences between the data and MC
523 efficiency for electrons is the same as that for photons – is supported by looking at the shapes of the photon ID
524 variables for MC electrons and photons. Fig. 5 shows the ratio of electron distribution to photon distribution for
525 the five photon ID variables under study. All photons and electrons are required to have $p_T \geq 30 \text{ GeV}$ and $H/E \leq$
526 0.05, be located in the ECAL barrel fiducial region, and be matched within $\Delta R = 0.3$ to a generator-level photon
527 or electron. γ +jet MC samples with $\hat{p}_T > 15 \text{ GeV}$ were used as the photon source while $Z \rightarrow ee$ MC was used as
528 the electron source. Only generator-level photons coming from the hard scatter were considered for MC matching,
529 while in the case of electrons, only electrons from Z decay were considered. The ratio distributions are flat for the
530 photon ID region of interest (the region to which the cuts on the photon variable restrict the photons), showing that
531 there is no significant shape difference. This is an important check that there are no real MC differences between
532 the behavior of the ID variables for photons and electrons.

533 3.1.5 Comparison of ϵ_{MC} for γ +Jet and ϵ_{MC} for the GGM Signal

534 Finally, we compare the MC efficiency of photons from γ +jet samples to the efficiency of neutralino decay photons
535 in our signal MC. Fig. 6 shows the ratio of the GGM signal photon efficiency to γ +jet photon efficiency. Signal
536 photons are required to have $p_T \geq 30 \text{ GeV}$ and $H/E \leq 0.05$, be in the EB fiducial region, and be matched within
537 $\Delta R \leq 0.3$ to a generator level photon from neutralino decay. Furthermore, the distance in R between the matched
538 neutralino decay photon and the nearest generator-level quark jet from the SUSY cascade decay must be ≥ 0.9 .
539 With these requirements, the γ +jet photon and signal photon efficiencies are nearly identical. Nevertheless, the
540 efficiency ratios are fit to a constant and we take the differences as another systematic error on the measured
541 data/MC scale factor.

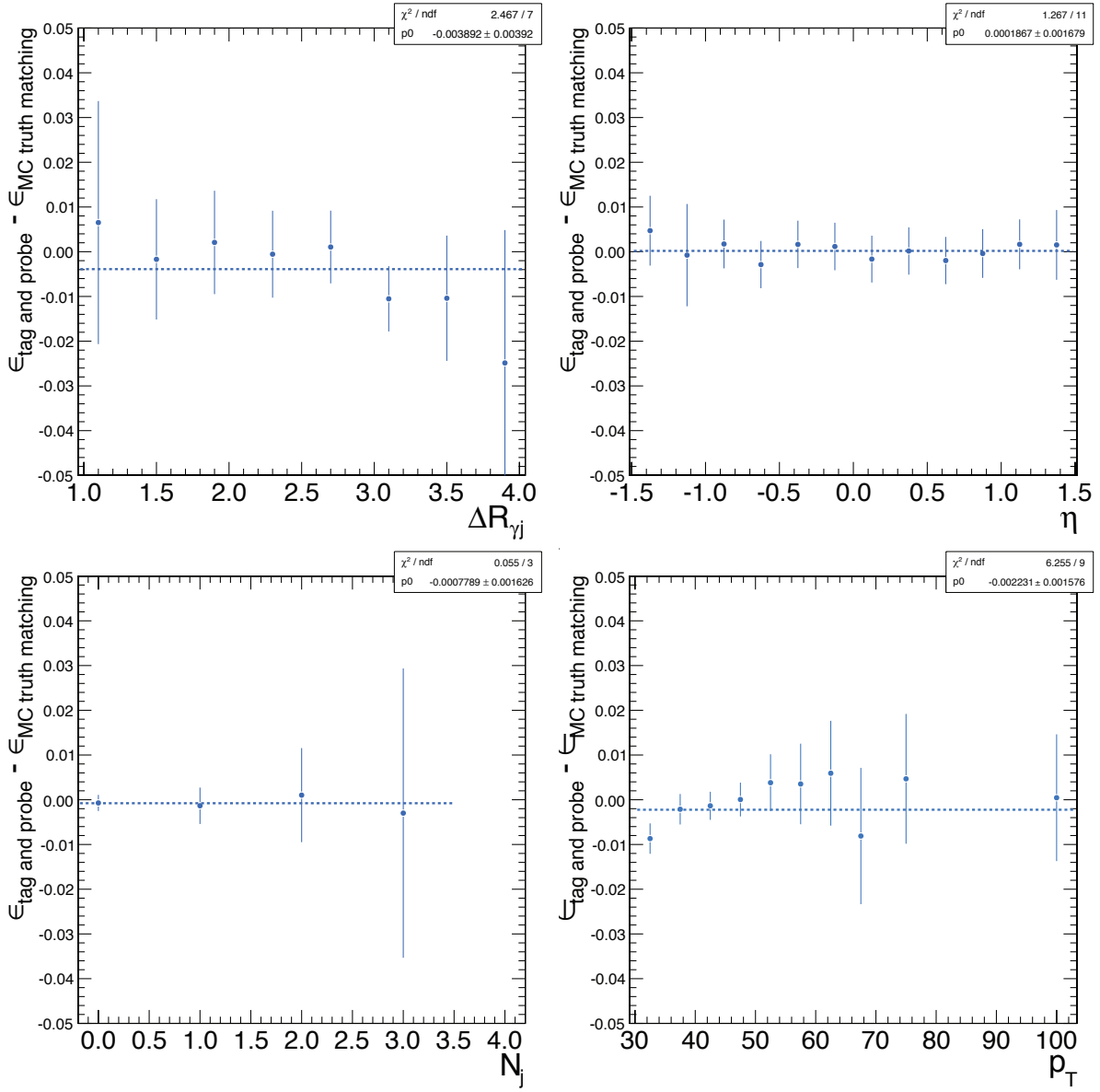


Figure 4: Efficiency ϵ_e^{MC} determined by the tag and probe method using reconstructed $Z \rightarrow ee$ MC events minus the MC truth for the same eventsVs. Top left: ΔR ; Top right: η ; Bottom left: N_{jets} ; Bottom right: p_T .

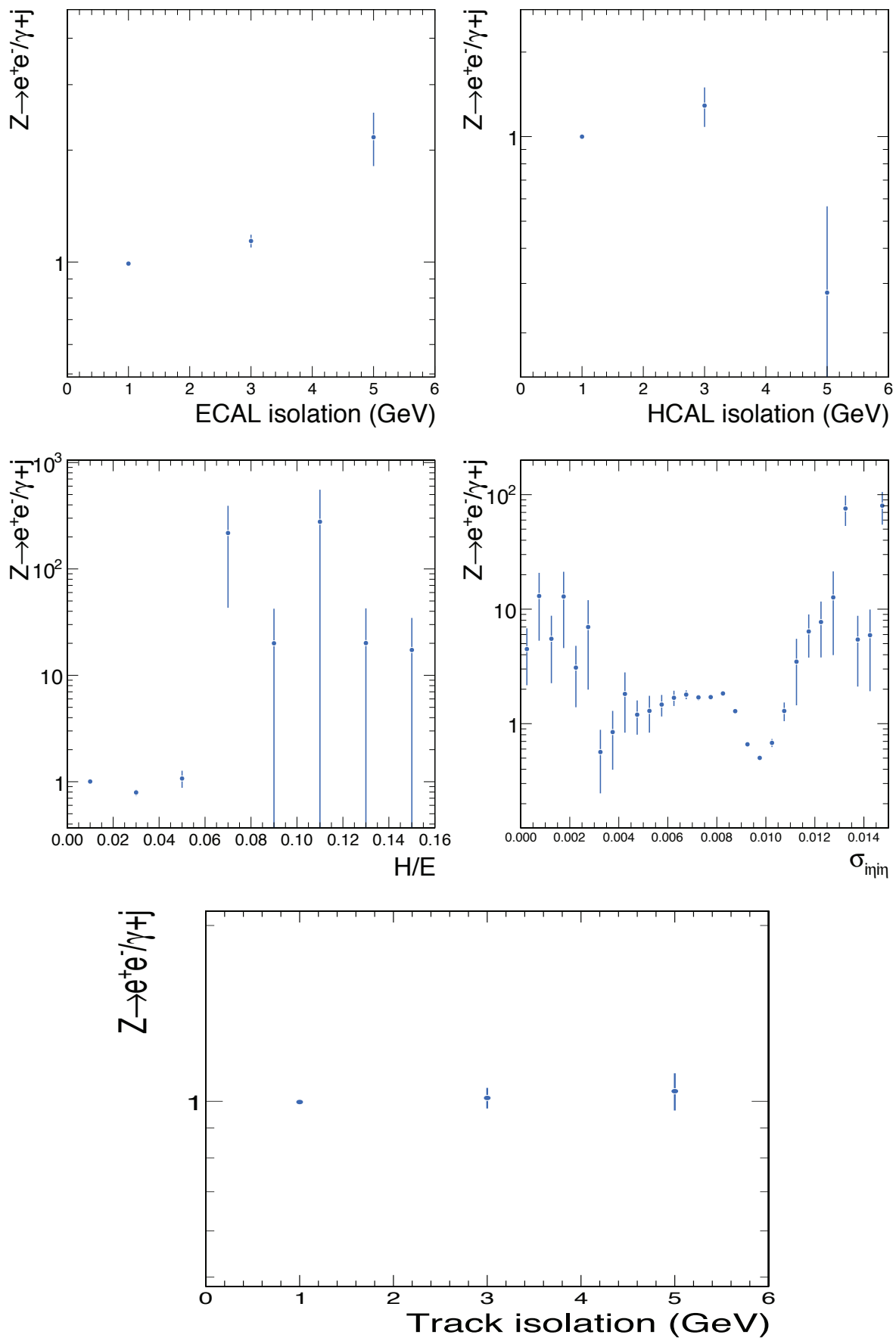


Figure 5: Ratio of electron distribution to photon MC distribution for the five photon ID variables: Top left: ECAL Isolation ; Top right: HCAL Isolation; Bottom left: H/E; Bottom right $\sigma_{inj\eta}$; Bottom Center: Track Isolation.

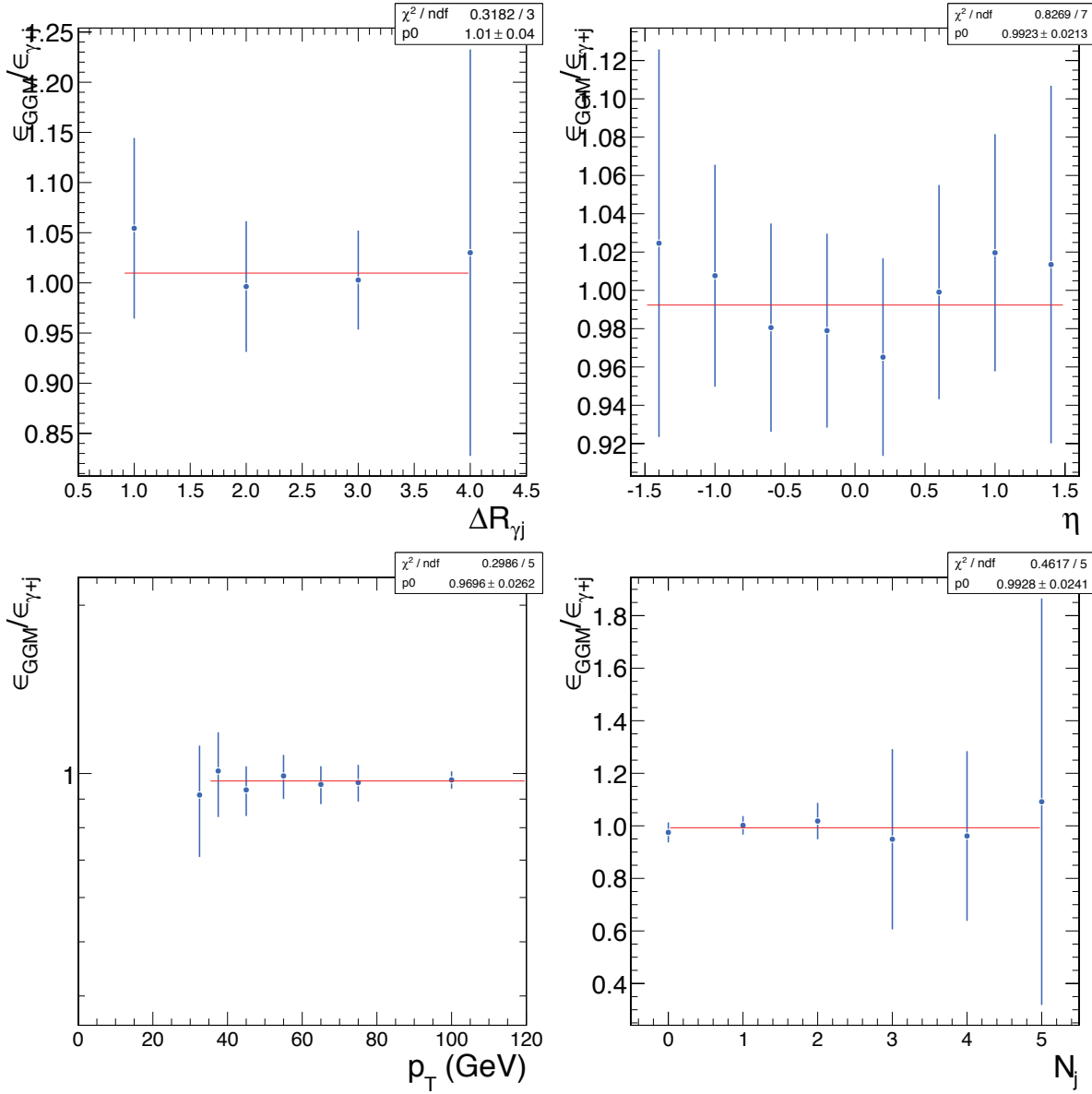


Figure 6: Ratio of the GGM signal photon efficiency to MC γ +jet photon efficiency Top Left - $\Delta R_{\gamma-jet}$; Top Right - η ; Bottom Left - jet p_T ; Bottom Right - N_{jets}

3.1.6 GGM Signal Photon Isolation

For signal photons where the distance between the generated neutralino decay photon and the nearest quark from the SUSY cascade decay is $\Delta R < 0.9$, the photon reconstruction fails to distinguish the two objects. Instead, the photon is reconstructed as a non-isolated photon, which fails the photon ID cuts and decreases the apparent signal photon efficiency. Therefore, we require that the minimum distance between a reconstructed photon and the nearest reconstructed jet be ≥ 0.9 , but this requirement does not remove the cases where a generated photon and generated jet are reconstructed as a single non-isolated object. Fig. 7 shows the correlation between $\Delta R_{RECO\gamma - RECOjet}$ and $\Delta R_{GEN\gamma - GENjet}$, in particular the region $\Delta R_{GEN\gamma - GENjet} < 0.9$, for signal photons passing the loose requirement described in the previous paragraph.

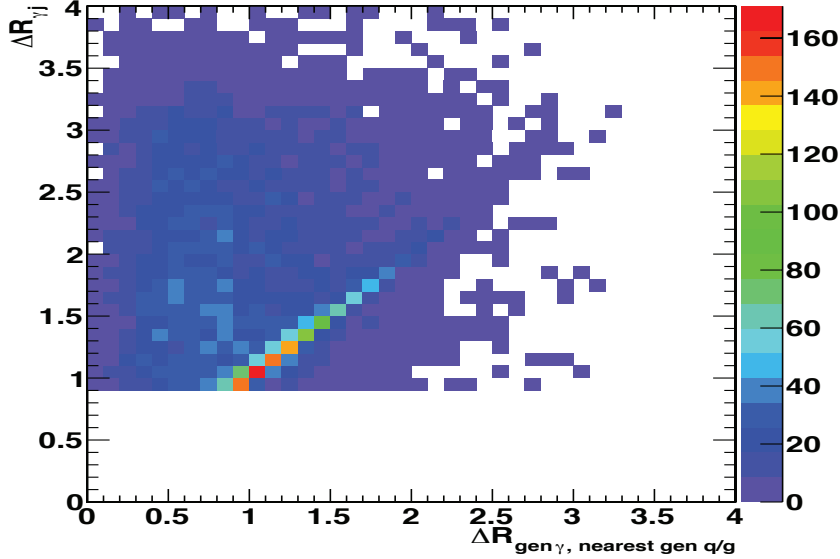


Figure 7: Correlation between $\Delta R_{RECO\gamma - RECOjet}$ and $\Delta R_{GEN\gamma - GENjet}$

Fig. 8 shows plots of the ECAL and HCAL isolation distributions of reconstructed photons matched to generated neutralino decay photons, separated by whether $\Delta R_{GEN\gamma - GENjet} < 0.9$ or ≤ 0.9 . The isolation energy tends to be larger for $\Delta R_{GEN\gamma - GENjet} < 0.9$.

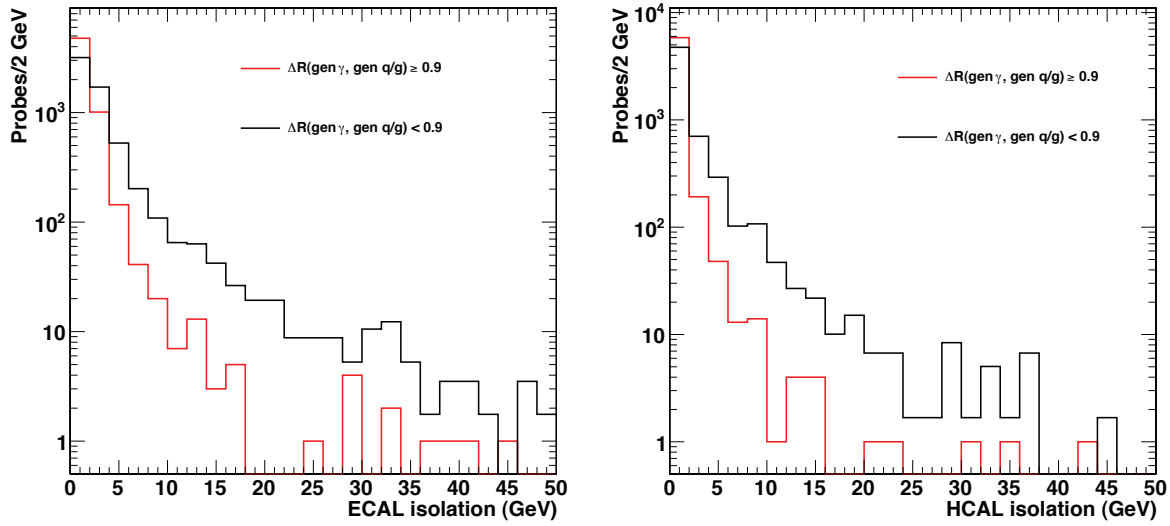


Figure 8: Energy deposits inside and outside the $\Delta R = 0.9$ isolation cones for reconstructed photons that are matched to generated neutralino decay photons for: Left - ECAL isolation energy; Right HCAL Isolation energy

Finally, Fig. 9 shows the signal photon ID efficiency as a function of $\Delta R_{GEN\gamma-GENjet}$. One clearly sees the turn-on around $\Delta R_{GEN\gamma-GENjet} = 0.9$. This efficiency plateaus at a value very close to the photon efficiency in $\gamma + \text{jet MC}$.

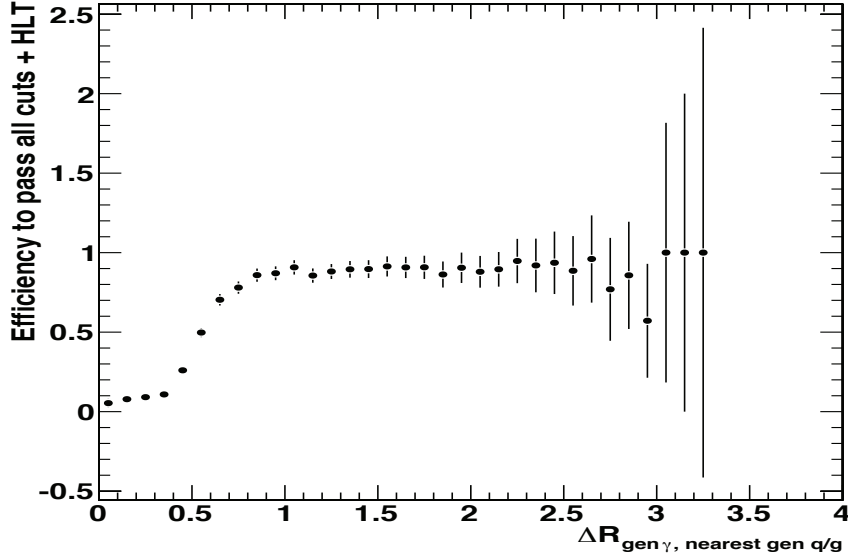


Figure 9: GGM signal photon ID efficiency as a function of $\Delta R_{GEN\gamma-GENjet}$.

The effect of this mis-reconstruction due to photon/jet overlaps is already included in the signal acceptance times efficiency. Once we exclude the effect from our comparisons between signal photon efficiency and $\gamma + \text{jet}$ efficiency, we see that the two are very nearly identical. Therefore, we consider the ratio $\gamma + \text{jet}$ efficiency - signal photon efficiency ($\Delta R_{GEN\gamma-GENjet} \geq 0.9$)/ $\gamma + \text{jet}$ efficiency) as a small error on the $\epsilon_e^{\text{data}}/\epsilon_e^{\text{MC}}$ scale factor. We then correct the photon MC acceptance times efficiency by the $\epsilon_e^{\text{data}}/\epsilon_e^{\text{MC}}$ scale factor as determined by electron tag and probe.

3.2 Electron Misidentification

An electron is misidentified as a photon if its ECAL supercluster does not have a reconstructed pixel match from the silicon tracker. We determine the efficiency for pixel match reconstruction by fitting the mass of the Z seen in the ee and $e\gamma$ mass spectra, and comparing the integrals of these fits.

3.2.1 Determination of the Electron Misidentification Fraction

We must measure the fraction of electrons that are misidentified as photons in order to properly normalize the $W\gamma$ EW background to the observed $\gamma\gamma$ spectrum. This $W\gamma$ background results from $W \rightarrow e\nu$ decays where the electron is misidentified as a photon and the addition photon is provided by either a true photon or a jet identified as a photon.

To extract the misidentification fraction, we extract the electron efficiency from the ee and $e\gamma$ spectrum using the number of observed $Z \rightarrow ee$ events in the ee mass spectrum $N_{ee} = f_e^2 N_{\text{true}Z's}$ where $N_{\text{true}Z's}$ is the true number of $Z \rightarrow ee$ events and f_e is the electron efficiency. With these definitions, the observed $Z \rightarrow ee$ peak in the $e\gamma$ spectrum is then $N_{e\gamma} = 2[f_e(1-f_e)]N_{\text{true}Z's}$ leading to $f_e = [1+0.5N_{e\gamma}/N_{ee}]^{-1}$. We can calculate, as a check, the number of $Z \rightarrow ee$ expected in the $N_{\gamma\gamma}$ spectrum using $N_{\gamma\gamma} = [(1-f_e)(1-f_e)]N_{ee}/[(f_e^2)]$

The electroweak background to the $\gamma\gamma$ sample can then be determined using f_e and the $e\gamma$ spectrum. The $e\gamma$ spectrum should be composed mostly of $W\gamma$ events where the W decays into $e\nu$ with a residual amount of $Z \rightarrow ee$ where one of the electrons is misidentified as a γ . To determine the electroweak background we use the number of events from the $e\gamma$ spectrum = $N_{e\gamma} = f_e N_{\text{true}W\text{decays}}$ so that $N_{\gamma\gamma}$ from W decays = $(1-f_e)N_{\text{true}W's} = N_{e\gamma}(1-f_e)/(f_e)$.

581 **3.2.2 Fitting the ee, e γ , and $\gamma\gamma$ Spectra**

582 For the fit of the Z peak in the ee spectrum we use a Crystal Ball function with a linear or constant background
 583 assumptions (see figure 10 for the linear background fit). For the e γ sample we use a Crystal Ball function and a
 584 linear or constant function to fit the Z signal plus background (see Fig. 11 for the linear background fit). The $\gamma\gamma$
 585 spectrum is fit with a Breit-Wigner convoluted with a Gaussian plus a linear background. The statistical errors are
 586 taken from the integrals of the fits, while the systematic errors are determined by comparing the differences in the
 587 integrals between the linear and constant background fits for the ee and e γ samples. For the fits all parameters are
 588 allowed to float.

589 Fitting the Z peak of the ee sample yields $3824.6 \pm 91.8(57.4syst)$ events. Fitting the Z peak of the e γ sample
 590 yields $103.5 \pm 26.7(8.0syst)$ events. From the fits we determine an efficiency of $98.65 \pm 0.37\%$. From this we
 591 determine the fraction of ee and e γ events misidentified as $\gamma\gamma$ events to be $(1.87 \pm 0.72) \times 10^{-4}$ and 0.014 ± 0.004
 592 respectively.

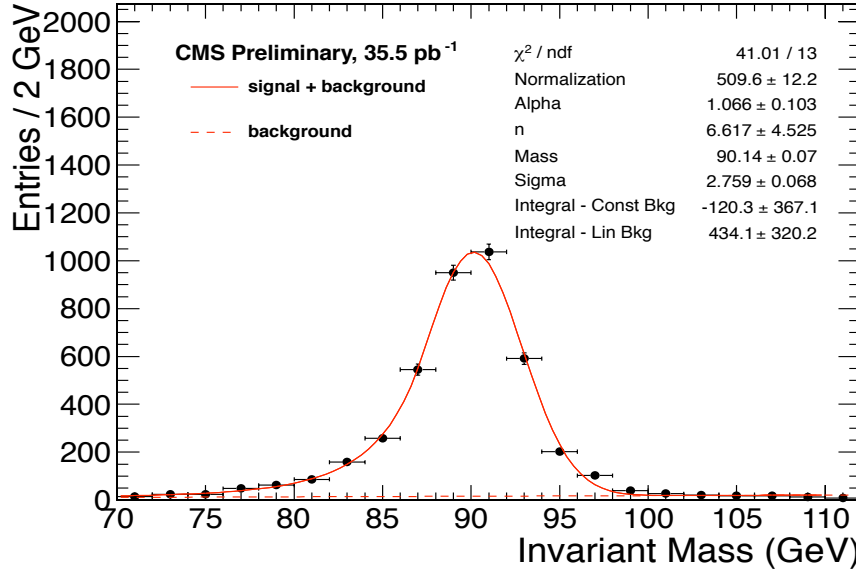


Figure 10: The invariant mass of two electron candidates; the Z peak is fit using a Crystal Ball function and a linear background.

593 **4 Estimation of MET Backgrounds**

594 After having selected a $\gamma\gamma$ sample with our photon cuts as described in section 2.3.1 which presumably contains
 595 the $\gamma\gamma$ di-photon SUSY events with large MET (specifically TcMET - track corrected MET), we must compare
 596 the shapes of the MET distribution in this sample of events to the expected QCD and EW background shapes.

597 Section 1 contains an overview of the possible backgrounds to $\gamma\gamma$ SUSY production. We must compare the shapes
 598 of the MET from the background control samples to the MET of the $\gamma\gamma$ sample and determine the contribution
 599 of each type of background to the MET region ≥ 50 GeV where we expect to see GGM SUSY production.

600 **4.1 Fake-Fake and $Z \rightarrow ee$ QCD Background Estimates**

601 Two control samples with two EM-like objects, ff and ee, can be used to measure the shape of the MET distri-
 602 bution for different types of backgrounds with false MET due to mismeasurements and fluctuations of hadron
 603 activity in the events.

604 **4.1.1 Correcting Differences Between $\gamma\gamma$ and ff and $Z \rightarrow ee$ Background diEM Spectra**

605 We must properly scale all the MET spectra from the two control samples to take into account that there is a
 606 slight difference in the diEM p_T spectrum of the candidates and the diEM p_T spectra of the two control samples

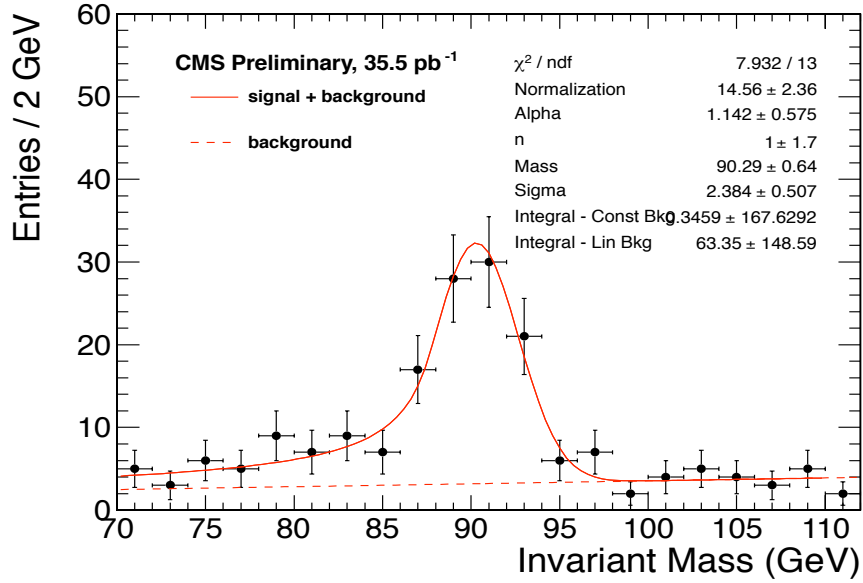


Figure 11: The invariant mass of electron and photon candidates; The $e\gamma$ distribution is fit with a Crystal Ball function plus a linear background.

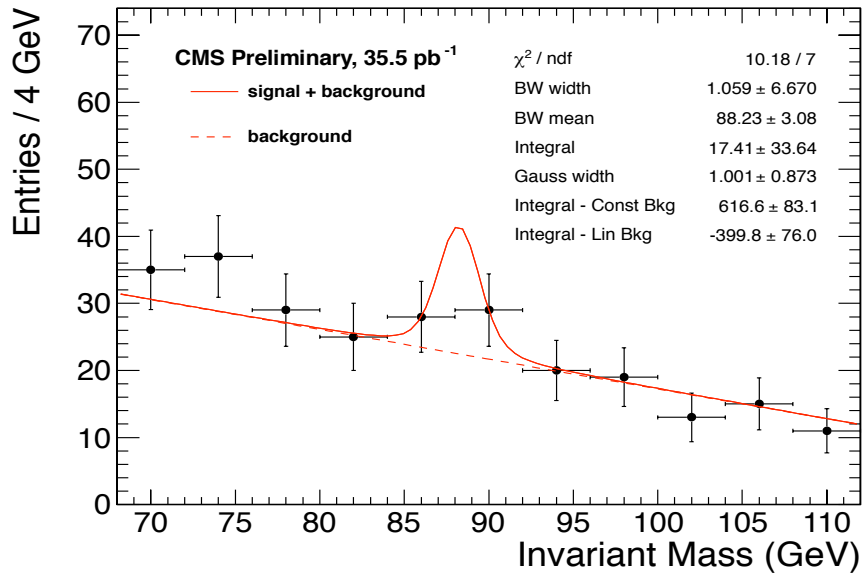


Figure 12: Invariant mass of two photon candidates fit using a Breit-Wigner convoluted with a Gaussian plus a linear background.

(see Fig. 13). This is assumed to be due to differences in the E_T of the hadronic recoil in the different topologies. In order to compensate for these differences in the diEM spectra, a given background is scaled to match the $\gamma\gamma$ diEM p_T distribution. To do this we form the ratio of the diEM spectrum from a background sample to the diEM spectrum of the candidate $\gamma\gamma$ events (see Fig. 14), fit the ratio to a linear expression, and scale each event in the given background using this fit to make the diEM spectra agree. The events replotted vs. MET are scaled by the ratio of the particular bin of diEM from which the event came.

The error in the scaled MET distribution due to the uncertainty in the diEM ratio is determined by taking each bin of the original diEM plot and distributing that bin's value about its central value with a Gaussian having a sigma equal to the statistical error on the bin in order to choose a new central value for each bin. This was done for each bin in order to form a new diEM plot with new central values for each bin but the same statistical error. We generate one thousand new diEM plots in this way. We then form new ratio plots from the new diEM plots to produce new MET plots with a range of values distributed relative to the original MET plot. Errors, which can be asymmetric, are then determined from fluctuations of MET in each bin using the thousand new MET plots. This procedure of scaling the MET distributions with the evaluation of the associated uncertainty is applied to the two control samples.

4.1.2 The QCD Background Estimate using fake-fake Sample

The MET distribution for the ff events is considered to represent the MET shape from all sources of backgrounds except those electroweak backgrounds determined using the $e\gamma$ sample. We normalize the ff MET spectrum so that the total number of ff events with $MET \leq 20$ GeV is equal to the number of $\gamma\gamma$ events with $MET \leq 20$ GeV (less the background prediction obtained with the $e\gamma$ sample for $MET \leq 20$ GeV). The MET distribution of the ff control sample after renormalization contains 83.2 ± 13.1 events, where 63.5 ± 10.4 events have $MET \leq 20$ GeV and 0.54 ± 0.40 events have $MET \geq 50$ GeV. Table 4 shows the predicted number of events from the ff control sample with $MET \geq 50$ GeV with the statistical uncertainty and errors due to scaling and normalization shown separately.

4.1.3 The QCD Background Estimate using the $Z \rightarrow ee$ Sample

The ee distribution can be treated in the same way as the ff distribution to give a prediction of all backgrounds except those EW backgrounds that are obtained from the $e\gamma$ sample. In this case, we normalize the ee events MET distribution so that the total number of ee events with $MET \leq 20$ GeV is equal to the number of $\gamma\gamma$ events with $MET \leq 20$ GeV (less the background prediction obtained with the $e\gamma$ sample with $MET \leq 20$ GeV). The MET distribution of the ee control sample after renormalization contains 81.9 ± 13.1 events, where 63.6 ± 10.4 events have $MET \leq 20$ GeV and 1.67 ± 0.66 events have $MET \geq 50$ GeV. Table 4 shows the predicted number of ee events from the ff and ee events treated using similar methods with $MET \geq 50$ GeV with statistical uncertainty and errors due to scaling and normalization shown separately.

4.2 Electroweak Background

There is also an electroweak background with real MET due to W leptonic decays where the electron is misidentified as a photon. We study this background using a control sample of events with one electron and one photon ($e\gamma$ sample). The electron misidentification fraction, as determined in section 3.2, is used on both ee and $e\gamma$ samples to estimate the rate of $\gamma\gamma$ backgrounds due to $Z \rightarrow ee$ and electroweak decays.

Using the measured electron identification efficiency from section 3.2, we multiply the MET distribution of the $e\gamma$ events by the factor of 0.014 ± 0.003 to estimate the contribution of the $e\gamma$ to the $\gamma\gamma$ sample given above. The MET distribution of the $e\gamma$ control sample after this scaling contains 0.59 ± 0.91 events. There are 0.083 ± 0.18 events with $MET \leq 20$ GeV and 0.04 ± 0.15 events with $MET \geq 50$ GeV in this MET spectrum. The number of expected $\gamma\gamma$ events $MET \geq 50$ GeV from the $e\gamma$ control sample is summarized in Table 4 with the statistical uncertainty and errors due to scaling and normalization shown separately.

4.3 Total Background Prediction with $MET \geq 50$ GeV

The previous section describes the determination of MET QCD and EW backgrounds. The QCD MET distribution of the candidate $\gamma\gamma$ events using either the MET distributions of the fake-fake events or the $Z \rightarrow ee$ events are compared in Figs. 15. Both options provide an estimation of the total QCD MET background. Both options

provide a cross-check of consistency of our determination of the QCD backgrounds. The $e\gamma$ spectrum as described above gives an estimate of background due to physics processes that have real MET .

We calculate the total background in the $MET > 50 \text{ GeV}$ range by adding individual background contributions and assuming uncorrelated individual uncertainties. Special care is taken when comparing error bars in closure plots due to the 100% correlation of normalization uncertainties in all bins. In Table 4 we give the predicted backgrounds for $MET \geq 50 \text{ GeV}$ for each technique in estimating backgrounds along with the number of events predicted by the GGM1 SUSY model defined in section 8.2 below.

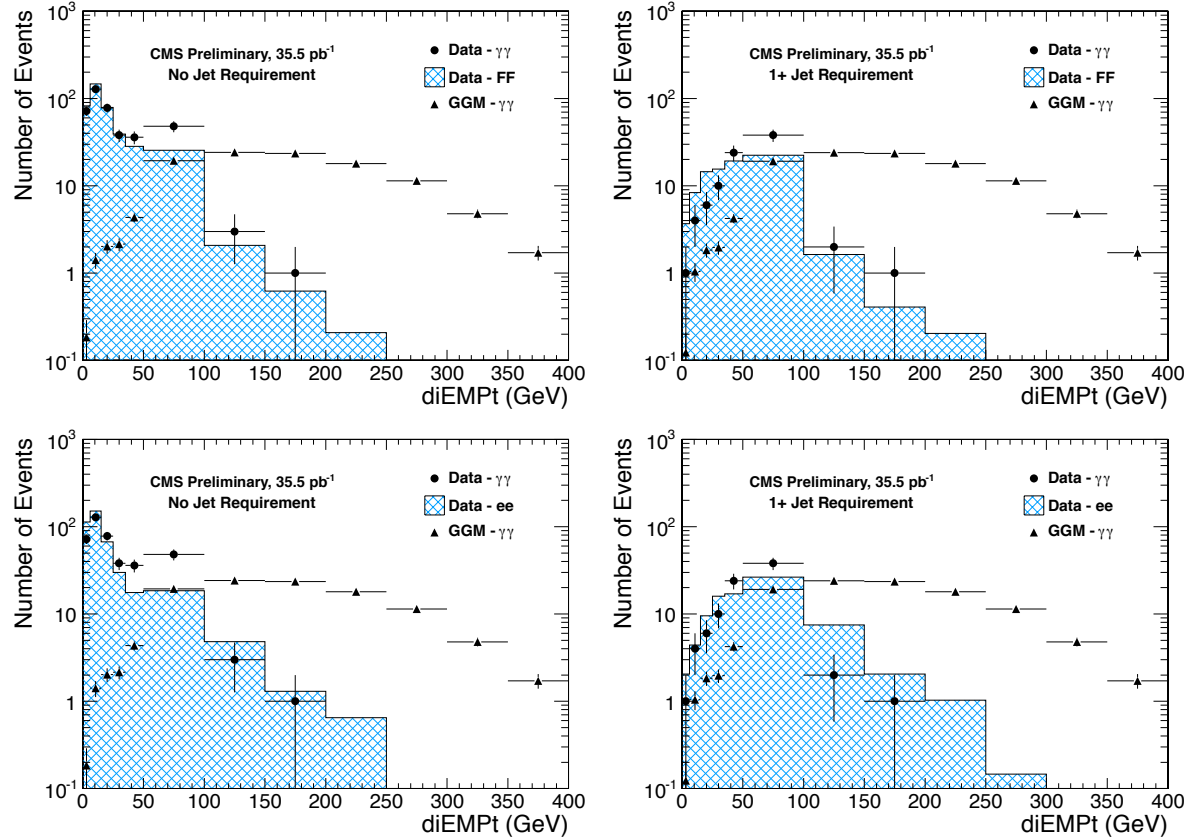


Figure 13: Top left: The diEM p_T spectrum for $\gamma\gamma$ and fake-fake events (histogram) with no jet requirement; Top right: The diEM p_T spectrum for $\gamma\gamma$ and fake-fake events (histogram) with ≥ 1 jet requirement; Bottom Left: The diEM p_T spectrum for $\gamma\gamma$ and $Z \rightarrow ee$ events (histogram) with no jet requirement; Bottom right: The diEM p_T spectrum for $\gamma\gamma$ and $Z \rightarrow ee$ events (histogram) with ≥ 1 jet requirement. We also show in all cases the expected diEM spectrum produced by the GGM1 SUSY model.

To show the effect of the reweighting obtained from the diEM, we show in Fig. 16, the MET plots for the fake-fake events with and without reweighting. There is almost not perceptible difference except that the errors are slightly smaller for the non-reweighted plot.

5 The $W\gamma$ EW Contribution to the MET Background

We have inspected the $e\gamma$ spectrum for any evidence of a contribution of the $W\gamma$ events. Shown in Fig. 17 is the $e\gamma$ spectrum (no requirement on the number of jets) compared to the expectation for this spectrum obtained using the MET spectrum from the $Z \rightarrow ee$ events plus the Monte Carlo of the $W\gamma$ production. As can be seen there is evidence that the $W\gamma$ spectrum (multiplied by a K factor of 1.8 to account for next to leading order enhancement of the production) peaks in the right place to make the agreement between the $e\gamma$ spectrum and the prediction of the total background better.

Since the $W\gamma$ electroweak background will contribute to high MET events in our search for new physics, we would like to determine its exact composition. It should be composed of events containing W decaying into electron plus neutrino accompanied by a real or fake photons due to a misidentified jet.

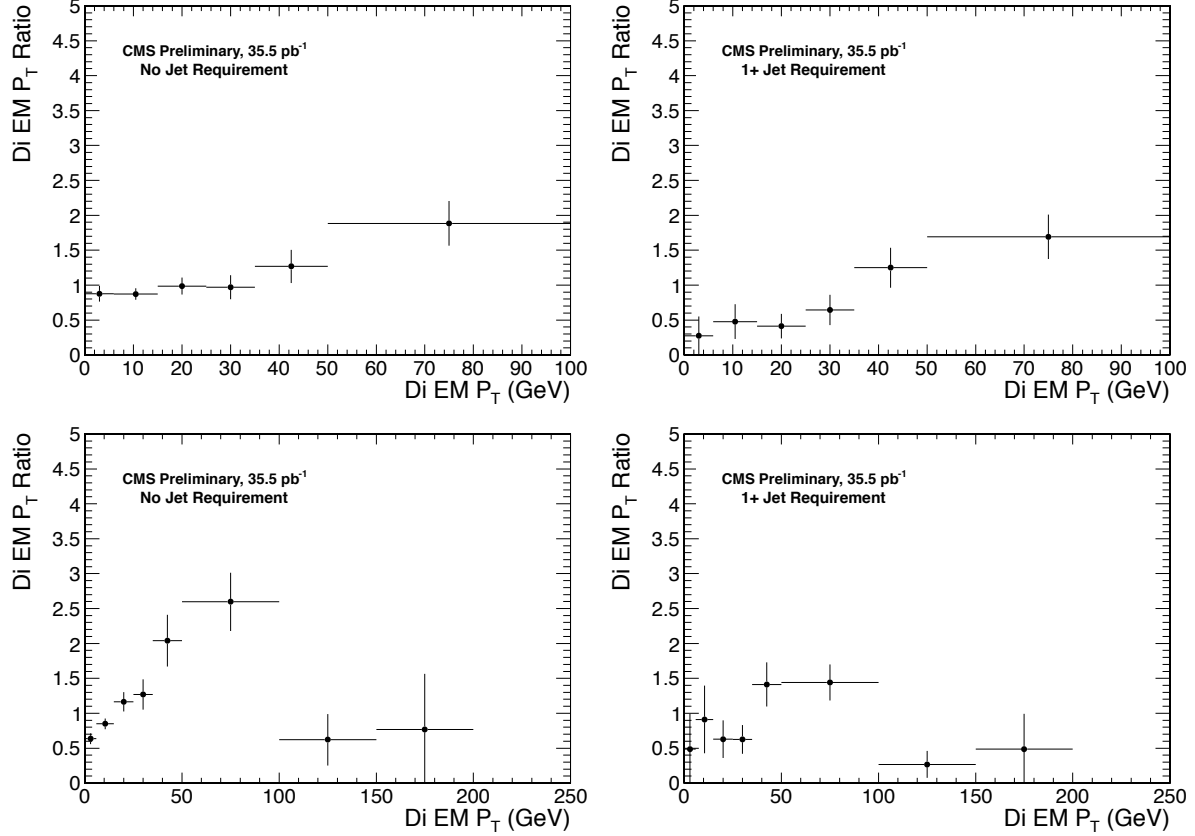


Figure 14: Top left: The $\gamma\gamma$ diEM/ff diEM ratio vs. diEM p_T for $\gamma\gamma$ and fake-fake events with no jet requirement; Top right: The $\gamma\gamma$ diEM/ff diEM vs. diEM p_T for $\gamma\gamma$ and fake-fake events with ≥ 1 jet requirement; Bottom Left: The $\gamma\gamma$ diEM/ee diEM vs. diEM p_T for $\gamma\gamma$ and $Z \rightarrow ee$ events with no jet requirement; Bottom right: The $\gamma\gamma$ diEM/ee diEM vs. diEM p_T for $\gamma\gamma$ and $Z \rightarrow ee$ events with ≥ 1 jet requirement.

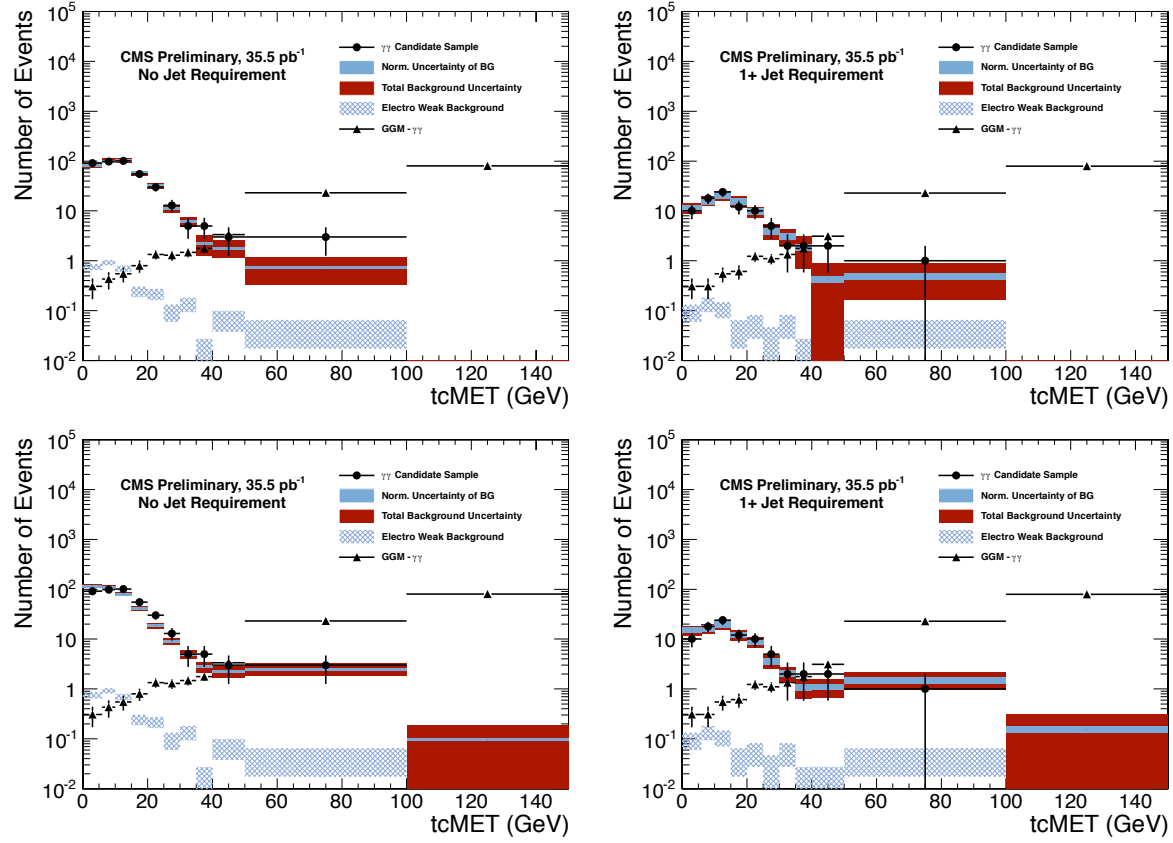


Figure 15: Top Left: The fake-fake events prediction of the QCD *MET* background is compared to the $\gamma\gamma$ spectrum (no jet requirement); Top Right: The same except requiring one or more jets; Bottom Left: The $Z \rightarrow ee$ events prediction of the QCD *MET* background (no jet requirement); Bottom Right: The same except with one or more jet requirement; The prediction of the GGM1 SUSY model (discussed in section 8.2) is shown in each plot. In addition, the yellow error bars and their red extensions represent respectively statistical errors (yellow) and extensions (red) of the statistical error when ratio scaling errors and renormalization errors (due to both ff and $e\gamma$) are added in quadrature.

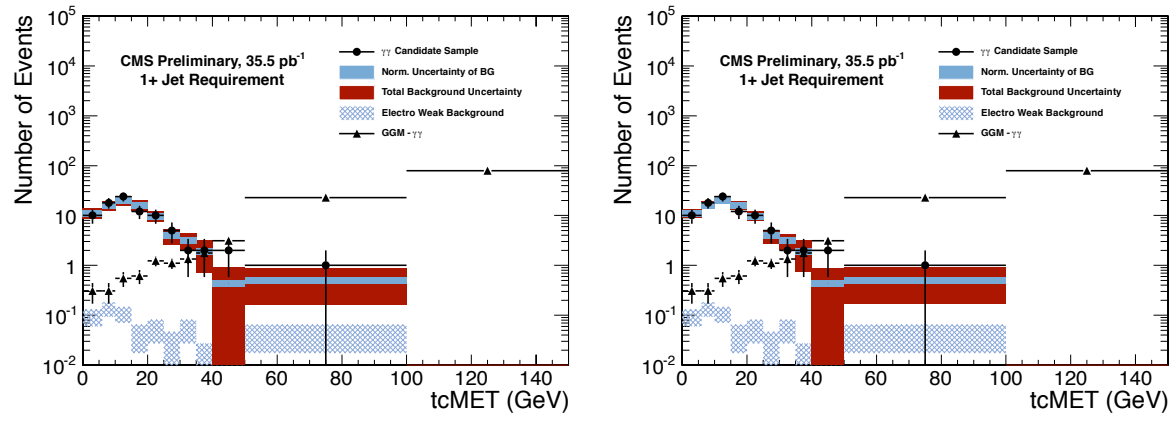


Figure 16: Top Left: The fake-fake events prediction of the QCD *MET* background compared to the $\gamma\gamma$ spectrum with one isolated jet requirement and diEM reweighting; Top Right: The same except without the diEM reweighting.

675 The breakdown of the $W\gamma$ spectrum is shown in Fig. 17. Approximately 33.6% of the $W\gamma$ spectrum is due to Wjet
 676 events where the jet is dominantly electromagnetic and passes the photon cuts. If we examine the MET region \geq
 677 30 GeV, the percentages of background there is 44.6% $W\gamma$, 22.5% Wjet, and 32.9% $Z \rightarrow ee$.

678 Table 3 quantifies the agreement between the observed numbers of events above a given MET and the expected
 679 numbers due to QCD and $W\gamma$ and Wjet EW backgrounds.

Table 3: Comparison between the number of integrated observed events above a given MET and the number expected due to QCD and $W\gamma$ and Wjet event where the jet is misidentified as a photon

$\geq MET$	Observed	QCD Background	$W\gamma$ and Wjet
≥ 20 GeV	42 events	20 ± 2 events	24 events
≥ 25 GeV	26 events	10 ± 1 events	20 events
≥ 30 GeV	19 events	5.5 ± 0.6 events	16 events
≥ 35 GeV	9 events	3.4 ± 0.4 events	12.7 events
≥ 40 GeV	8 events	2.0 ± 0.2 events	9.6 events
≥ 50 GeV	3 events	0.9 ± 0.1 events	4.5 events

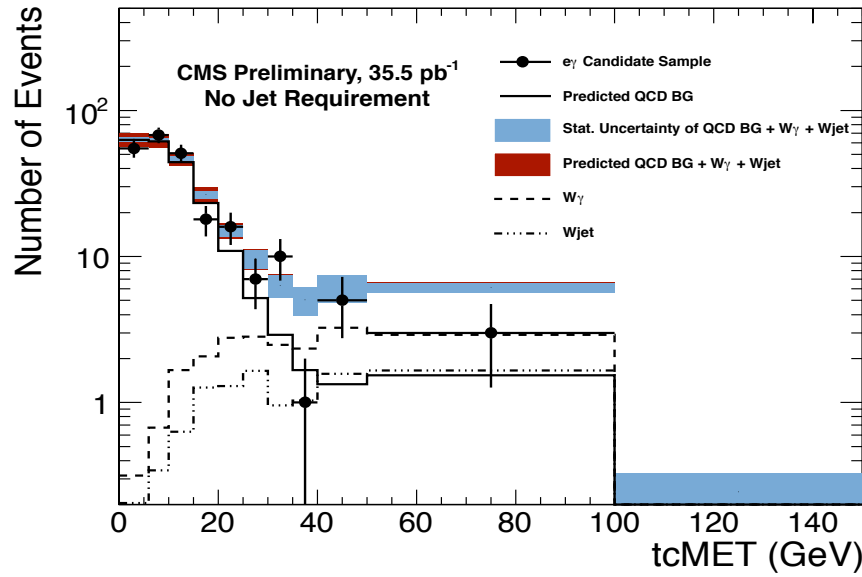


Figure 17: The MET of the $e\gamma$ candidates (no jet requirement) compared to the QCD expectation for this spectrum plus a Monte Carlo of $W\gamma$ production (boosted by a K factor of 1.8 to take into account next to leading order production). The prediction of the QCD background is estimated using the $Z \rightarrow ee$ MET spectrum. The contribution of the $W\gamma$ and Wjet MET backgrounds to the overall MET spectrum of $e\gamma$ events is displayed. Here the Wjet contribution occurs when the jet is misidentified as a photon.

680 6 Table of Backgrounds

681 We have assembled in Table 4 the number of observed events and the various backgrounds predicted for $MET \geq$
 682 50 GeV.

683 Therefore, we estimate a MET background ≥ 50 GeV due to QCD and EW sources of 0.53 ± 0.40 and 1.71 ± 0.66
 684 events (depending on whether we use the MET of fake-fake or $Z \rightarrow ee$ events). We combine these two results to
 685 obtain a background estimate of 1.2 ± 0.8 .

686 We observe on $\gamma\gamma$ event with $MET \geq 50$ GeV that contains at least one isolated jet. We show the various event
 687 displays for this event in Fig. 18.

Table 4: The number of events with $MET \geq 50$ GeV from $\gamma\gamma$, fake-fake, and $Z \rightarrow ee$ as well as the total number of background events with $MET \geq 50$ GeV using either the fake-fake events or the $Z \rightarrow ee$ data. The final line gives the number of events or our GGM example predicted for $MET \geq 50$ GeV without or with a K factor of 1.66. We give the numbers with both no jet requirement and a ≥ 1 jet requirement. We display in the final three columns the contributions to the errors of the statistics, the error due to the scaling technique, and the error due to the normalization. The components of the error are quoted for the ≥ 1 jet data sample.

Type	no jet cut	≥ 1 jet	stat error	scaling error	normalization error
$\gamma\gamma$ events	3.0 ± 1.7	1.0 ± 1.0	± 1.0	± 0.0	± 0.0
fake-fake QCD background estimate	0.78 ± 0.44	0.49 ± 0.37	± 0.36	± 0.06	± 0.07
$Z \rightarrow ee$ QCD background estimate	2.62 ± 0.77	1.67 ± 0.64	± 0.46	± 0.38	± 0.23
background from $e\gamma$ evts	0.04 ± 0.20	0.04 ± 0.15	± 0.15	± 0.0	± 0.01
Total Background ≥ 50 GeV (using ff)	0.82 ± 0.49	0.53 ± 0.40			
Total Background ≥ 50 GeV (using ee)	2.66 ± 0.79	1.71 ± 0.66			

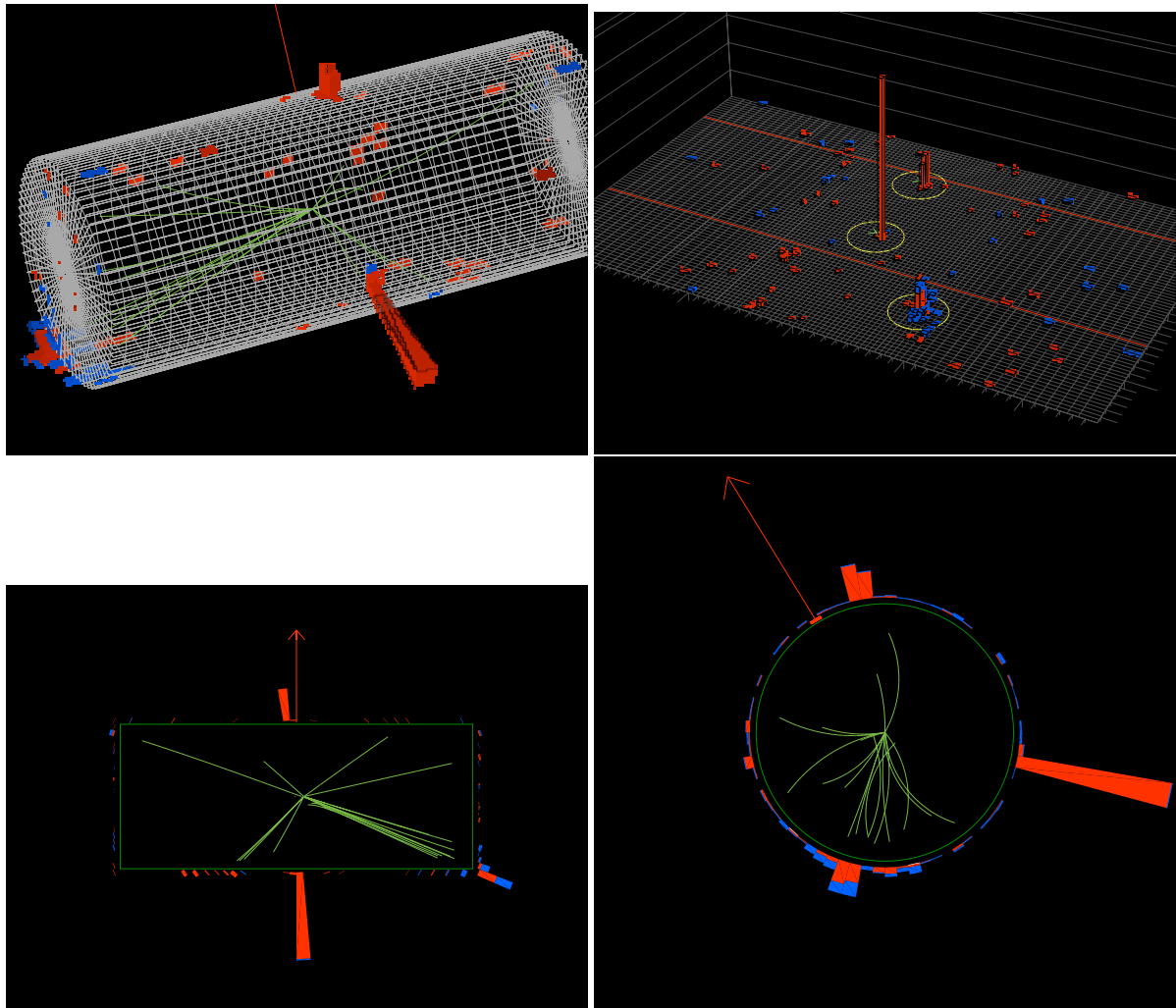


Figure 18: Top Left: the 3D event display of the one observed $MET \geq 50$ GeV event; Top Right: the lego event display of the event; Bottom Left: The rz display of the event; Bottom Right: the xy display of the event.

688 7 Table of Uncertainties

689 The calculation of cross section for observation or for upper limits on SUSY production depend on several param-
 690 eters which we define in Table 5.

Table 5: Critical parameters and errors for determination of SUSY cross sections

Parameter	Value	Total Err.	Stat. Err.	Syst. Err.	
Luminosity (l)	35.5 pb^{-1}	$\pm 3.9 \text{ pb}^{-1}$			
Acceptance (a)	26.8%	± 0.0076	± 0.004	± 0.0065	
Pixel seed veto efficiency	96.64%			$\pm 0.45\%$	
Photon scale factor (ϵ_γ)	1.002	0.0051	0.005	0.001	
Pileup Systematic		1%			
Electron MisID ($MID\epsilon_{elect}$)	1.4%	$\pm 0.4\%$			
Jet Energy Scale		$< 2.0\%$			
Renormalization Scale		13%			
Background (b)	1.71	± 0.66			

691 The acceptance and the efficiencies depend to some extent on the particular point in the space of squark, gluino,
 692 and neutralino masses at which the determination is performed. We give “typical” values in Table 5 for the point
 693 squark, gluino, and neutralino masses of 560, 400, and 150 GeV respectively. The background is that determined
 694 using the $Z \rightarrow ee$ MET spectrum when ≥ 1 jet is required.

695 8 Estimation of Upper Limit Contours for the GGM SUSY

696 8.1 Upper Limits Using the Bayesian Method

697 The outcome of our experiment is potentially the observation of N events in the MET distribution of $\gamma\gamma$ sample \geq
 698 50 GeV above background. The probability distribution of the outcome depends on the GGM cross section σ as
 699 shown below.

$$p(\sigma|N) = \frac{L(N|\sigma)\pi(\sigma)}{\int L(N|\sigma')\pi(\sigma') d\sigma'} \quad (2)$$

700 where $L(N|\sigma)$ is a joint probability distribution function (p.d.f.) for data to observe N events as a function of σ ,
 701 and $\pi(\sigma)$ is the prior p.d.f. that reflects the state of our knowledge about σ . We use

$$\pi(\sigma) = \begin{cases} 0 & \text{if } \sigma < 0 \\ 1 & \text{if } \sigma \geq 0 \end{cases} \quad (3)$$

702 The denominator serves to normalize $p(\sigma|N)$ to unity.

703 The probability distribution for the outcome depends on three parameters: integrated luminosity l , amount of
 704 background b , and the total acceptance times efficiency for the signal ϵ . These parameters are known with limited
 705 accuracy. Each parameter represents a non-negative value and is modeled as a p.d.f. centered about its nominal
 706 value with a standard deviation equal to the parameter error. The joint p.d.f to observe N events can be expressed
 707 as:

$$L(N|\sigma) = \int L(N|\sigma, l, \epsilon, b) \pi(l) \pi(\epsilon) \pi(b) dl d\epsilon db \quad (4)$$

708 where

$$L(N|\sigma, l, \epsilon, b) = \frac{(\sigma l \epsilon + b)^N}{N!} e^{-(\sigma l \epsilon + b)} \quad (5)$$

709 With zero signal candidates observed after all selection cuts, we set a 95% C.L. on the signal cross section as
 follows:

$$0.95 = \int_0^{CL95} p(\sigma|0) d\sigma \quad (6)$$

710 or

$$0.95 = \frac{\int_0^{CL95} e^{-(\sigma l \epsilon + b)} \pi(l) \pi(\epsilon) \pi(b) dl d\epsilon db d\sigma}{\int_0^{\infty} e^{-(\sigma' l \epsilon + b)} \pi(l) \pi(\epsilon) \pi(b) dl d\epsilon db d\sigma'} \quad (7)$$

711 As discussed above, we test Gaussian, log-normal, and gamma shapes for $\pi(b)$, $\pi(l)$, and $\pi(\epsilon)$ as different models
 712 to incorporate uncertainties on the total background rates

713 8.2 Example of an Upper Limit Calculation

714 As an example of this method, we estimate the limit obtained using our *MET* measurements for a particular
 715 choice of the parameters for the GGM SUSY signal.

716 8.2.1 GGM Example Calculations

717 As a first example, we choose a GGM1 point which is not excluded by our measurement. We set $\tan\beta$ to 20, the
 718 squark mass to $800 \text{ GeV}/c^2$, the gluino mass to $1920 \text{ GeV}/c^2$, and the $\tilde{\chi}_1^0$ mass to $150 \text{ GeV}/c^2$. After all selection
 719 criteria are applied, we find a total acceptance time efficiency of $0.2677 \pm 0.0041(\text{stat}) \pm 0.0065(\text{syst})$. The
 720 predicted cross section for GGM given by PYTHIA for these parameters is $(8.8 \pm 0.76) \times 10^{-2}$ (PDF uncertainty)
 721 pb cross section using a K factor of 1.12. This cross section implies an

722 Using the acceptance times efficiency of $0.268 \pm 0.004(\text{stat}) \pm 0.0065(\text{syst})$ for the $\gamma\gamma$ sample with $MET \geq$
 723 50 GeV, we determine 95% CL upper limits shown in Table 6 for our GGM example for our measurement using
 724 the Bayesian method [5] described in section 8.1. We give in Table 6 the upper limits for both the ff and $Z \rightarrow ee$
 725 QCD *MET* backgrounds ≥ 50 GeV for three different choices of background probability distributions (Gaussian,
 726 log-normal, and Gamma).

Table 6: Upper limits for fake-fake and $Z \rightarrow ee$ of QCD backgrounds and background uncertainty distributions

Data sample	Background	Gaussian	log-normal	Gamma
combined backgrounds	1.2 ± 0.8 evts	0.454 pb	0.443 pb	0.437 pb
fake-fake QCD <i>MET</i> background	0.53 ± 0.40 evts	0.477 pb	0.470 pb	0.461 pb
$Z \rightarrow ee$ QCD <i>MET</i> background	1.71 ± 0.66 evts	0.436 pb	0.425 pb	0.422 pb
no backgrounds	0.0 ± 0.0 evts	0.529 pb	0.513 pb	0.512 pb

727 The variation of the result between different models is negligible, and therefore we set an upper limit at the 95%
 728 CL for a GGM cross section of ≤ 0.454 pb for the particular choice of squark, gluino, and neutralino masses for
 729 our example. This particular point has a 0.383 probability at the 95% CL and cannot be excluded.

730 As a second example, we take a point that is excluded by our measurement. We consider the GGM point with the
 731 squark mass $= 720 \text{ GeV}/c^2$, the gluino mass $= 720 \text{ GeV}/c^2$, and the $\tilde{\chi}_1^0$ mass $= 150 \text{ GeV}/c^2$. The leading order signal
 732 cross-section with K factor of 1.45 for this point is 0.712 pb, efficiency time acceptance is $0.218 \pm 0.0041(\text{stat})$
 733 $\pm 0.0054(\text{syst})$, and PDF and scale uncertainties are 18.4% and 13% respectively. The expected number of events
 734 for this point for an integrated luminosity of 35.5 pb^{-1} is 5.5 ± 1.2 events. The upper limits arrived at from this
 735 measurement are 0.557 pb, 0.544 pb, and 0.536 pb for the assumptions of a Gaussian, log-normal, and Gamma
 736 background uncertainty distribution respectively. The variation of the result among different background models
 737 is negligible, and, therefore, we set an upper limit of ≤ 0.544 pb at the 95% CL for the GGM cross section for our
 738 example using the log-normal result. The expected cross section upper limit at the 95% CL that we would expect
 739 from an observation of one event is 0.584 pb. The probability to observe one or zero events with the expected
 740 GGM cross section is 0.016 and, therefore, this point is excluded by our measurement.

741 We have performed similar calculations for the entire squark vs. gluino mass plane from 400 GeV to 2000 GeV
 742 for several neutralino masses. We show in Fig. 19, the variation of the 95% CL upper limits (pb) across the
 743 squark-gluino mass planes for 50, 150 and 500 GeV/c^2 neutralino masses.

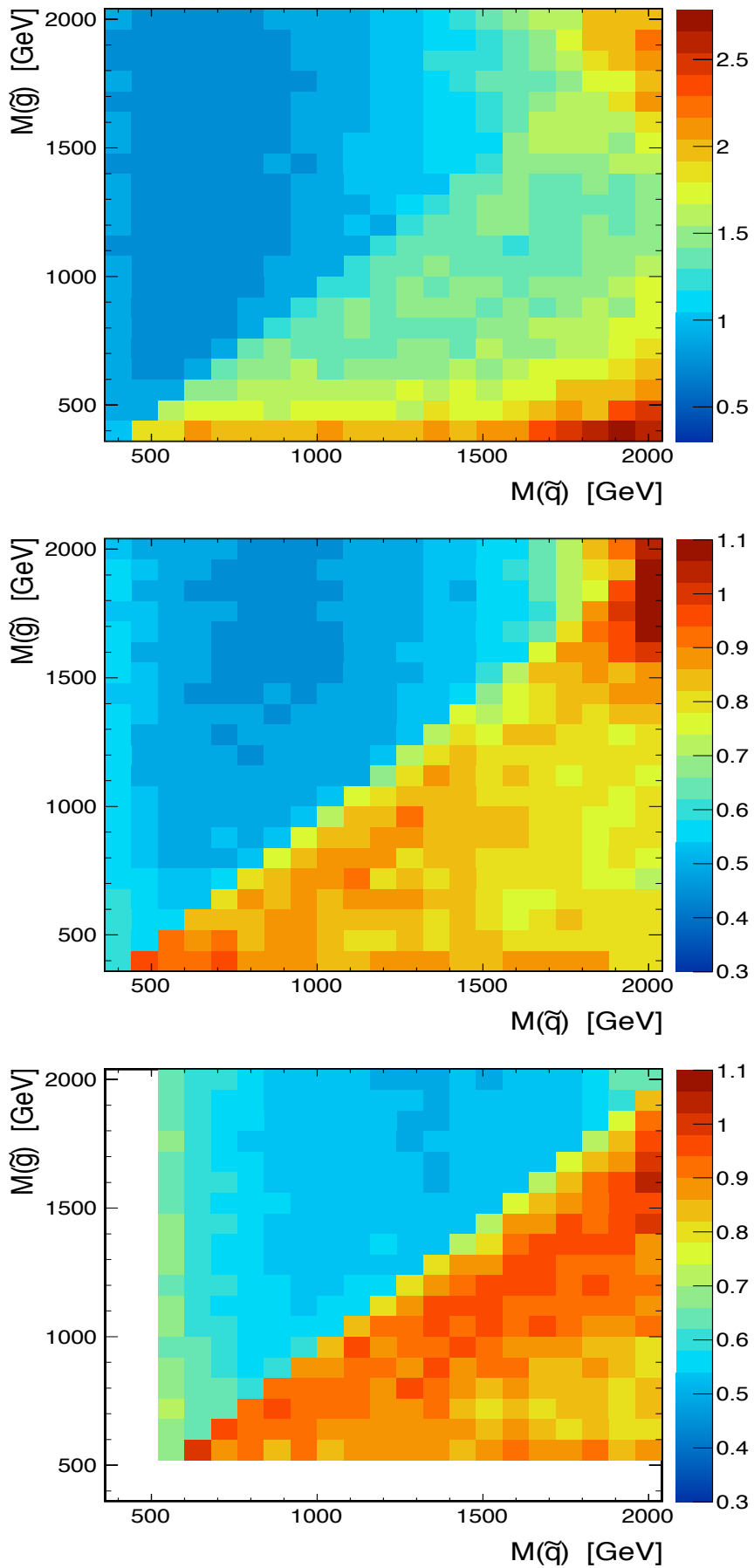


Figure 19: 95% CL upper limits for the squark-gluino mass plane and for Top plot: 50, Middle plot: 150, and Bottom Plot: 500 GeV/c^2 neutralino masses; The units are pb.

744 8.3 Construction of GGM Exclusion Regions

745 We have calculated in the same manner a set of upper limits for a set of GGM SUSY points chosen to cover the
 746 region in gluino-squark mass space from 400 to 2000 GeV for a range of $\tilde{\chi}_1^0$ neutralino masses. The 95% CL upper
 747 limit contours derived for this raster of points is shown in Fig. 23 in the squark-gluino mass plane for the choices
 748 of a 50 GeV $\tilde{\chi}_1^0$ neutralino mass and the PDF's and PDF uncertainties for our 35.5 pb^{-1} measurement.

749 In addition to the factors and errors affecting the determination of upper limits, there are additional factors that
 750 affect the exclusion region that have to do with the calculation of the theoretical cross section. These include
 751 the uncertainty in the Parton Distribution Functions (PDFs). We show in Fig. 20 the variation of cross section
 752 ratios (K factors) between leading order PDFs next to leading order PDF's and in Fig. 21 the uncertainty in the
 753 squark-gluino mass plane of the PDF functions for a particular choice of PDF [6].

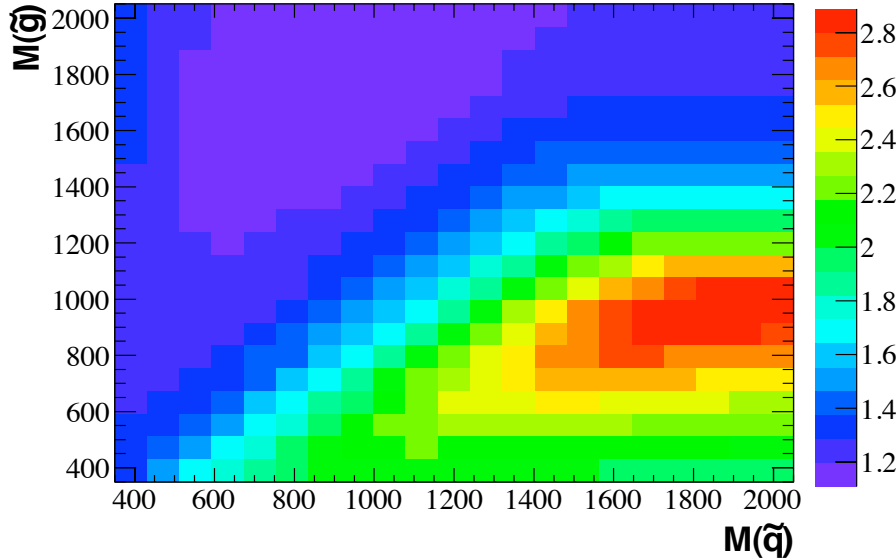


Figure 20: K factor ratio as a function of squark-gluino masses

754 The PDFs and associated uncertainties are the result of use of the prescription for generating PDFs recommended
 755 by the PDF4LHC. The cross sections as a function of squark and gluino mass is shown in Fig. 22.

756 Using these plots together with the variation of acceptance vs. squark and gluino masses, construct exclusions
 757 regions determined for our measurement.

758 9 Summary

759 In summary, we have searched for evidence of GGM SUSY in diphoton plus single jet events in the MET spectrum
 760 beyond 50 GeV in an early data set with an integrated luminosity of 35.5 pb^{-1} . We find no evidence of GGM SUSY
 761 production and have set upper limits for a range of parameters for the GGM SUSY. We have defined exclusion
 762 regions in GGM SUSY parameter space of squark, gluino and neutralino mass at the level of 0.5 to 1.0 pb cross
 763 section.

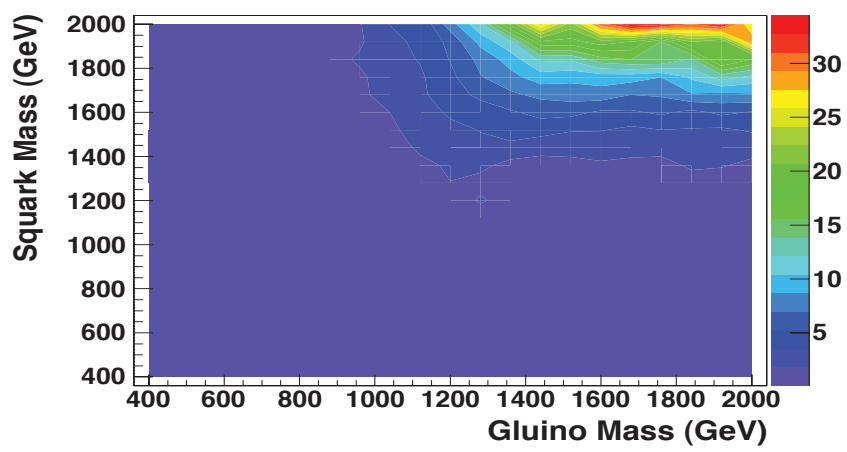
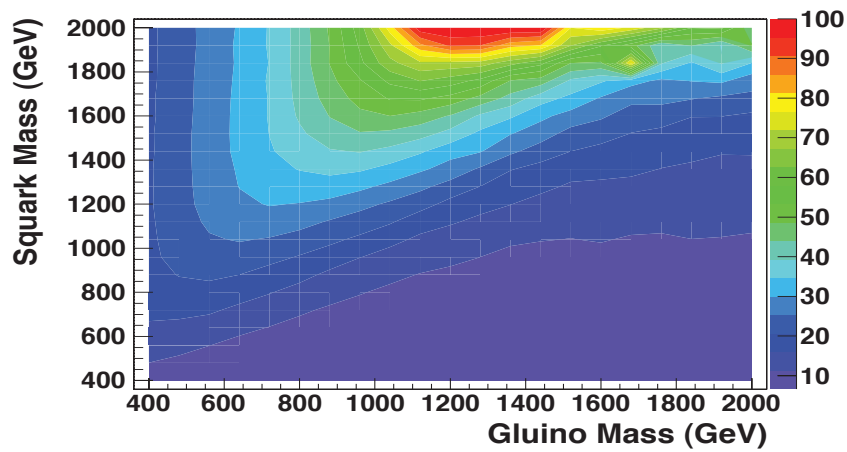


Figure 21: Top: PDF uncertainties as a function of squark-gluino masses; Bottom: Acceptance uncertainties

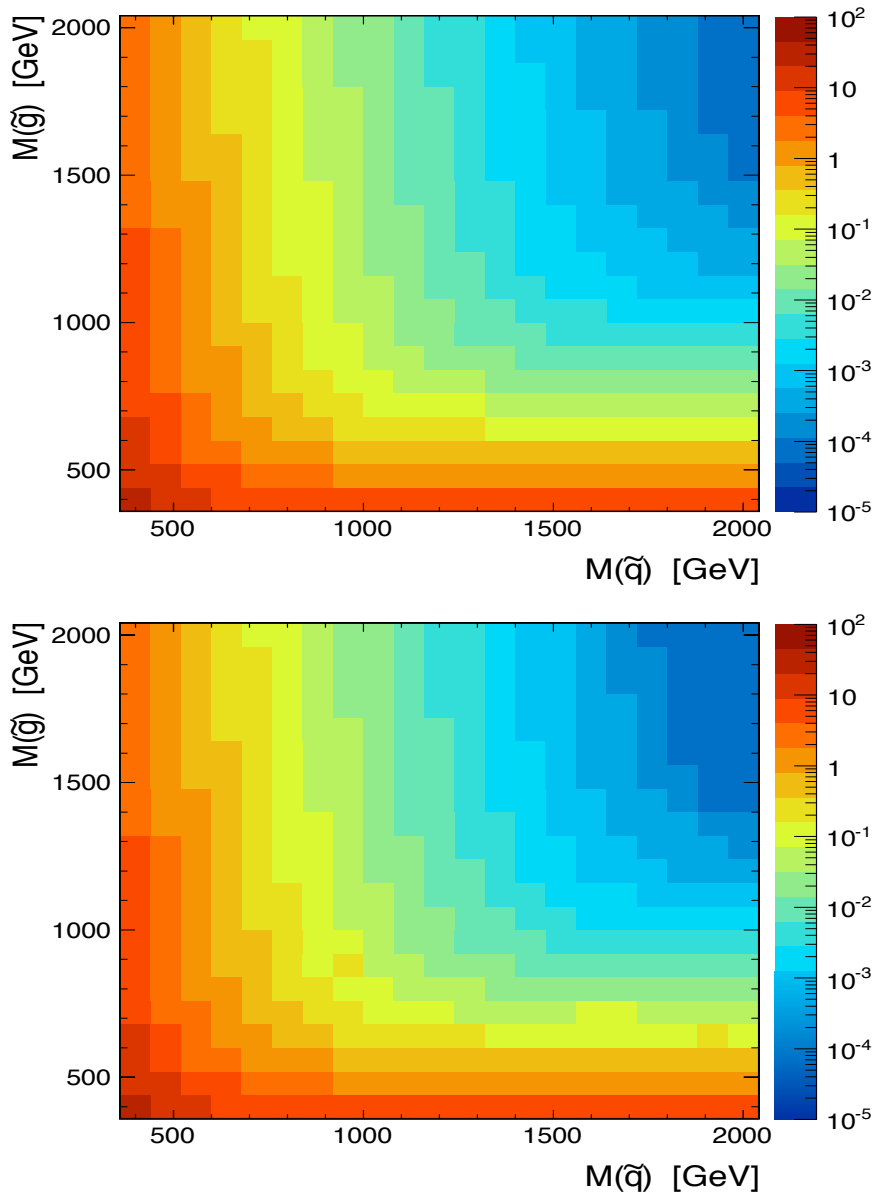


Figure 22: Cross sections for GGM production as a function of squark and gluino masses with a neutralino mass of Top: 50 GeV/c², Bottom: 150 GeV/c²; The units are pb.

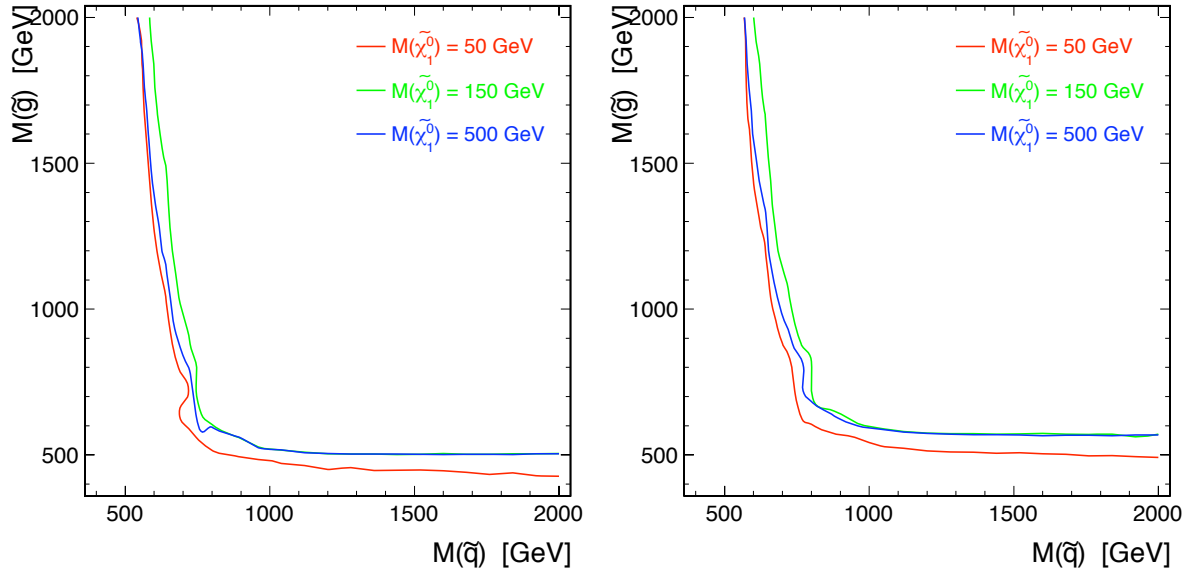


Figure 23: Exclusion contours in the squark-gluino mass plane for 50, 150, and 500 GeV/c^2 neutralino masses for GGM SUSY: Left: without K factors; Right: with K factors.

765 Several studies have been done to investigate both data and MC aspects of the analyses covered above in the body
 766 of this note. We give additional plots from these studies in this appendix.

767 A Breakdown of Various Effects on Signal Acceptance

768 There are several steps in the obtaining the final $\gamma\gamma$ signal sample, each of which has some effect on the acceptance.
 769 We use our signal MC to study each step and the attendant loss of acceptance for the selection. The results are shown
 770 in Fig. 24 for a particular point in the squark-gluino-neutralino mass space of squark mass = 880 GeV/c², gluino
 771 mass = 560 GeV/c², and neutralino mass = 500 GeV/c². As shown in Fig. 24 as a function of the number of quarks
 772 and gluons from GGM SUSY decays, first step in obtaining a signal $\gamma\gamma$ sample is the requirement that the MC
 773 contains two generator photons with $p_T \geq 30$ GeV/c and $|\eta| \leq 1.38$. An efficiency of approximately 65% is
 774 obtained essentially flat with number of partons from SUSY decays. Asking that these photons be reconstructed
 775 makes essentially no difference. When we ask that photons pass the photon ID cuts that are listed in the body of
 776 AN271, the efficiency essentially drops to between 40-50% for at the low end of the parton from SUSY number
 777 spectrum and then decreases with increasing parton number due to the increasing probability of overlaps of the
 778 partons with the photons. Subsequent requirements of at least one jet separated from all photons in the event and
 779 additional photon selection requirements make almost no difference. Fig. 24 also shows the distribution of the
 780 multiplicity of partons from SUSY which peaks at 4 for this point in squark-gluino-neutralino mass space.

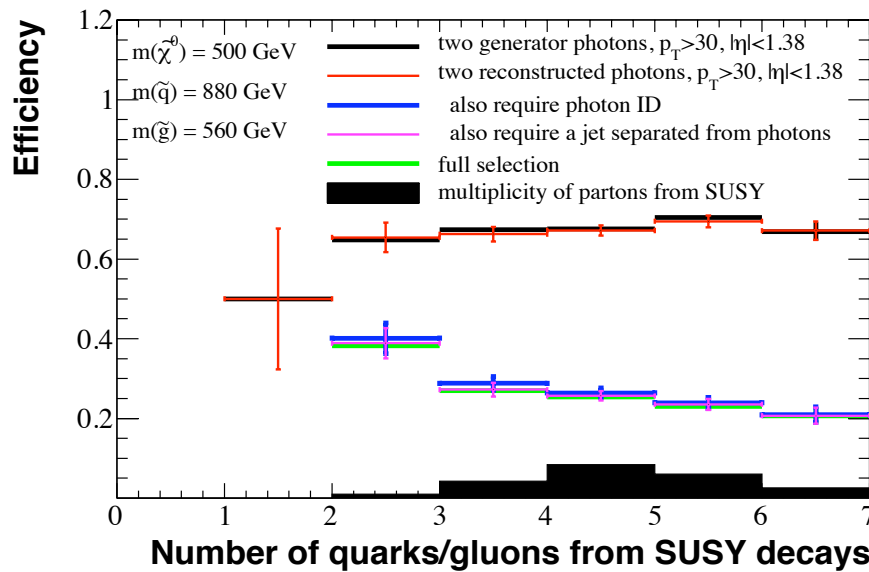


Figure 24: Breakdown of factors in determining the acceptance for $\gamma\gamma$ events due to SUSY

781 The most significant factor in the determining the level of the acceptance for accepting $\gamma\gamma$ events is the E_T cuts on
 782 the lead and trail photons. Both are subject to a cut $E_T \geq 30$ GeV. We plot in Fig. 25 the E_T distribution for the
 783 lead and trail photons before the E_T for the squark-gluino mass point of 880 and 560 GeV/c² respectively for two
 784 neutralino masses, 50 and 500 GeV/c². The E_T cut at 30 GeV on the lead and trail photons are much more severe
 785 for the lower mass than for the higher mass neutralino.

786 Finally, we show in Fig. 26 that the η distributions for photons from the quite different neutralino masses of 50 and
 787 500 GeV/c² are essentially identical and therefore the η requirement of ≤ 1.36 produces almost no difference in
 788 acceptances for photons from states with very different mass neutralinos.

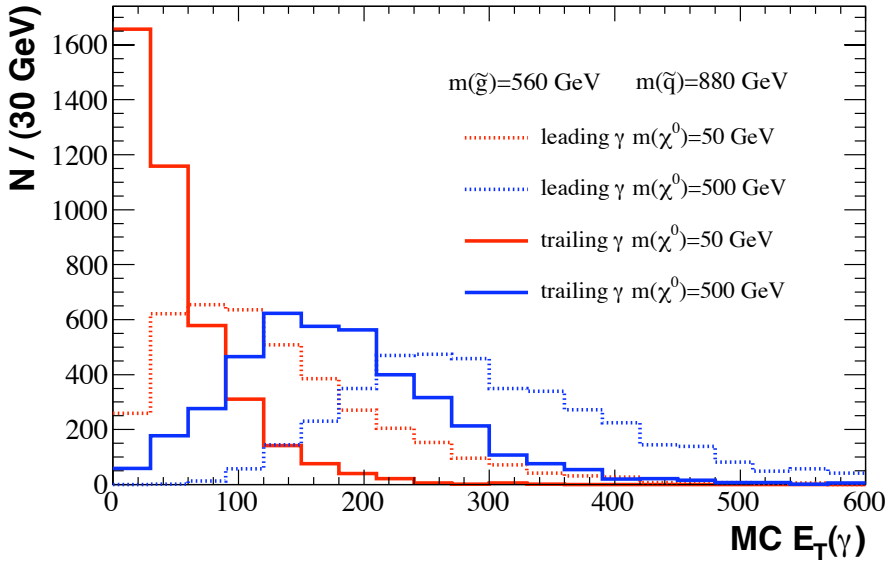


Figure 25: Distribution of E_T for the lead and trail photons from 50 and 150 GeV/c^2 neutralinos from squark-gluino mass states of 880 and 560 GeV/c^2 respectively

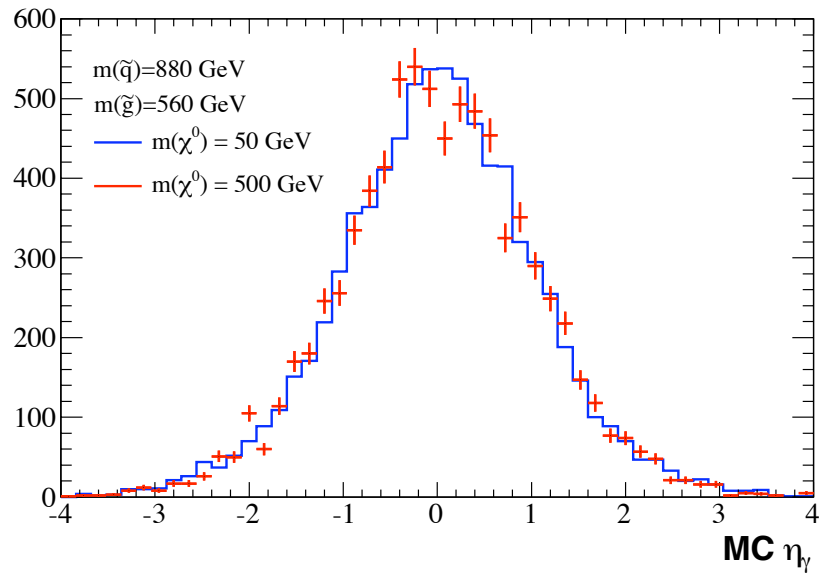


Figure 26: η distributions for photons from 50 and 500 GeV/c^2 neutralino decays

789 B Effect of Loosening the Tight Photon Analysis Requirement

790 Our tight photon requirements are imposed to eliminate QCD backgrounds. To check the effect of requiring a loose
 791 analysis cut on the lead photons. The loose cut differs from the tight cut by a relaxed $\sigma_{inj\eta}$ cut and a tightening of
 792 the track isolation cut as shown below:

- 793 • E_T of the tracks in the track isolation cone $< 0.001 * E_T + 2.0 \text{ GeV}$ tightened to $< 0.001 * E_T + 3.5 \text{ GeV}$;
 794 • $\sigma_{inj\eta} < 0.013$ dropped;

795 The $\sigma_{inj\eta}$ criterion is the most problematic although from Fig. 27, the $Z \rightarrow ee$ and fake fake samples are very
 796 different and would suggest that loosening this cut is not productive.

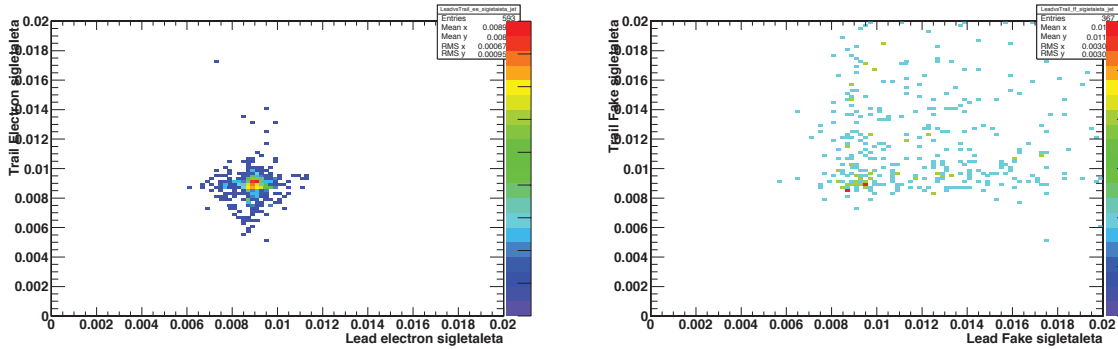


Figure 27: Left: $\sigma_{inj\eta}$ plot of lead vs. trail electron for the $Z \rightarrow ee$ sample; Right: same for the fake-fake QCD sample.

797 Since our $\gamma\gamma$ candidate events have very much the same $\sigma_{inj\eta}$ distributions for the lead and trail photons as the lead
 798 and trail electrons from the $Z \rightarrow ee$ events as shown in Fig. 28, we expect that we will gain background at the
 799 expense of gaining few extra signal events if we loosen the photon cuts.

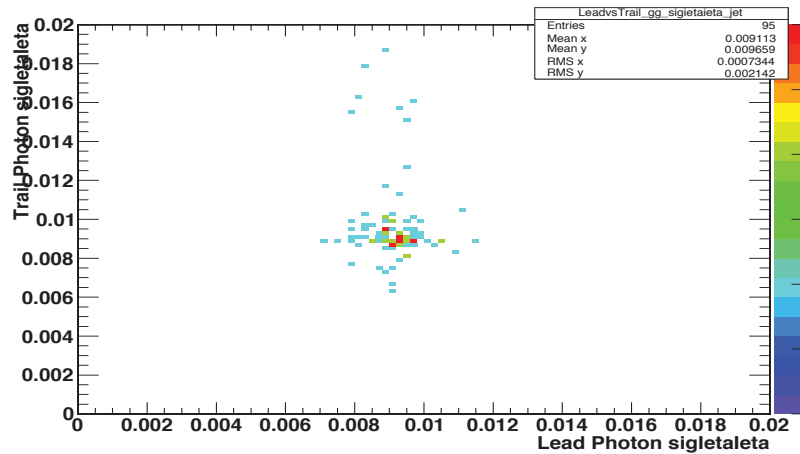


Figure 28: $\sigma_{inj\eta}$ plot of lead vs. trail γ candidate for the $\gamma\gamma$ candidate sample.

800 We quantify this assertion by using three different samples, the $\gamma\gamma$ candidates, the fake-fake events, and the
 801 $Z \rightarrow ee$ events to determine the composition of our $\gamma\gamma$ sample. We then see how this composition changes by

802 going to a loose photon definition.

803 Under the assumptions that the $Z \rightarrow ee$ sample is completely dominated by Z production and has no backgrounds,
 804 the fake-fake events are completely QCD and the efficiency for the $\sigma_{inj\eta}$ cut is the same for photons and electrons,
 805 then we can write for N_Z , the number of Z decays

- 806 • $N_{\gamma\gamma} = \epsilon_1 \epsilon_2 N_Z$
- 807 • $N_{\gamma fake} = \epsilon_1 (1 - \epsilon_2) N_Z$
- 808 • $N_{fake\gamma} = (1 - \epsilon_1) \epsilon_2 N_Z$
- 809 • $N_{fakefake} = (1 - \epsilon_1)(1 - \epsilon_2) N_Z$

810 where ϵ_1 and ϵ_2 are the efficiencies for the lead and trail electrons to pass whatever photon cuts we impose. Here
 811 the N's represent the number of events passing or failing the photon cuts as the case may be in the Z sample. These
 812 equations are then solved for the ϵ s.

813 Similar equations can be written for the fake-fake sample:

- 814 • $N_{\gamma\gamma} = f_1 f_2 N_{ff}$
- 815 • $N_{\gamma fake} = f_1 (1 - f_2) N_{ff}$
- 816 • $N_{fake\gamma} = (1 - f_1) f_2 N_{ff}$
- 817 • $N_{fakefake} = (1 - f_1)(1 - f_2) N_{ff}$

818 where f_1 and f_2 are the probabilities for helead and trail objects to pass the photon cuts.

819 Now overall our samples of $\gamma\gamma$, fake-fake, fake- γ and γ -fake are given by

- 820 • $N_{\gamma\gamma} = \epsilon_1 \epsilon_2 N_{\gamma\gamma} + \epsilon_1 f_2 N_{\gamma f} + f_1 \epsilon_2 N_{f\gamma} + f_1 f_2 N_{ff}$
- 821 • $N_{\gamma f} = \epsilon_1 (1 - \epsilon_2) N_{\gamma\gamma} + \epsilon_1 (1 - f_2) N_{\gamma f} + f_1 (1 - \epsilon_2) N_{f\gamma} + f_1 (1 - f_2) N_{ff}$
- 822 • $N_{f\gamma} = (1 - \epsilon_1) \epsilon_2 N_{\gamma\gamma} + (1 - \epsilon_1) f_2 N_{\gamma f} + (1 - f_1) \epsilon_2 N_{f\gamma} + (1 - f_1) f_2 N_{ff}$
- 823 • $N_{ff} = (1 - \epsilon_1)(1 - \epsilon_2) N_{\gamma\gamma} + (1 - \epsilon_1)(1 - f_2) N_{\gamma f} + (1 - f_1)(1 - \epsilon_2) N_{f\gamma} + (1 - f_1)(1 - f_2) N_{ff}$

824 which when taken with the equations above give us a system of four equations and four unknowns. We solve these
 825 equations to give us the composition of the $N_{\gamma\gamma}$ sample for any set of criteria that we impose.

826 Comparing the loose photon to the tight photon cut criteria compositions of $N_{\gamma\gamma}$ sample we show in Table 7

Table 7: Composition of $N_{\gamma\gamma}$ candidates for loose and tight photon cuts

Photon Cuts	$\gamma\gamma$ %	γ -fake %	fake-fake
Tight-Tight	81.0%	19.0%	0 %
Tight-Loose	74.6%	25.4%	0 %

827 C Study of ΔR Criterion for Proximity of Isolated Jets to γ Candidates

828 We show in Fig. 29a scatterplot for jets in $\gamma\gamma$ data events of ΔR between the jets and the leading photon vs. the
 829 ΔR between the jets and the trailing photon for before applying the ΔR criteria. The $\Delta R \geq 0.9$ region is shown.
 830 The clustering of events in ΔR on the respective axes, will most likely fail the ECAL and HCAL isolation cuts
 831 and the events above the ΔR will by and large survive to the final data sample. The criteria for accepting an event
 832 is that at least one jet in the event is at a distance greater than $R=0.9$ from the lead and trail photons in the event.

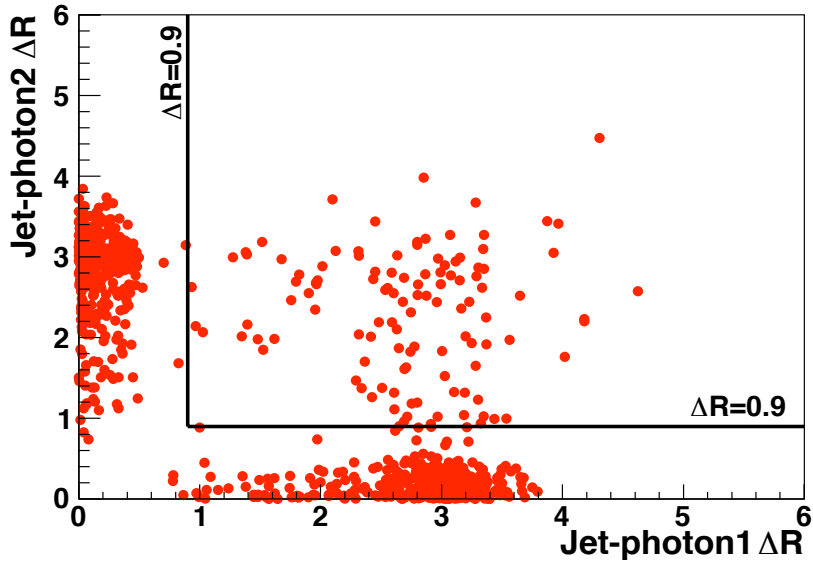


Figure 29: Scatterplot of ΔR between jets and the leading photon vs. the ΔR between the jets and the trailing photon for $\gamma\gamma$ data events before applying the ΔR criteria.

833 The question of how close an isolated jet can be to one of our photon candidates without affecting acceptance
 834 is a complicated one. The question of how much loss is experienced in our signal modes when we demand at
 835 least one isolated jets that is separated by ΔR greater than 0.9 from both the lead and trail photon, could affect
 836 our acceptance for GGM events which have multiple jets associated with them. Accordingly in this section we
 837 investigate the relationship between the ΔR criterion and the loss of efficiency for GGM signal as a function of
 838 the number of jets in the events. We have looked at the relationship for every one of the regions in the squark vs.
 839 gluino mass plane using our GGM signal Monte Carlos.

840 We show in Figs. 30 the relationship of efficiency for the the ΔR cut for a typical region (squark mass= 640 GeV,
 841 gluino mass= 640 GeV, neutralino mass =150 GeV).

842 As can be seen, as the number of jets in the events increases, the average distance of the closest jet to the lead
 843 photon will decrease. This will unavoidably cause a lower efficiency regardless of our choice for an isolation cut
 844 since, as also can be seen, the HCAL and ECAL isolation cuts will begin to cause the photon to fail. The efficiency
 845 to go to zero by $\Delta R = 0.5$. If no jet proximity cut is imposed then the question of how corrupted the photon is by
 846 the proximity of the jet comes into play.

847 A simple way to look at the effect of the ΔR requirement of at least one jet with $\Delta R \geq 0.9$ in the event is to simply
 848 plot the acceptance of the GGM signal for a typical point in the squark-gluino mass plane as a function of the
 849 number of jets in the events with and without the $\Delta R \geq 0.9$ requirement. This plot is given in Fig. 31 for a typical
 850 point, squark mass = $640 \text{ GeV}/c^2$, gluino mass = $640 \text{ GeV}/c^2$, and neutralino mass = $150 \text{ GeV}/c^2$. As can be seen,
 851 there is almost no difference in acceptance caused by imposition of the ΔR requirement.

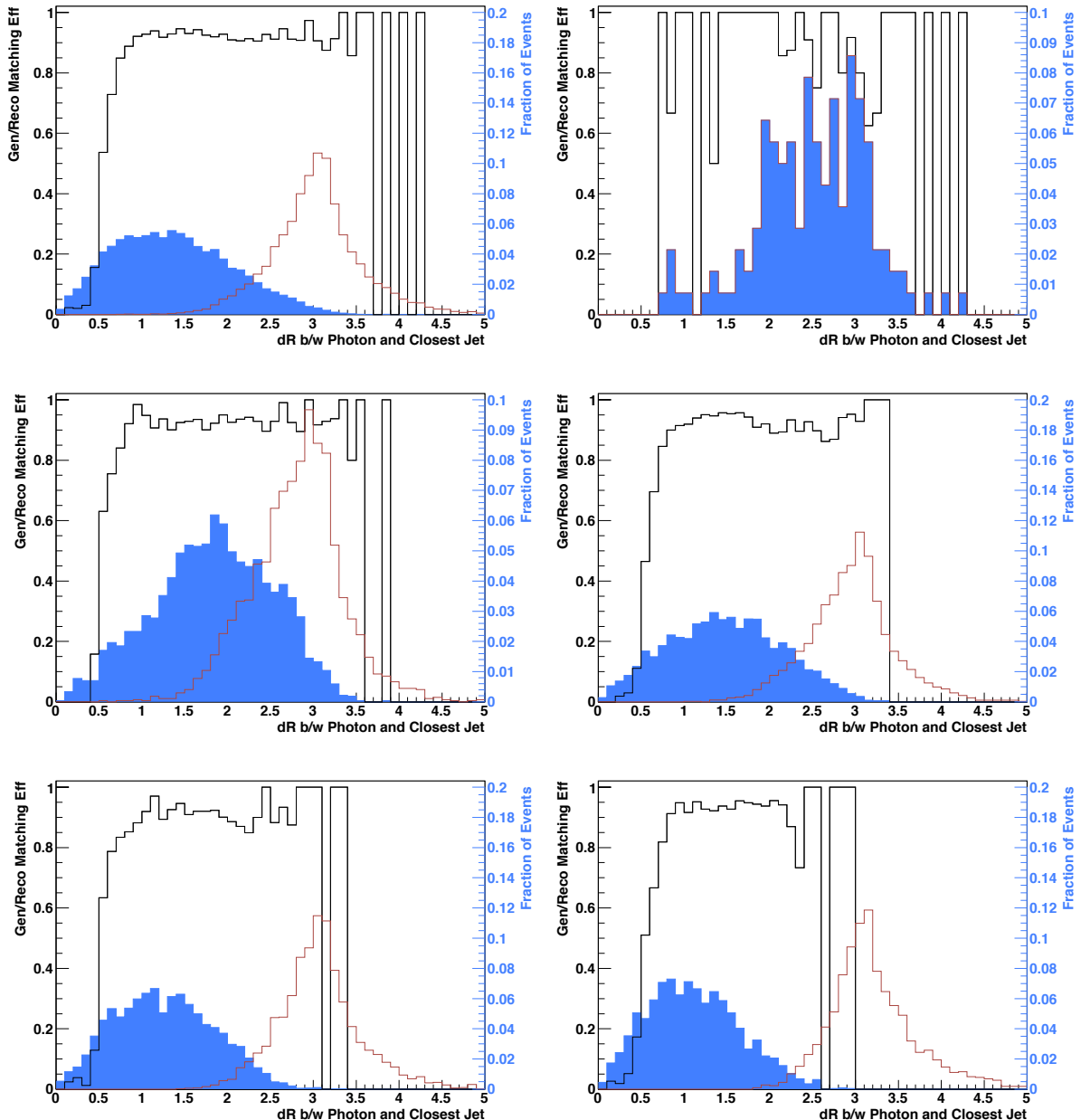


Figure 30: In each plot the black histogram is the efficiency, the blue solid histogram is the fraction of events as a function of ΔR of the closest jet, and the red histogram is the plot of the distance of the most distant jet from the lead photon. Each plot is made for events with different numbers of jets; 1st Row Left: $N_{jets}=1$; 1st Row Right: $N_{jets}=2$; 2nd Row Left: $N_{jets}=3$; 2nd Row Right: $N_{jets}=4$; 3rd Row Left: $N_{jets}=5$; 3rd Row Right: $N_{jets}=6$.

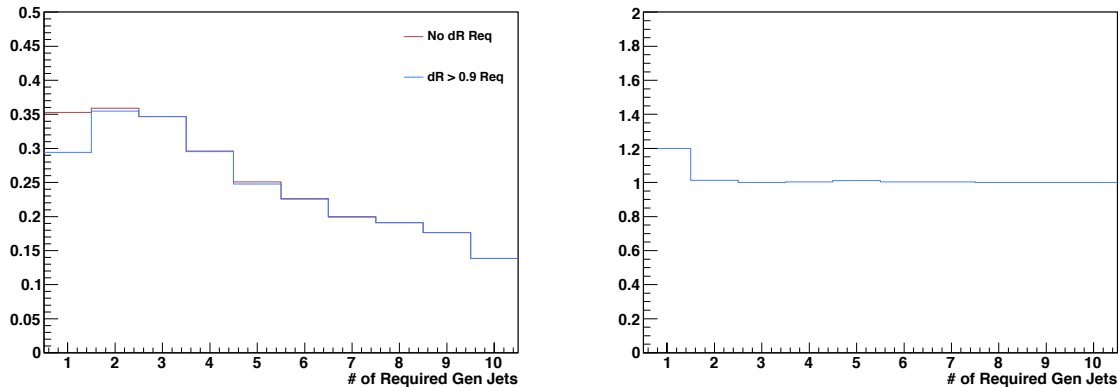


Figure 31: Left: Acceptance for GGM singal events with and without the ΔR requirement of at least one jet with $\Delta R \geq 0.9$ as a function of the number of jets in the events; Right: Ratio of acceptances without to the acceptances with the $\Delta R \geq 0.9$ requirement. The GGM point used is squark mass = $640 \text{ GeV}/c^2$, gluino mass = $640 \text{ GeV}/c^2$, and neutralino mass = $150 \text{ GeV}/c^2$.

D Effect of Number of Jets on Acceptances

We show in Fig. 32 the average number of jets in each region of the squark-gluino mass plane for the GGM SUSY model. The number of jets in each region results in the acceptance times efficiency variation shown in Fig. 33. The regions of highest jet density obviously have the lowest acceptance times efficiency because of the jet/photon overlaps which causes the photons to be lost because of failing the ECAL and HCAL isolation criteria.

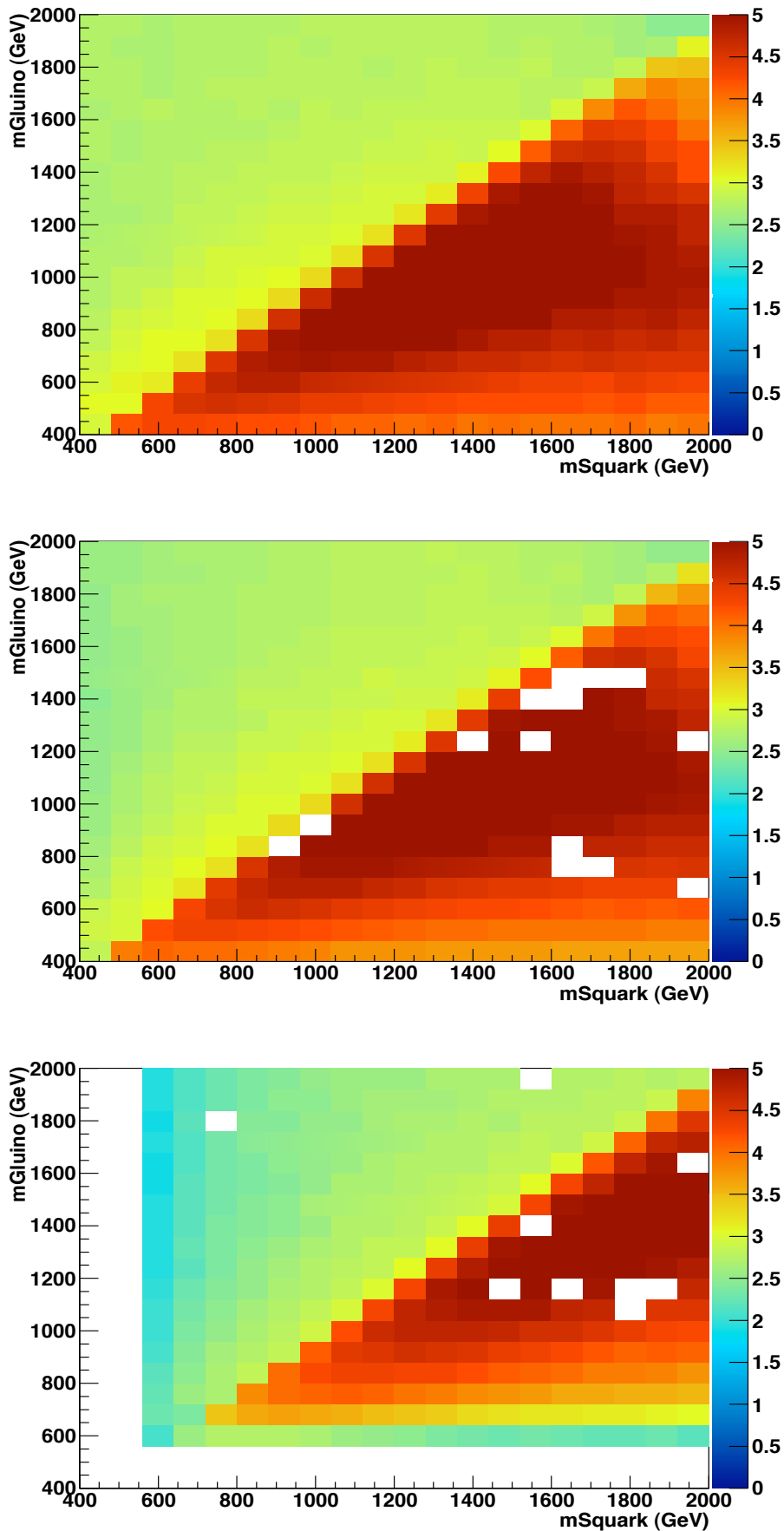


Figure 32: Number of jets in the event vs. squark-gluino masses for Top: 50, Middle: 150, and Bottom: 500 GeV/c² neutralino masses.

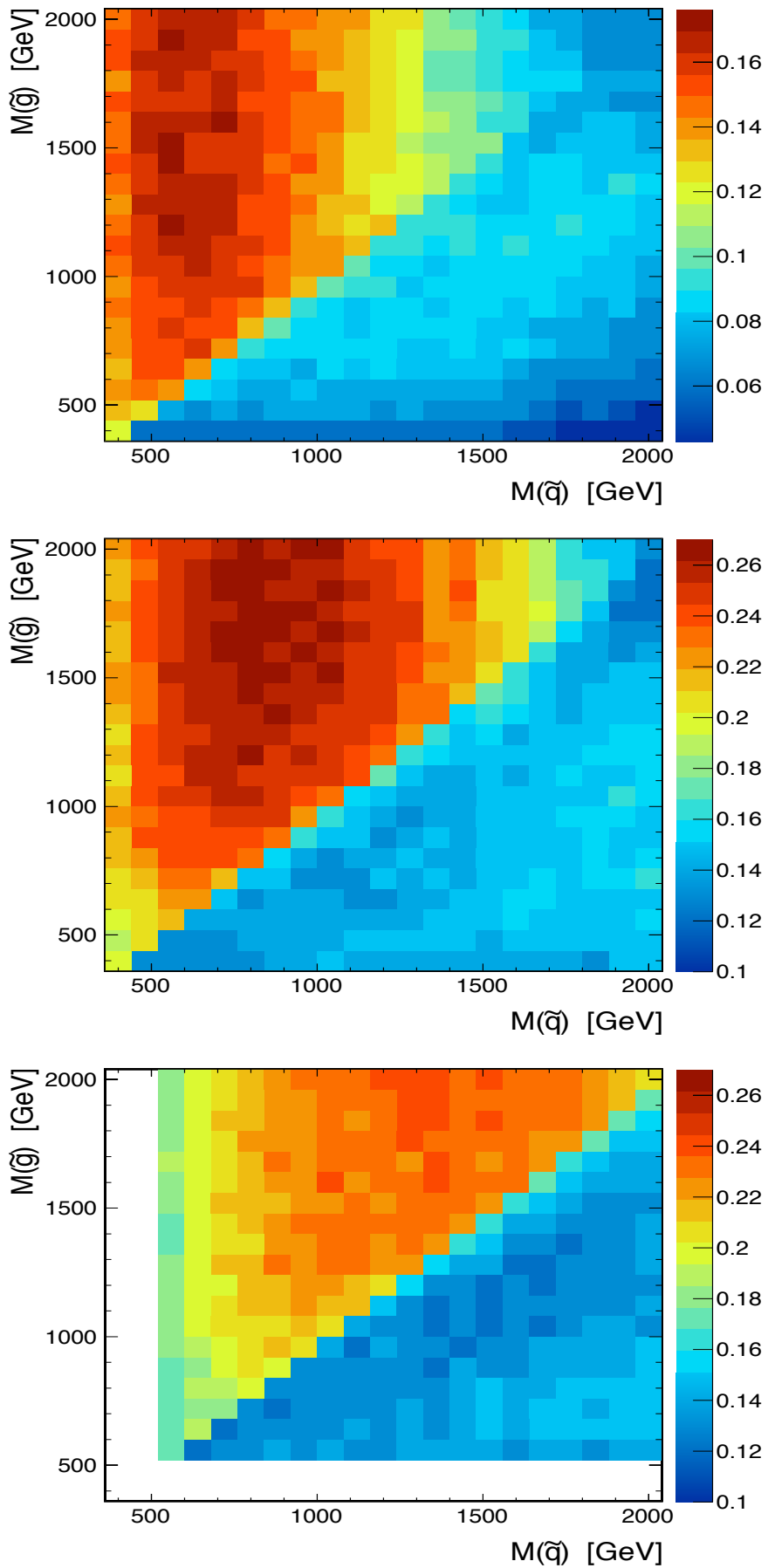


Figure 33: Acceptance times efficiency vs. squark-gluino mass with Top plot: 50, Middle plot: 150, and Bottom plot: 500 GeV neutralino masses.

857 E Comparison of TcMET and PfMET

858 The analysis of *MET* in diphoton events has been done using TcMET. We compare in Fig. 34 TcMET to PfMET
 859 for our $\gamma\gamma$ events to see if there are striking differences in the two *METs*. As can be seen, the two different
 860 *METs* show are reasonably correlated as much as can be determined for this level of statistics.

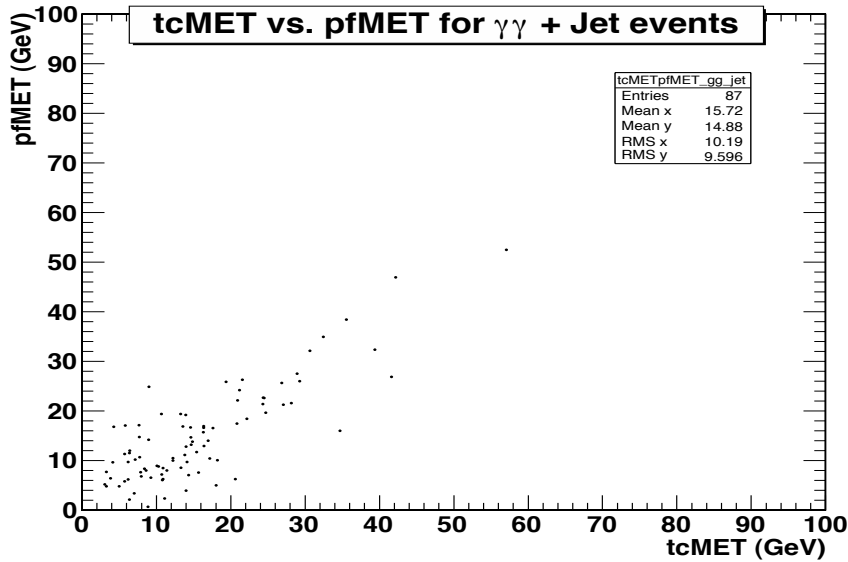


Figure 34: TcMET vs. PfMET for $\gamma\gamma$ data events.

861 Continuing to compare the *MET* distributions arrived at by use of different types of jets, we compare the MET
 862 distribution from our $\gamma\gamma$ plus jets events obtained for a large subset of our existing data (27.3 pb^{-1}) where the
 863 jet selection was based on use of particle flow jets. The corresponding “Loose 09 jet” jet ID requirements were
 864 applied for each type of jet since particle flow jets have different jet ID requirements than jet plus track (JPT) jets.
 865 Fig. 35 compares the *MET* distributions for three cases:

- 866 1. track corrected *MET* for $\gamma\gamma$ events with a 30 GeV JPT jet required (shown in black).
- 867 2. track corrected *MET* for $\gamma\gamma$ events with a 30 GeV particle flow jet selected (shown in blue).
- 868 3. particle flow *MET* for $\gamma\gamma$ events with a 30 GeV particle flow jet selected (shown in red).

869 In all three cases the requirement imposed on the two photons are the same as those used in the rest of the analysis.
 870 As can be seen, there are only minor differences among the three spectra and the event above 50 GeV is the same
 871 event In all cases.

872 F Pixel Seed Veto Systematics

873 We depend on the presence of a pixel seed to help distinguish between an electron and a photons so it is important
 874 to determine the efficiency of the veto and its uncertainty. The origin of the uncertainty in the pixel veto uncertainty
 875 is in the uncertainty of the geometry of the pixel itself. We determine the pixel inefficiency using a MC simulation
 876 of response of the pixel for the nominal thickness and the extremes X0min and X0max of the pixel geometry.
 877 The mean and RMS of the obtained inefficiencies is $3.36 \pm 0.45\%$ (i.e. a 96.65% average efficiency with a 0.5%
 878 uncertainty). So the systematic uncertainty in the veto inefficiency is taken to be 0.5% for one photon or 1% for
 879 two.

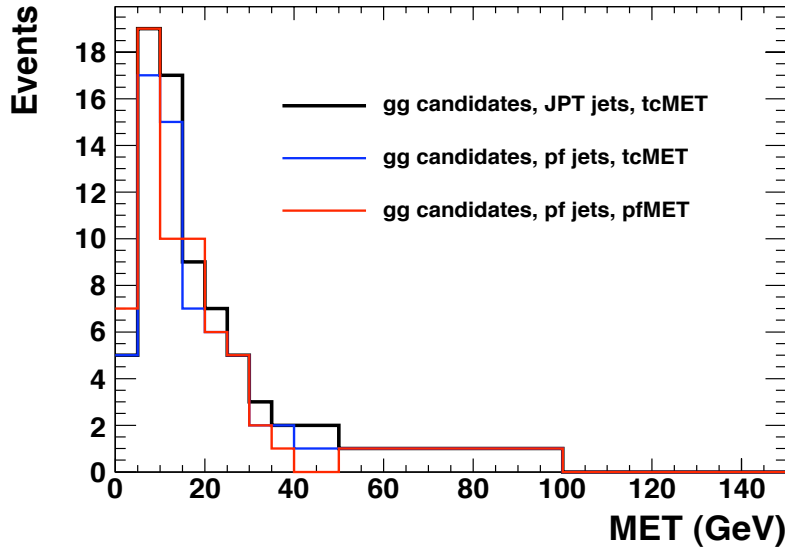


Figure 35: Track corrected MET for $\gamma\gamma$ events with a 30 GeV JPT jet required (shown in black); Track corrected MET for $\gamma\gamma$ events with a 30 GeV particle flow jet selected (shown in blue); particle flow MET for $\gamma\gamma$ events with a 30 GeV particle flow jet selected (shown in red).

880 G Comparison of Lead Jet η Distributions for $\gamma\gamma, Z \rightarrow ee$, QCD fake- 881 fake, and GGM Event Samples

882 We display the leading jet η distributions of our various data samples after all cuts including the isolation cuts
883 in comparison to the GGM signal events to answer two questions. Do our cuts (isolation cut in particular) force
884 our jets into the ECAL endcaps and does our signal difference dramatically from our $\gamma\gamma$ candidate jet distribution
885 significantly? As can be seen, in Figs. 36, the answer to both of those questions is no.

886 The distribution of the various data samples and the GGM MC lead jets is quite similar. There is no evidence for
887 the cuts forcing the jets to be preferentially in the end caps. Various GGM points and been checked the conclusions
888 remain the same.

889 H Use of TCjets vs. PFjets

890 The question of what jets to use in the analysis was raised. The analysis has been done to date using TCjets and
891 to redo it at this stage use PFjets would require using the complete ensemble of physics objects constructed with
892 particle flow. Instead we compare in Table 8 the TCjet and PFjet results for the highest three jets in the one $\gamma\gamma$
893 event with $MET \geq 50$ GeV (shown in Fig. 18 to show that the two different jet construction techniques give
894 comparable results.

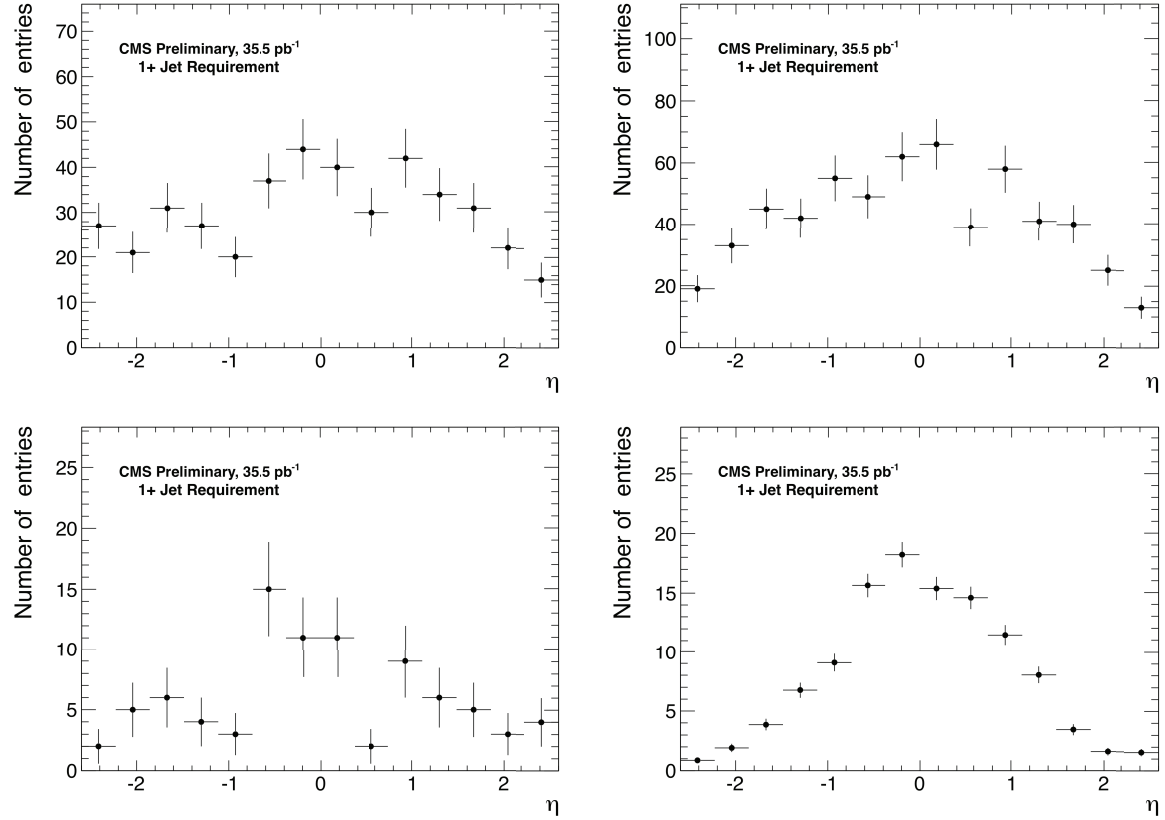


Figure 36: Top left: Lead jet η for QCD events; Top right: lead jet η for Z events; Bottom left Lead jet η for $\gamma\gamma$ events; Bottom right: Lead jet η for GGM example point.

Table 8: Comparison of TCjet and PFjet Content of Event with $MET \geq 50$ GeV

Jets	TCjet	PFjet
Jet 1		
E_T	51.8 GeV	49.0 GeV
η	1.633	1.628
ϕ	-1.881	-1.911
Jet 2		
E_T	13.3 GeV	10.2 GeV
η	-0.927	-1.065
ϕ	-1.489	-1.511
Jet 3		
E_T	9.8 GeV	9.1 GeV
η	-0.957	-0.924
ϕ	-3.016	-3.006

I Comparison of QCD MET Spectra from ff and $Z \rightarrow ee$ Events

We have two different methods to determine the QCD MET spectrum form the data, either using the fake-fake or the $Z \rightarrow ee$ MET distributions. The question is how well do these MET distributions agree. We normalize the two distributions to each other as shown in Fig. 37 in order to perform the comparison. The top plots shows the two distributions overlaid with each other. The bottom plots shows the ratio of the distributions with the error including the normalization error. A KS test yields a value of 0.58 for agreement of the two spectra in the top plot. The χ^2 per degree of freedom is 1.27 for agreement of the two spectra.

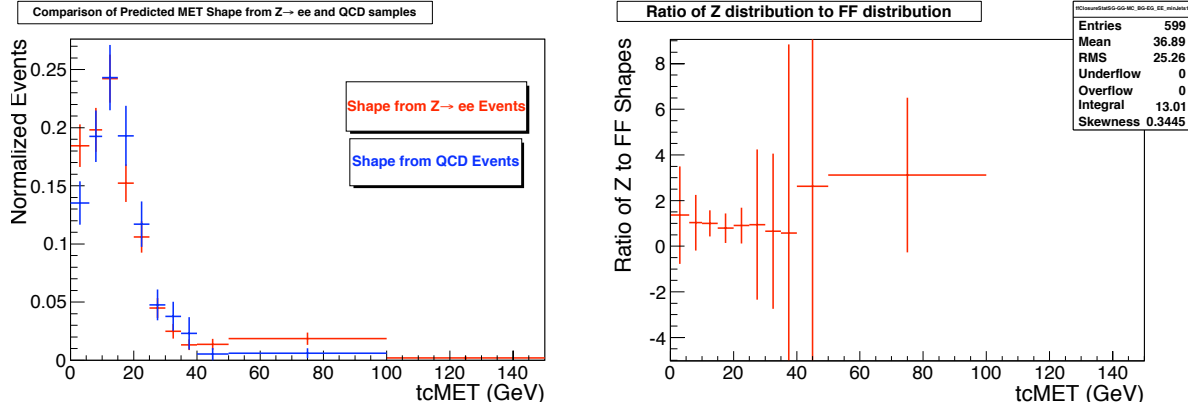


Figure 37: Left: The fake-fake and $Z \rightarrow ee$ MET distributions normalized to each other for comparison; Right: Ratio of QCD MET distribution from $Z \rightarrow ee$ data to QCD MET from fake-fake events.

902 J Check of Effects of Use of Corrected Jets in TcMET

903 We check that the use of JEC corrected jets in TcMET (which otherwise uses uncorrected jets) does not change
 904 our data samples appreciably. We extract the uncorrected jets p_T from TcMET and replace them with the p_T of
 905 JEC corrected jets. We then compare, as shown in Fig. 38, the TcMET distribution in our $\gamma\gamma$ events determined
 906 using uncorrected jets compared to the same spectrum using corrected jets. As can be seen, within errors, the
 907 two spectra agree.

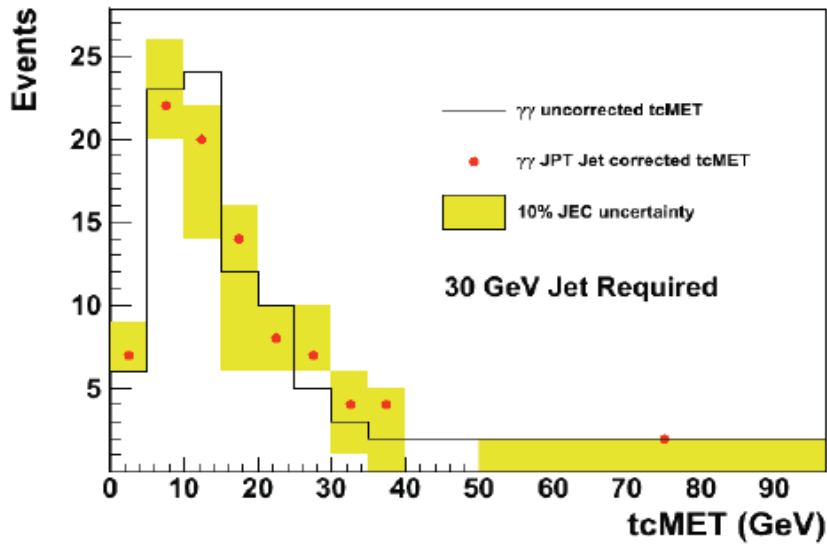


Figure 38: TcMET in $\gamma\gamma$ events with uncorrected jets (histogram) compared to $\gamma\gamma$ TcMET using corrected jets (dots). The bands are the 10% uncertainties due to JEC uncertainties.

908 K Effect of Overcleaning on the GGM Signal

909 In order to ascertain the effect of possible loss of photons and an accompanying shift of MET below the ≥ 50
 910 GeV signal region due to overcleaning, we study the effect on a representative set of GGM MC points. We show in
 911 Fig. 39 the effect on the MET of doing the most severe overcleaning, i.e. losing the lead photon in the GGM MC,
 912 for various representative SUSY points. We compare in all the plots the normal and overcleaned MET spectra for
 913 the $\gamma\gamma$ candidates.

914 As can be seen from the plots, the percentage of GGM events at the various points that were checked that migrated
 915 below the $MET=50$ GeV threshold for the “signal” region is very small in all cases. Indeed, in some cases the
 916 GGM signal event actually migrated above the 50 GeV cutoff. The conclusion is that we expect minimal loss of
 917 signal due to overcleaning.

918 In addition, we check in a sample data that have had the overcleaning problem corrected to see how many $\gamma\gamma$
 919 events that we gain in the properly cleaned data sample. We gain one event above the 300 that we already in the
 920 overcleaned sample.

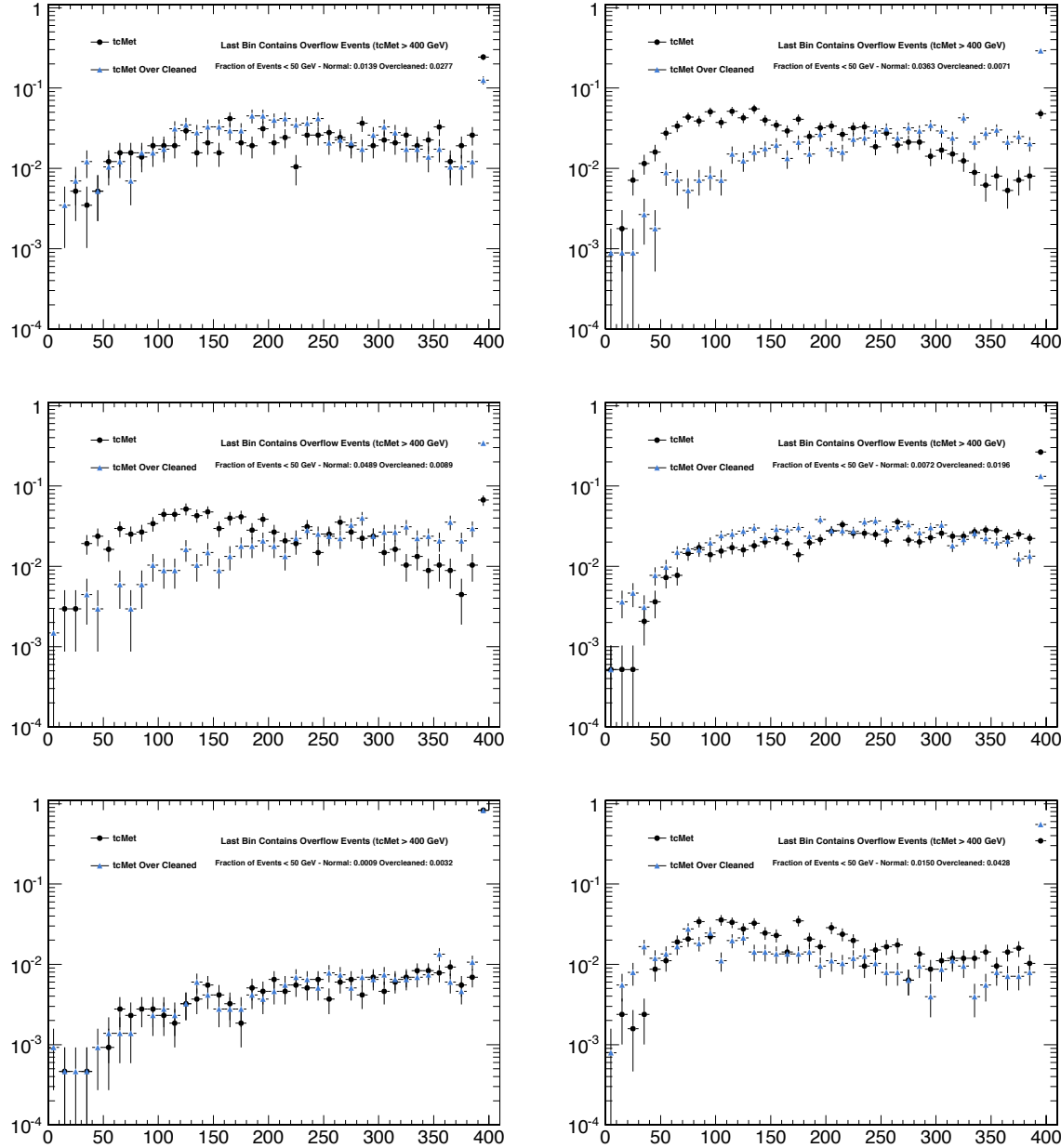


Figure 39: 1st row left: GGM MET spectra normal and cleaned - gluino,squark,neutralino masses 640,1840,500 resp.; 1st row right: GGM MET spectra normal and cleaned - gluino,squark,neutralino masses 640,640,50 resp.; 2nd row left: GGM MET spectra normal and cleaned - gluino,squark,neutralino masses 1840,640,50 resp.; 2nd row right: GGM MET spectra normal and cleaned - gluino,squark,neutralino masses 1840,640,500 resp.; 3rd row left: GGM MET spectra normal and cleaned - gluino,squark,neutralino masses 2000,2000,1500 resp.; 3rd row right: GGM MET spectra normal and cleaned - gluino,squark,neutralino masses 2000,2000,150 resp.

L Effect of Variation of p_T Cuts on Jet and Photon Transverse Momenta

We study the issue of the effect of variation of cuts on the transverse momentum of the lead and trail jets on the results of our analysis. In Fig. 40 we show the bottom line, the “closure” plots obtained with different lead jet and trail photon p_T cuts. These plots are to be compared to the standard plots with $p_T \geq 30$ GeV/c on both the lead and trail photons shown on the right hand side of Fig. 15. As can be seen in Fig. 40, there is little if no variation in these plots in the agreement of QCD +EW MET with the $\gamma\gamma$ events.

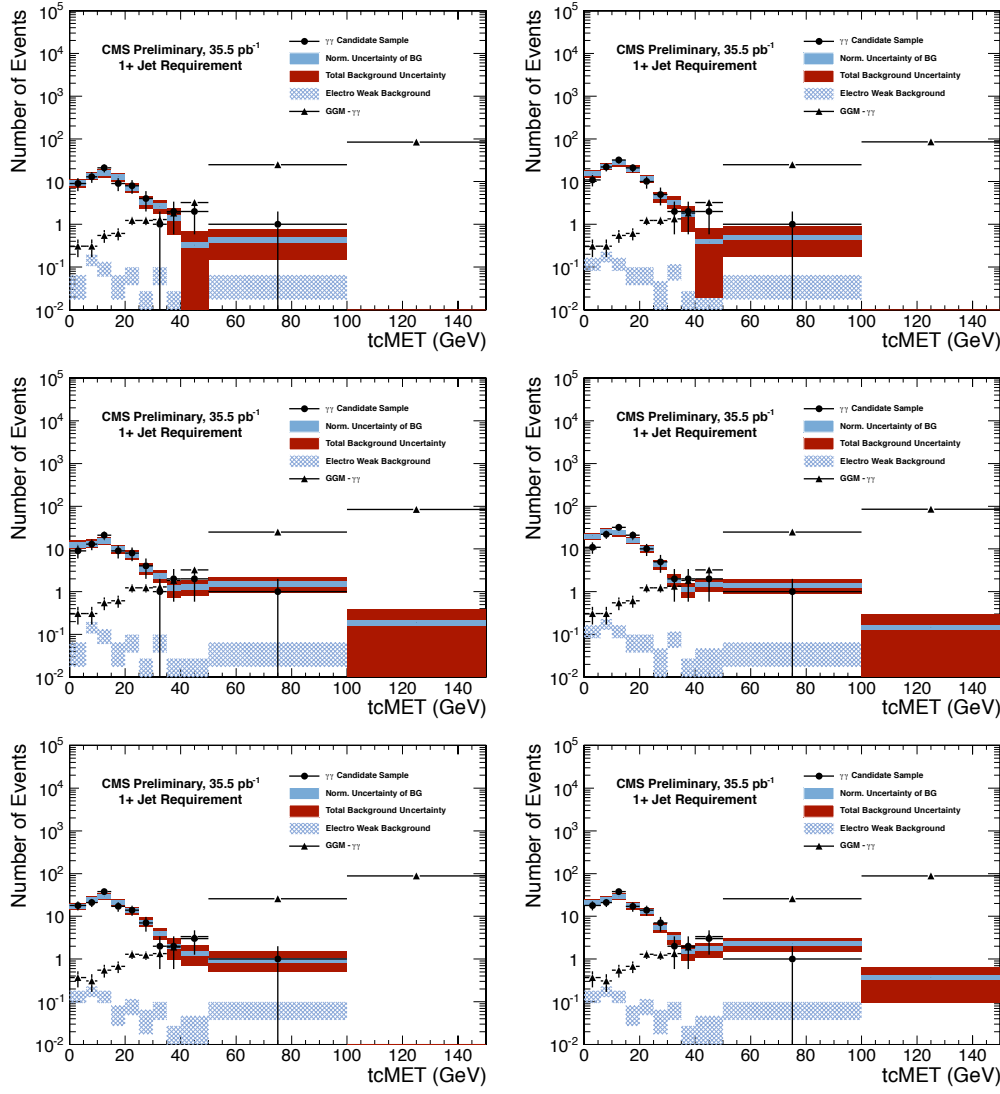


Figure 40: All plots in this figure show the sum of the QCD plus EW MET background compared to the MET from our sample of $\gamma\gamma$ events. They differ by whether the QCD background is determined from fake-fake events or $Z \rightarrow ee$ events: 1st Row Left : ff MET with lead jet $p_T \geq 35$ GeV; 1st Row Right: ff MET with lead jet $p_T \geq 25$ GeV; 2nd Row Left : ee MET with lead jet $p_T \geq 35$ GeV; 2nd Row Right: ee MET with lead jet $p_T \geq 25$ GeV; 3rd Row Left : ff MET with trail photon $p_T \geq 20$ GeV; 3rd Row Right: ee MET with trail photon $p_T \geq 20$ GeV.

927 M Kinematic Plots with No Jet and ≥ 1 Jet Requirements

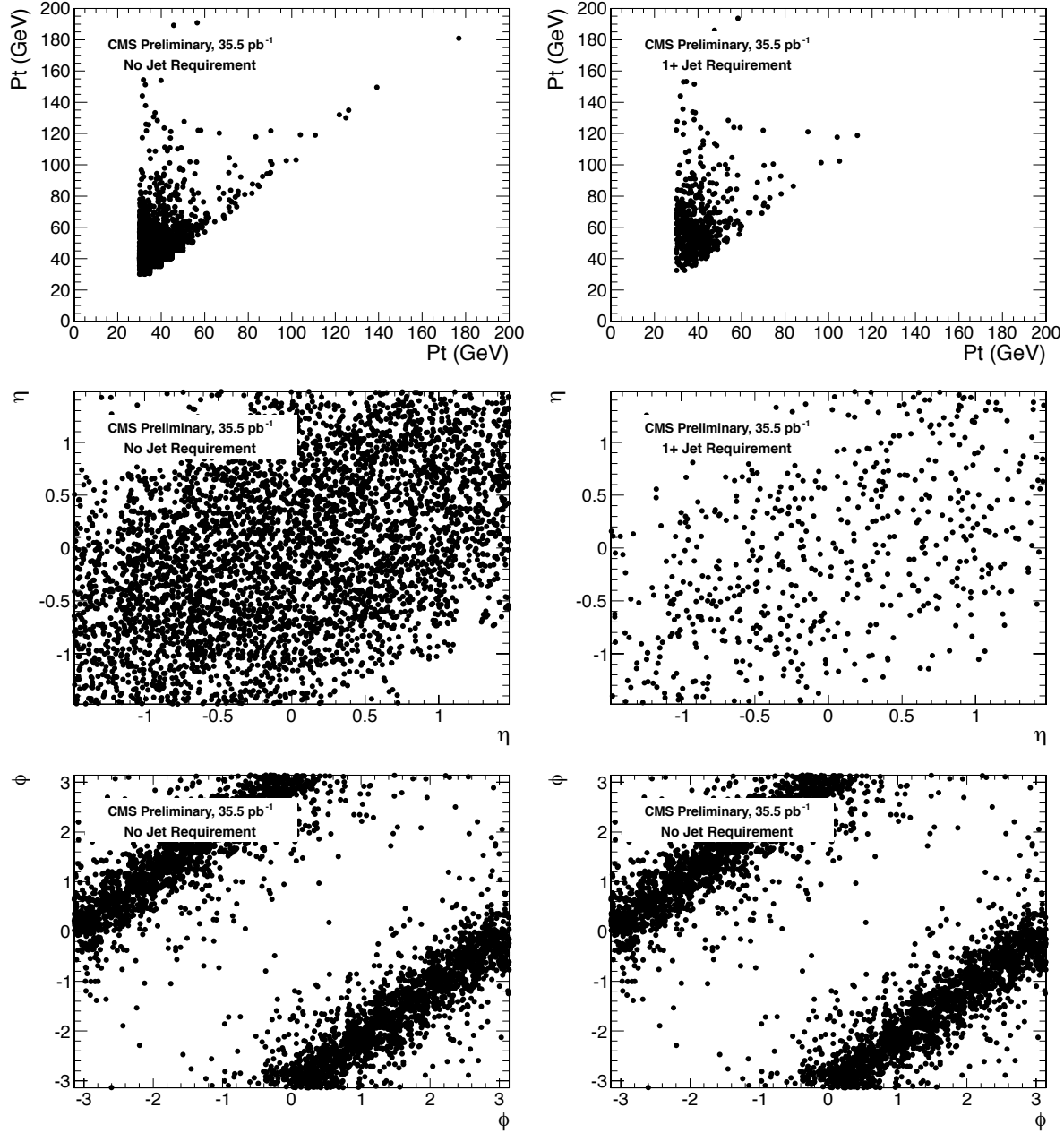


Figure 41: left plots: leading electron vs. trailing electron with no jet requirement for E_T , η , and ϕ respectively; right plots: leading electron vs. trailing electron with ≥ 1 jet for E_T , η , and ϕ respectively

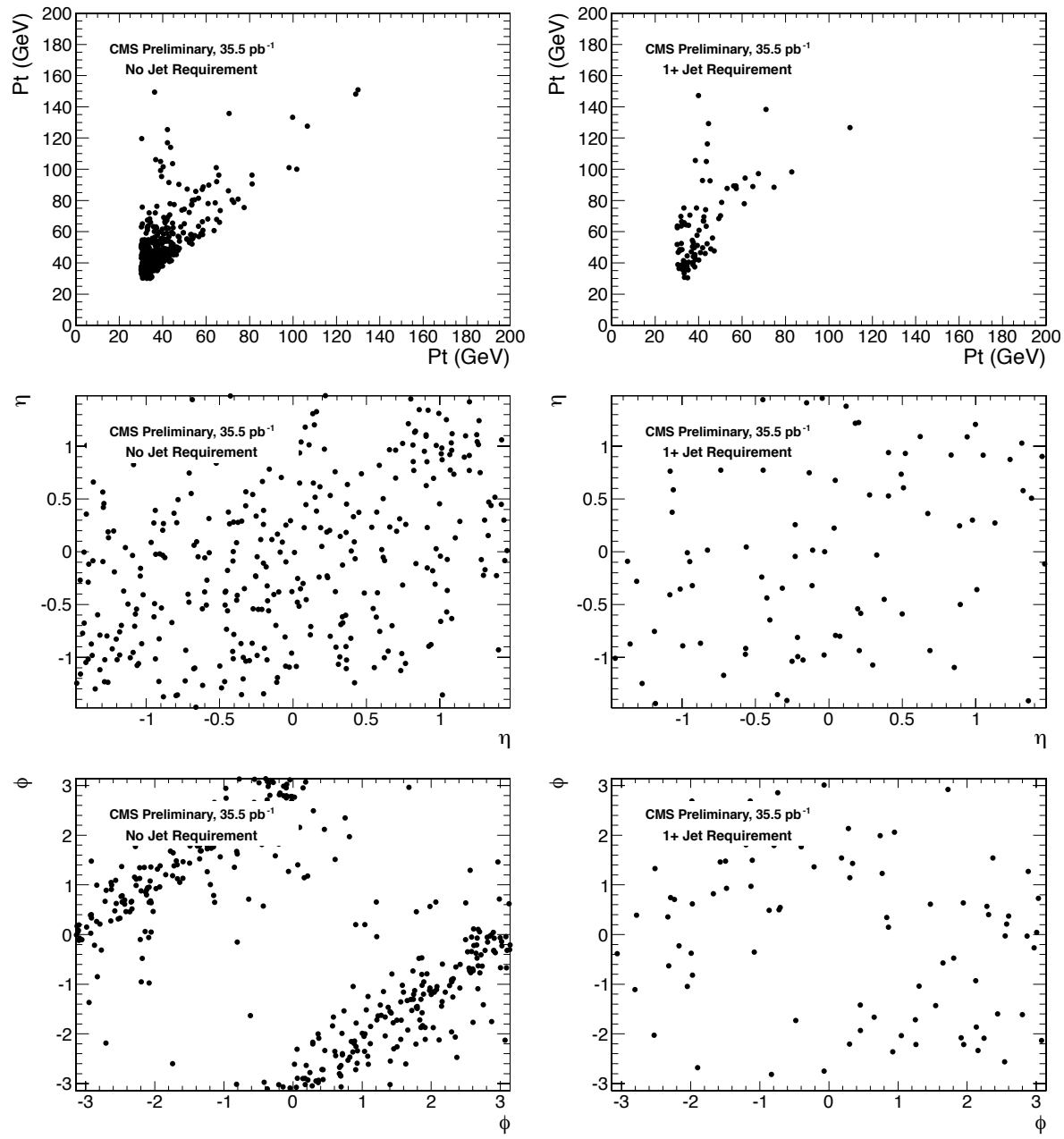


Figure 42: left plots: leading photon vs. trailing photon with no jet requirement for E_T , η , and ϕ respectively; right plots: leading photon vs. trailing photon with ≥ 1 jet for E_T , η , and ϕ respectively

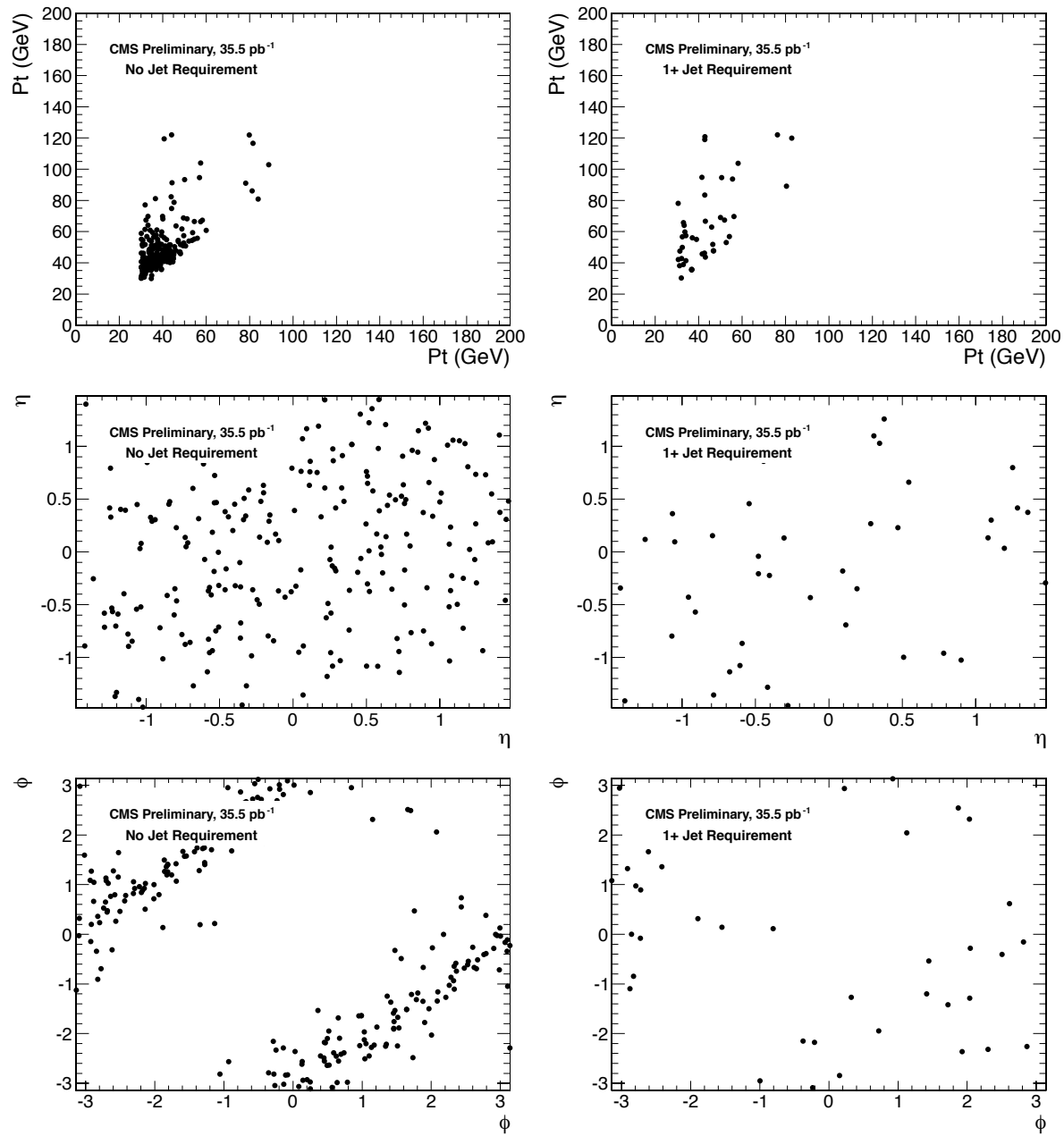


Figure 43: left plots: leading or electron photon vs. trailing photon or electron with no jet requirement for E_T , η , and ϕ respectively; right plots: leading photon or electron vs. trailing photon or electron with ≥ 1 jet for E_T , η , and ϕ respectively; these plots are made for $e\gamma$ events

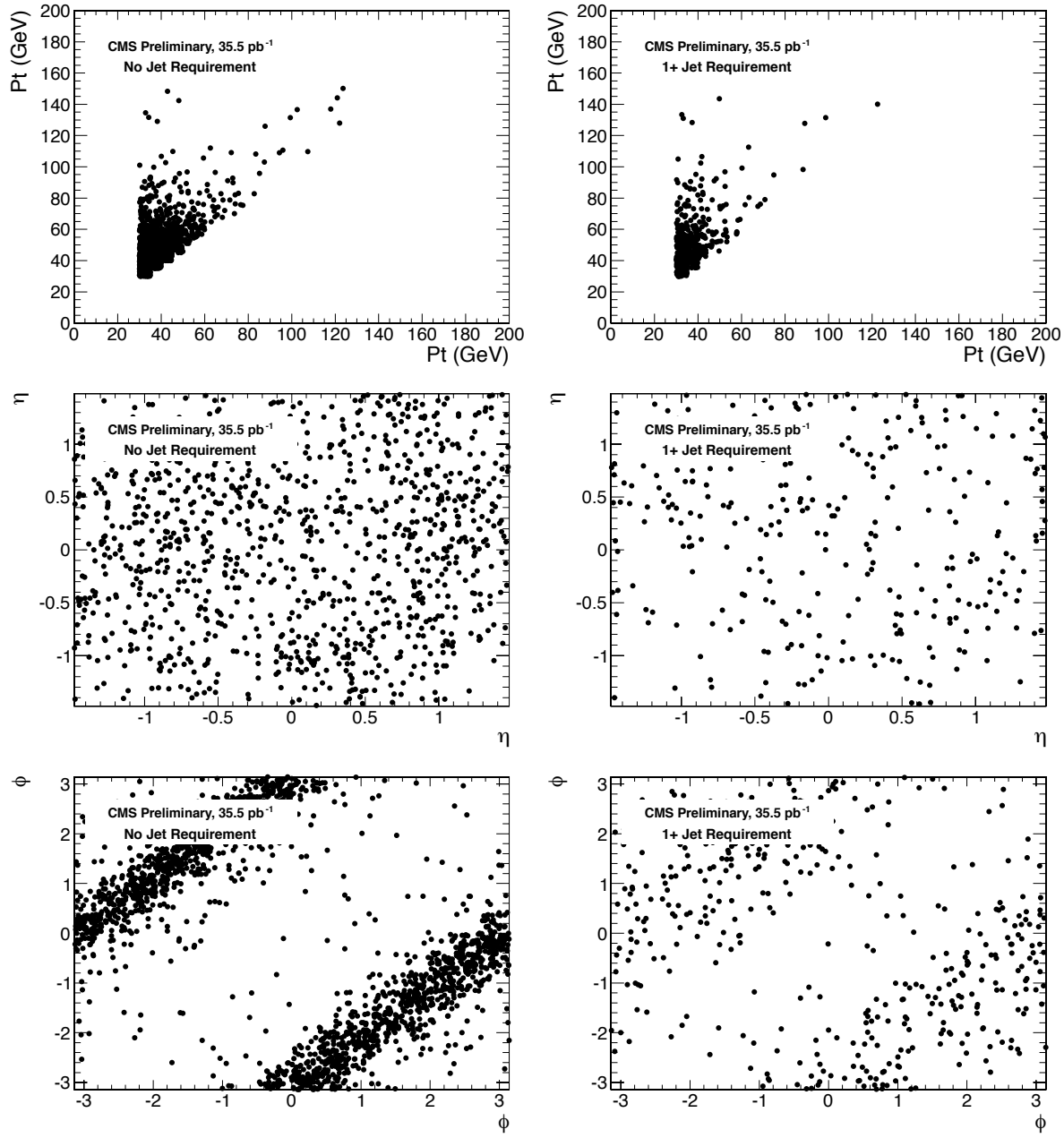


Figure 44: left plots: leading fake vs. trailing fake with no jet requirement for E_T , η , and ϕ respectively for fake fake events; right plots: leading fake vs. trailing fake with ≥ 1 jet for E_T , η , and ϕ respectively for fake fake

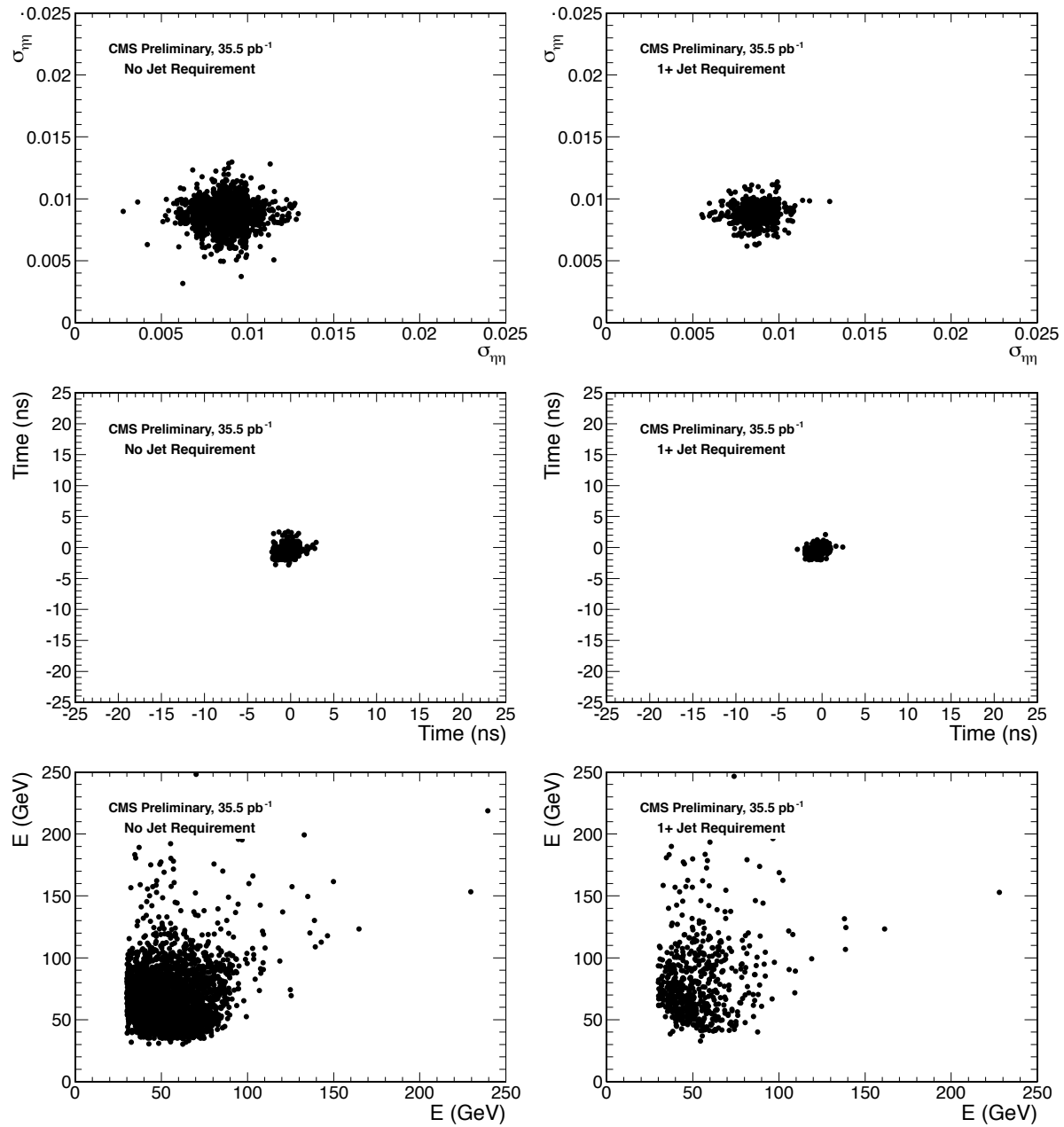


Figure 45: left plots: leading electron vs. trailing electron with no jet requirement for $\sigma_{\eta\eta}$, Time, and Energy respectively for ee events; right plots: leading electron vs. trailing electron with ≥ 1 jet for $\sigma_{\eta\eta}$, Time, and Energy respectively for ee events

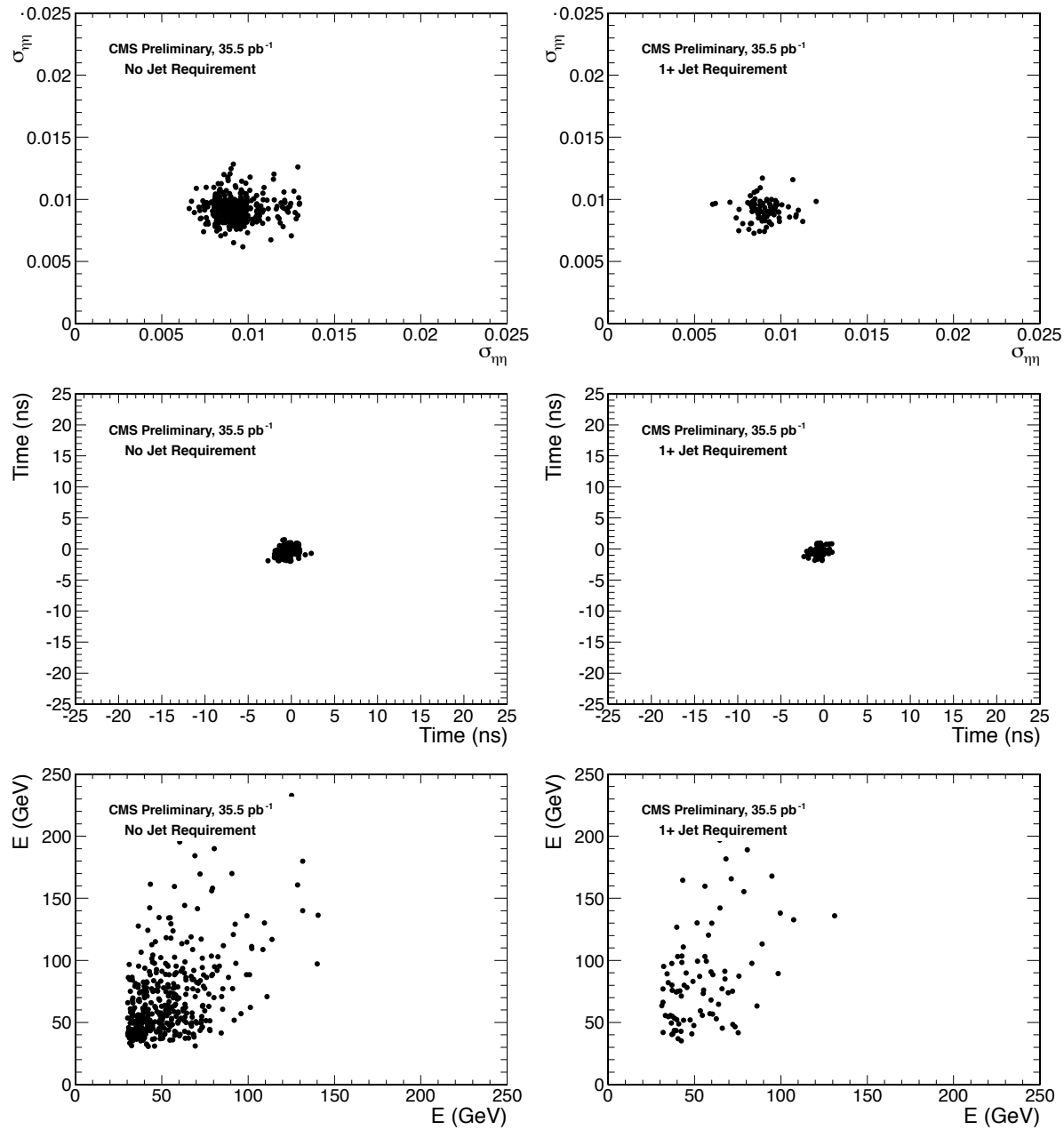


Figure 46: left plots: leading photon vs. trailing photon with no jet requirement for $\sigma_{\eta\eta}$, Time, and Energy respectively for $\gamma\gamma$ events; right plots: leading photon vs. trailing photon with ≥ 1 jet for $\sigma_{\eta\eta}$, Time, and Energy respectively for $\gamma\gamma$ events

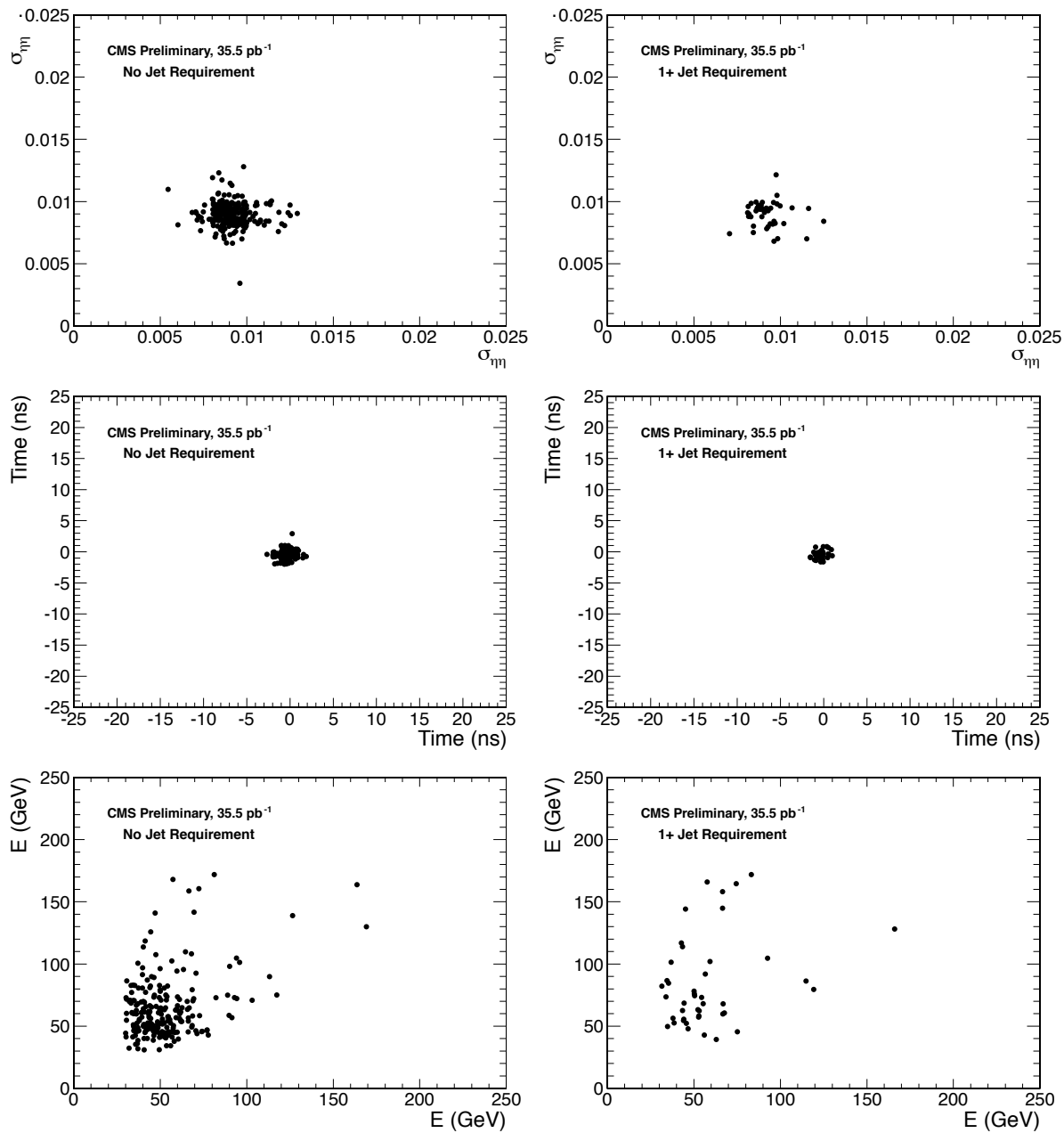


Figure 47: left plots: leading electron or photon vs. trailing electron or photon with no jet requirement for $\sigma_{\eta\eta}$, Time, and Energy respectively for $e\gamma$ events; right plots: leading electron or photon vs. trailing electron or photon with ≥ 1 jet for $\sigma_{\eta\eta}$, Time, and Energy respectively for $e\gamma$ events

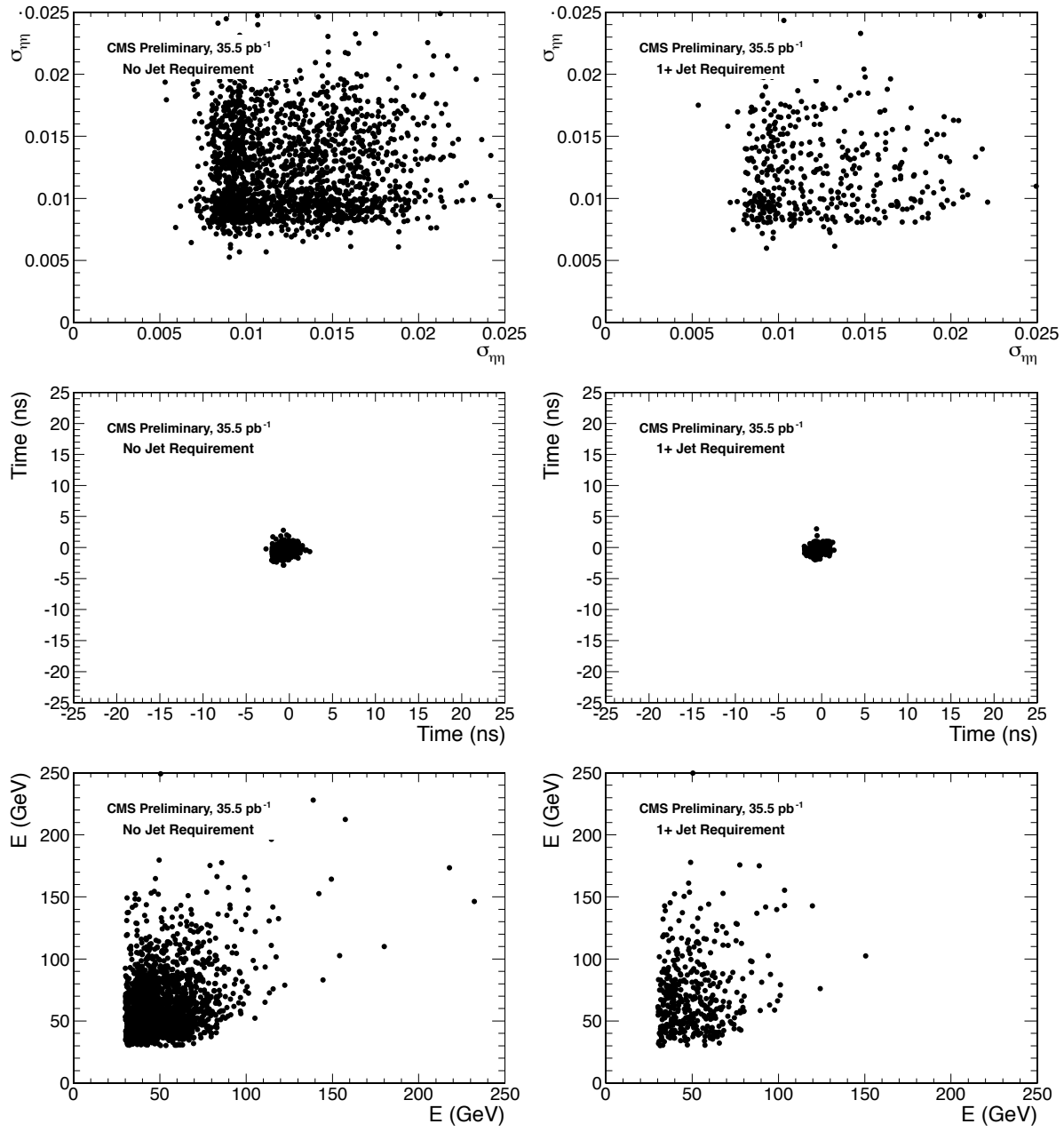


Figure 48: left plots: leading fake vs. trailing fake with no jet requirement for $\sigma_{\eta\eta}$, Time, and Energy respectively; right plots: leading fake vs. trailing fake with ≥ 1 jet for $\sigma_{\eta\eta}$, Time, and Energy respectively

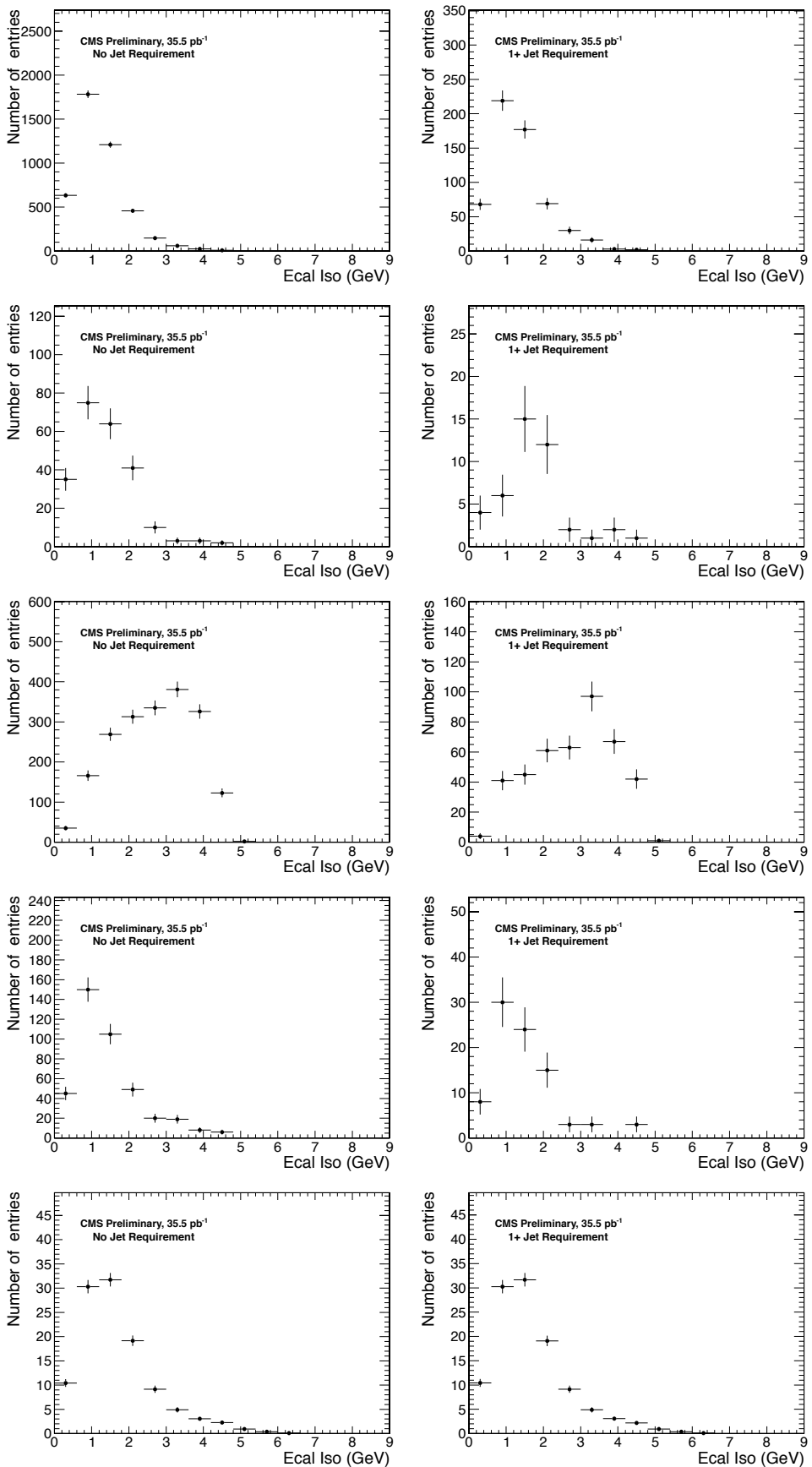


Figure 49: 1st row left plot: ee events leading photon with no jet requirement ECAL iso; right plots: same except ≥ 1 jet requirement; 2nd row left plot: e γ events leading photon with no jet requirement ECAL iso; right plots: same except with ≥ 1 jet requirement; 3rd row left plot: ff events leading photon with no jet requirement ECAL iso; right plots: same except with ≥ 1 jet requirement; 4th row left plot: $\gamma\gamma$ events leading photon with no jet requirement ECAL iso; right plots: same except with ≥ 1 jet requirement; 5th row left plot: GGM events leading photon with no jet requirement ECAL iso; right plots: same except with ≥ 1 jet requirement;

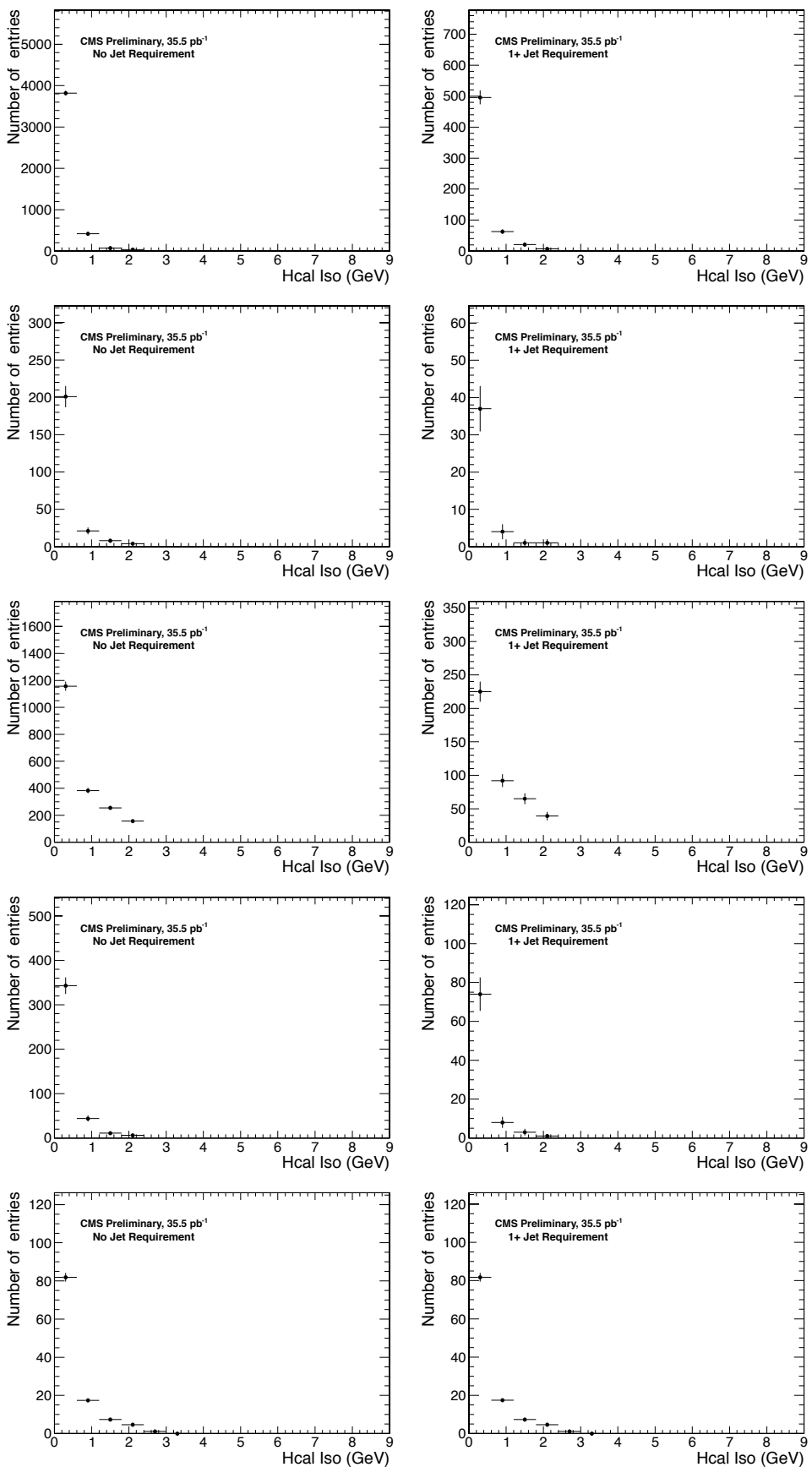


Figure 50: 1st row left plot: ee events leading photon with no jet requirement HCAL iso; right plots: same except ≥ 1 jet requirement; 2nd row left plot: $e\gamma$ events leading photon with no jet requirement HCAL iso; right plots: same except with ≥ 1 jet requirement; 3rd row left plot: ff events leading photon with no jet requirement HCAL iso; right plots: same except with ≥ 1 jet requirement; 4th row left plot: $\gamma\gamma$ events leading photon with no jet requirement HCAL iso; right plots: same except with ≥ 1 jet requirement; 5th row left plot: GGM events leading photon with no jet requirement HCAL iso; right plots: same except with ≥ 1 jet requirement;

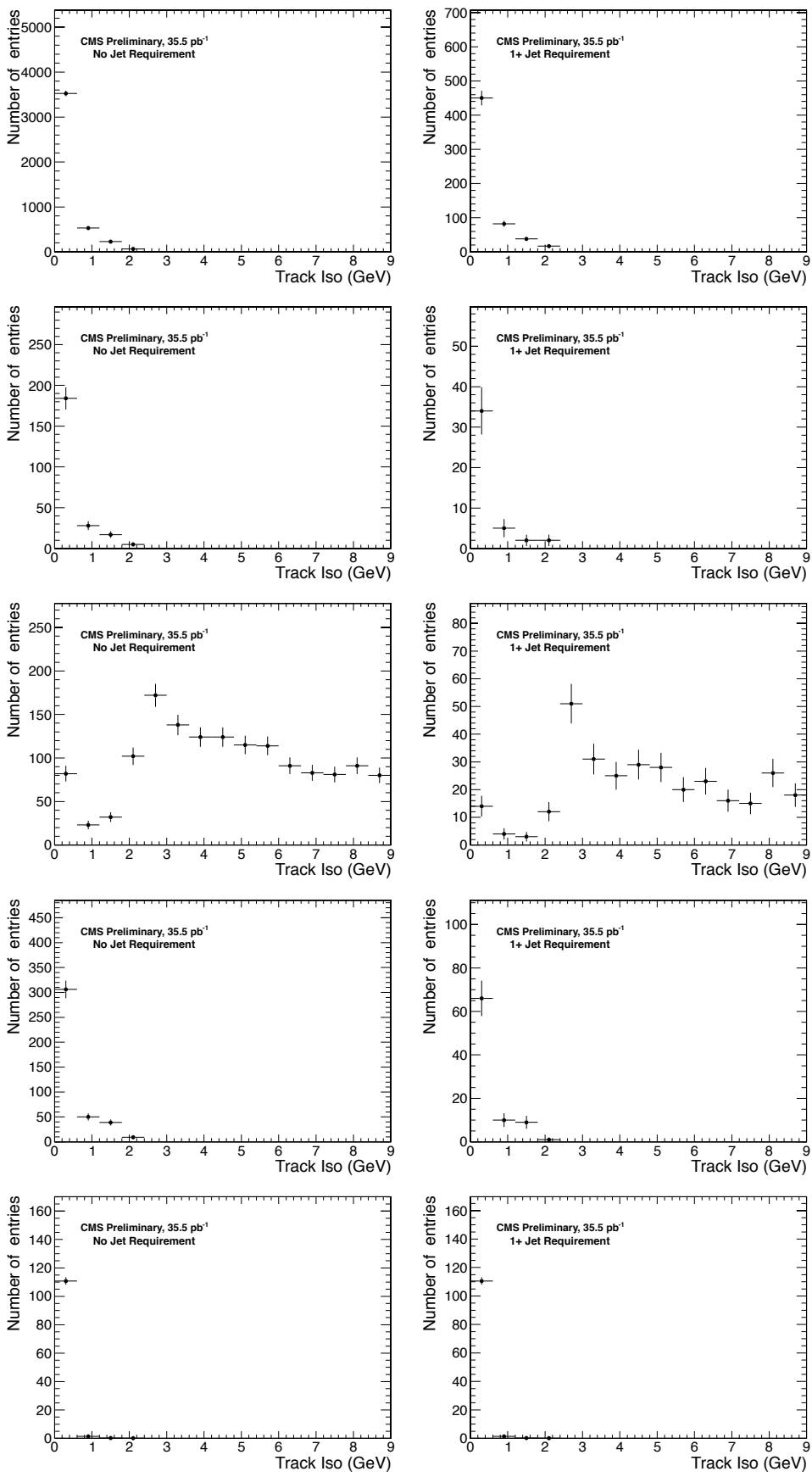


Figure 51: 1st row left plot: ee events leading photon with no jet requirement Track iso; right plots: same except ≥ 1 jet requirement; 2nd row left plot: $e\gamma$ events leading photon with no jet requirement Track iso; right plots: same except with ≥ 1 jet requirement; 3rd row left plot: ff events leading photon with no jet requirement Track iso; right plots: same except with ≥ 1 jet requirement; 4th row left plot: $\gamma\gamma$ events leading photon with no jet requirement Track iso; right plots: same except with ≥ 1 jet requirement; 5th row left plot: GGM events leading photon with no jet requirement Track iso; right plots: same except with ≥ 1 jet requirement;

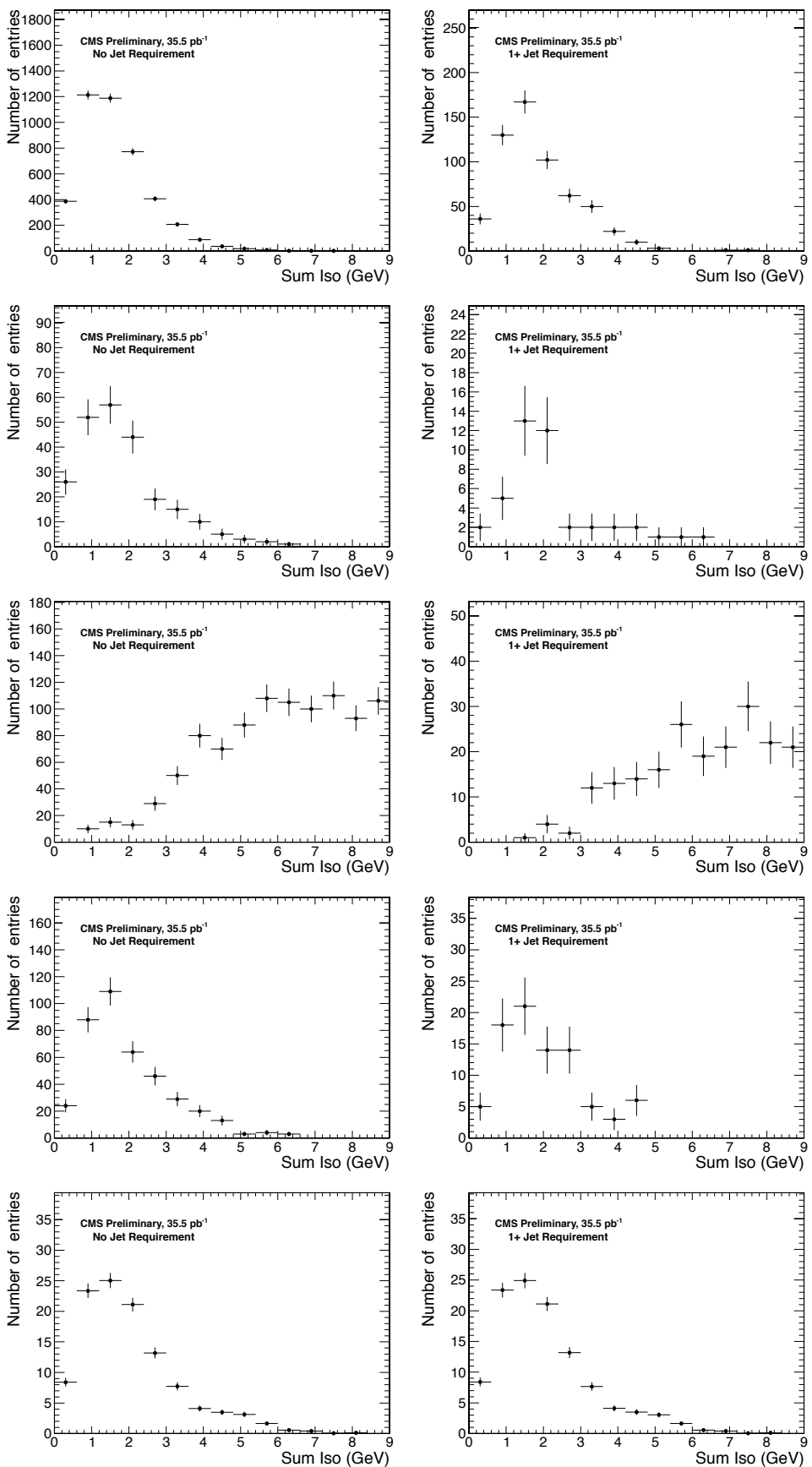


Figure 52: 1st row left plot: ee events leading photon with no jet requirement Sum iso; right plots: same except ≥ 1 jet requirement; 2nd row left plot: $e\gamma$ events leading photon with no jet requirement Sum iso; right plots: same except with ≥ 1 jet requirement; 3rd row left plot: ff events leading photon with no jet requirement Sum iso; right plots: same except with ≥ 1 jet requirement; 4th row left plot: $\gamma\gamma$ events leading photon with no jet requirement Sum iso; right plots: same except with ≥ 1 jet requirement; 5th row left plot: GGM events leading photon with no jet requirement Sum iso; right plots: same except with ≥ 1 jet requirement;

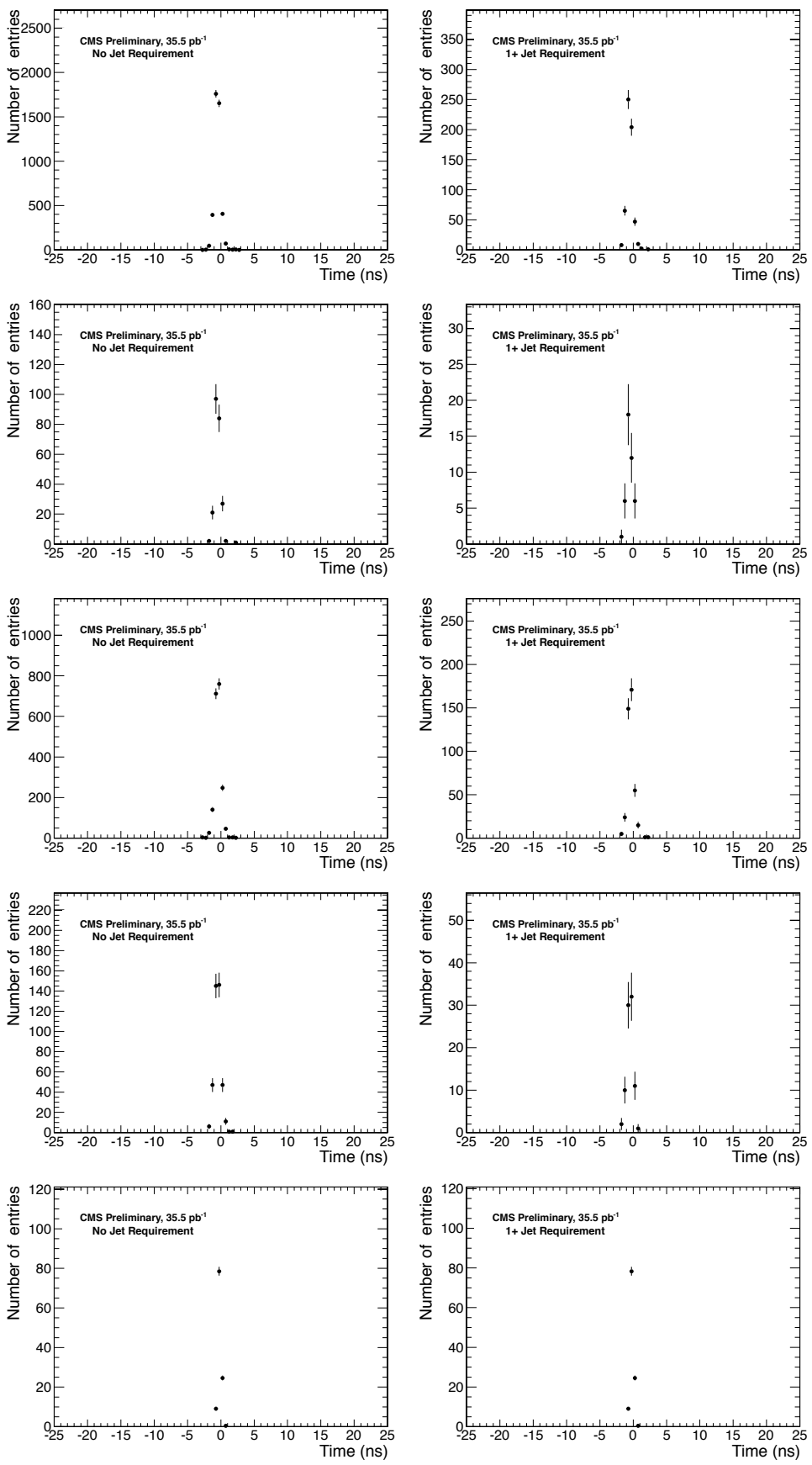


Figure 53: 1st row left plot: ee events Time leading photon with no jet requirement; right plots: same except ≥ 1 jet requirement; 2nd row row left plot: e γ events Time leading photon with no jet requirement; right plots: same except with ≥ 1 jet requirement; 3rd row left plot: ff events Time leading photon with no jet requirement; right plots: same except with ≥ 1 jet requirement; 4th row left plot: $\gamma\gamma$ events Time leading photon with no jet requirement; right plots: same except with ≥ 1 jet requirement; 5th row left plot: GGM events Time leading photon with no jet requirement; right plots: same except with ≥ 1 jet requirement

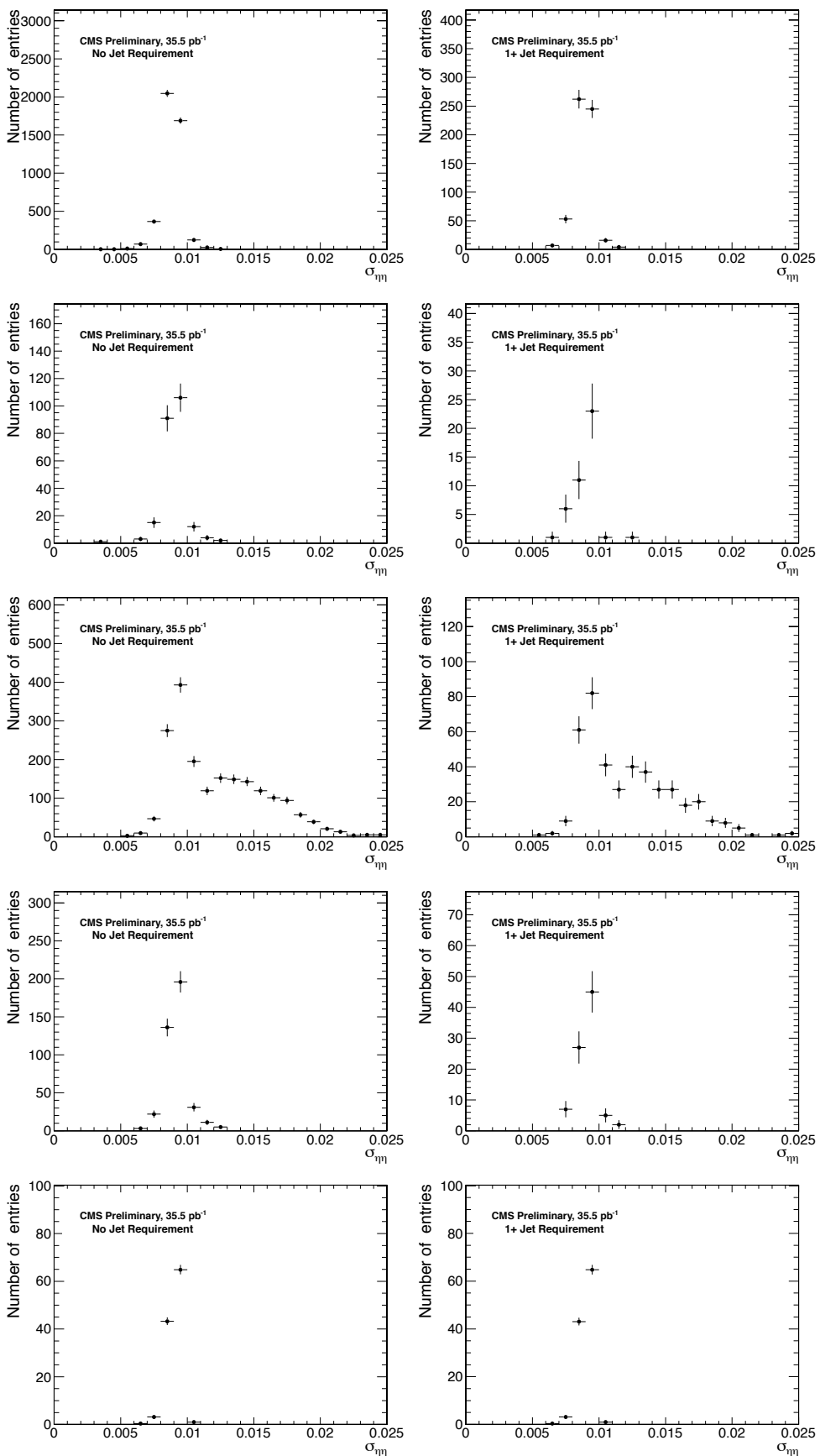


Figure 54: 1st row left plot: ee events $\sigma_{inj\eta}$ leading photon with no jet requirement; right plots: same except ≥ 1 jet requirement; 2nd row left plot: $e\gamma$ events $\sigma_{inj\eta}$ leading photon with no jet requirement; right plots: same except with ≥ 1 jet requirement; 3rd row left plot: ff events $\sigma_{inj\eta}$ leading photon with no jet requirement; right plots: same except with ≥ 1 jet requirement; 4th row left plot: $\gamma\gamma$ events $\sigma_{inj\eta}$ leading photon with no jet requirement; right plots: same except with ≥ 1 jet requirement; 5th row left plot: GGM events $\sigma_{inj\eta}$ leading photon with no jet requirement; right plots: same except with ≥ 1 jet requirement

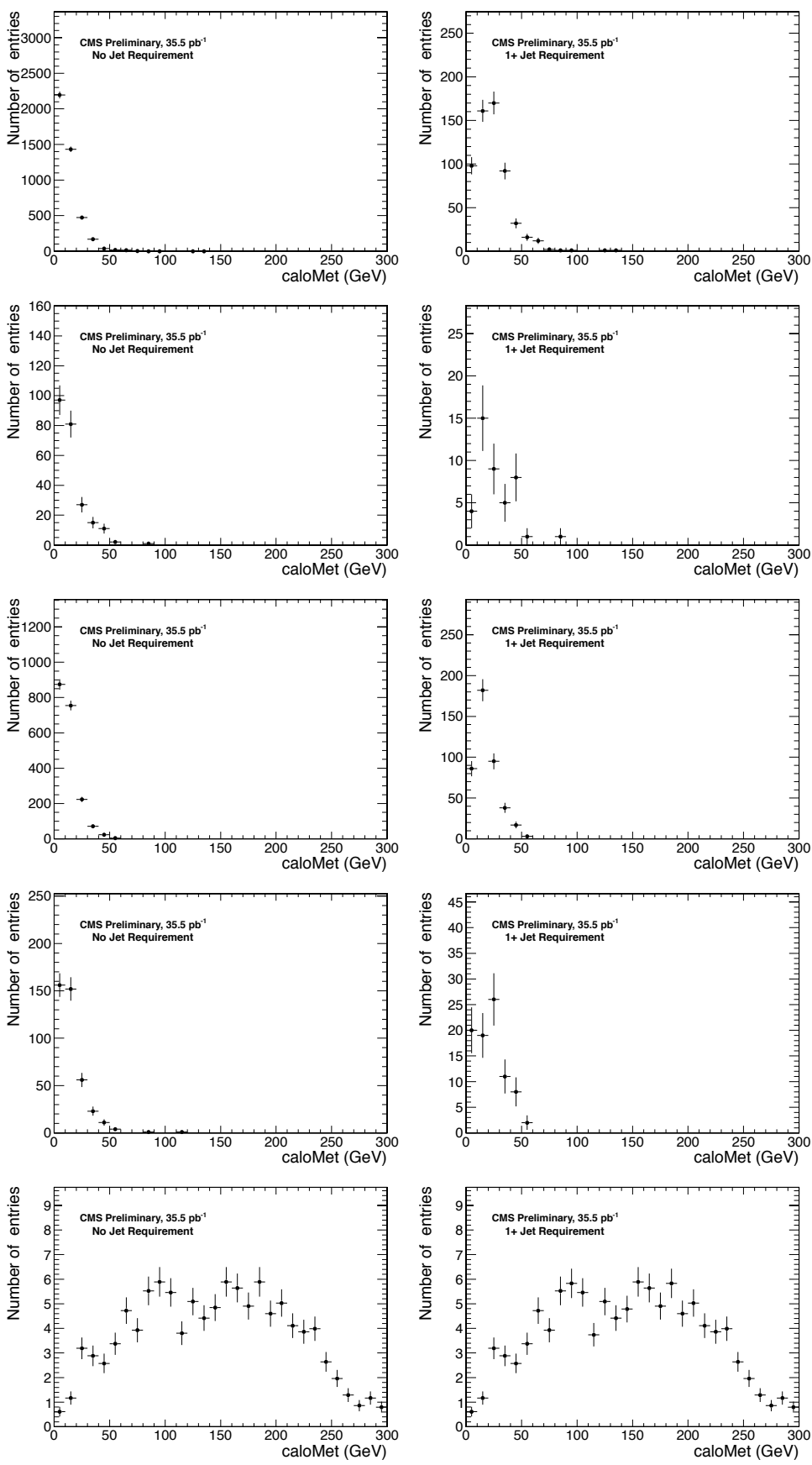


Figure 55: 1st row left plot: ee events caloMet with no jet requirement; right plots: same except ≥ 1 jet requirement; 2nd row left plot: $e\gamma$ events caloMet with no jet requirement; right plots: same except with ≥ 1 jet requirement; 3rd row left plot: ff events caloMet with no jet requirement; right plots: same except with ≥ 1 jet requirement; 4th row left plot: $\gamma\gamma$ events caloMet with no jet requirement; right plots: same except with ≥ 1 jet requirement; 5th row left plot: GGM events caloMet with no jet requirement; right plots: same except with ≥ 1 jet requirement

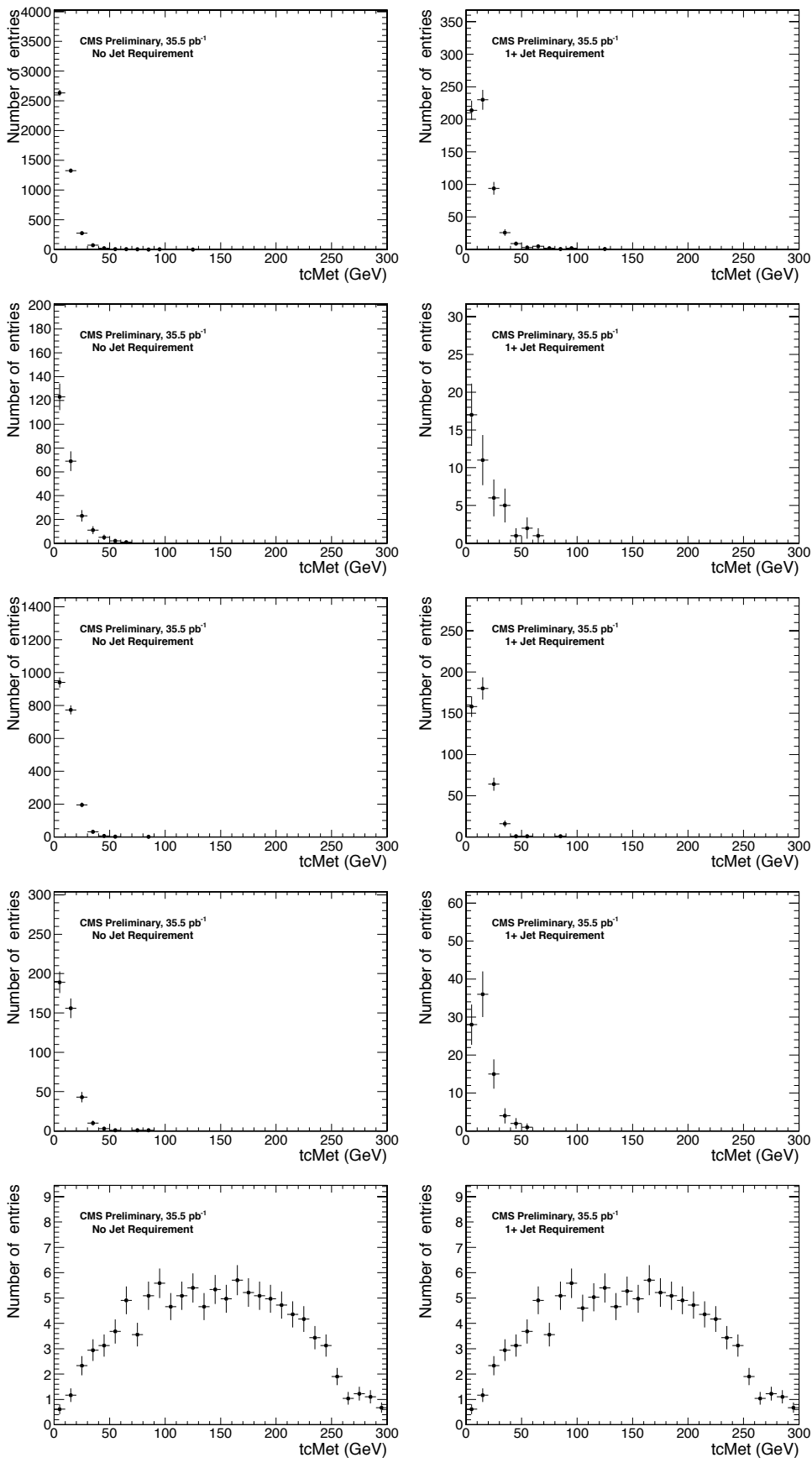


Figure 56: 1st row left plot: ee events tcmet with no jet requirement; right plots: same except ≥ 1 jet requirement; 2nd row row left plot: e γ events tcmet with no jet requirement; right plots: same except with ≥ 1 jet requirement; 3rd row left plot: ff events tcmet with no jet requirement; right plots: same except with ≥ 1 jet requirement; 4th row left plot: $\gamma\gamma$ events tcmet with no jet requirement; right plots: same except with ≥ 1 jet requirement; 5th row left plot: GGM events tcmet with no jet requirement; right plots: same except with ≥ 1 jet requirement;

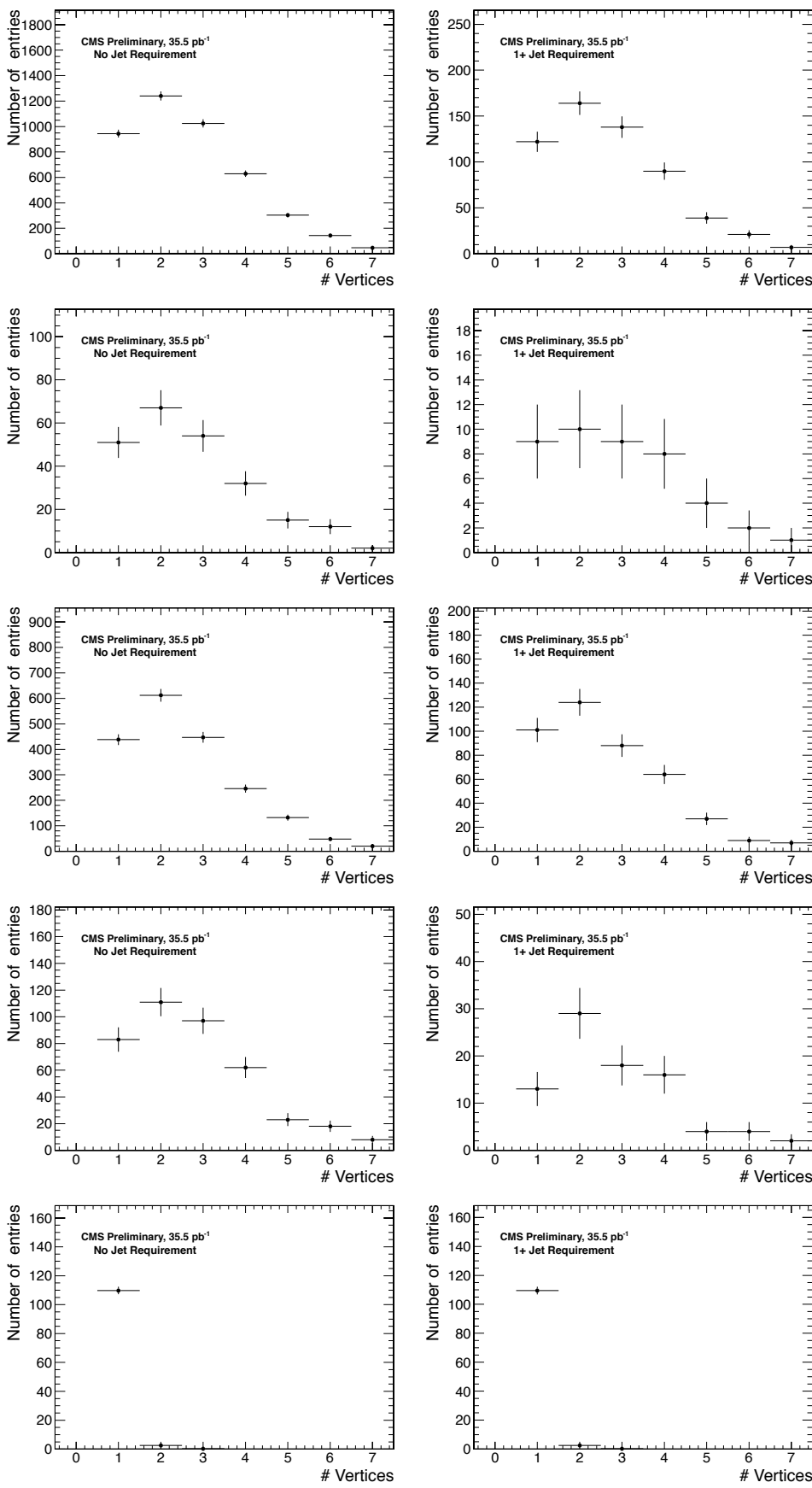


Figure 57: 1st row-left plot: ee events-number of vertices with no jet requirement; right plot: same except with ≥ 1 jet requirement; 2nd row-left plot: e γ events-number of vertices with no jet requirement; right plot: same except with ≥ 1 jet requirement; 3rd row-left plot: ff events-number of vertices with no jet requirement; right plot: same except with ≥ 1 jet requirement; 4th row-left plot: $\gamma\gamma$ events-number of vertices with no jet requirement; right plot: same except with ≥ 1 jet requirement; 5th row-left plot: GGM events-number of vertices with no jet requirement; right plot: same except with ≥ 1 jet requirement

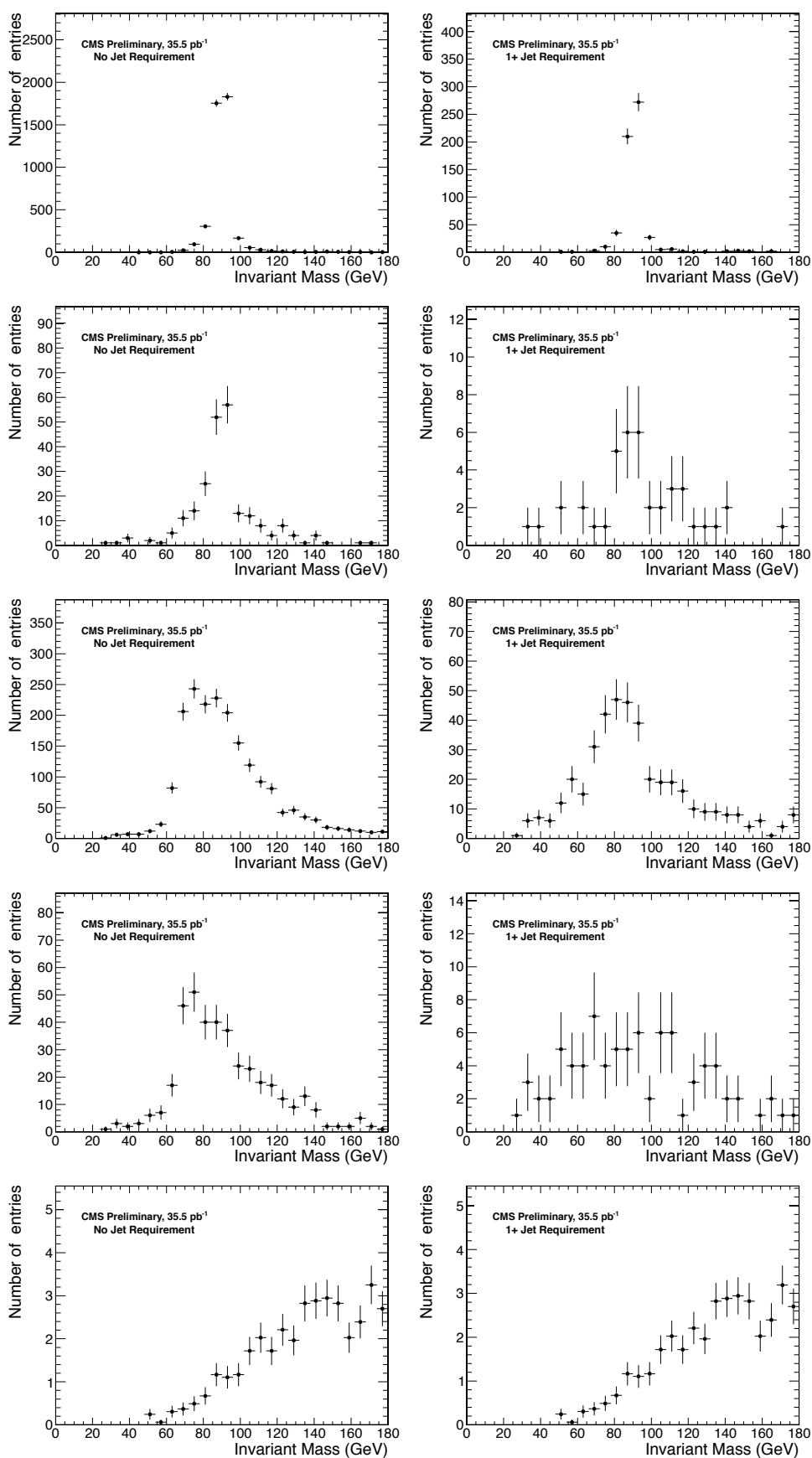


Figure 58: left plots: masses for ee, $e\gamma$, ff, $\gamma\gamma$ and GGM events with no jet requirement; right plots: same sequence except with ≥ 1 jet requirement

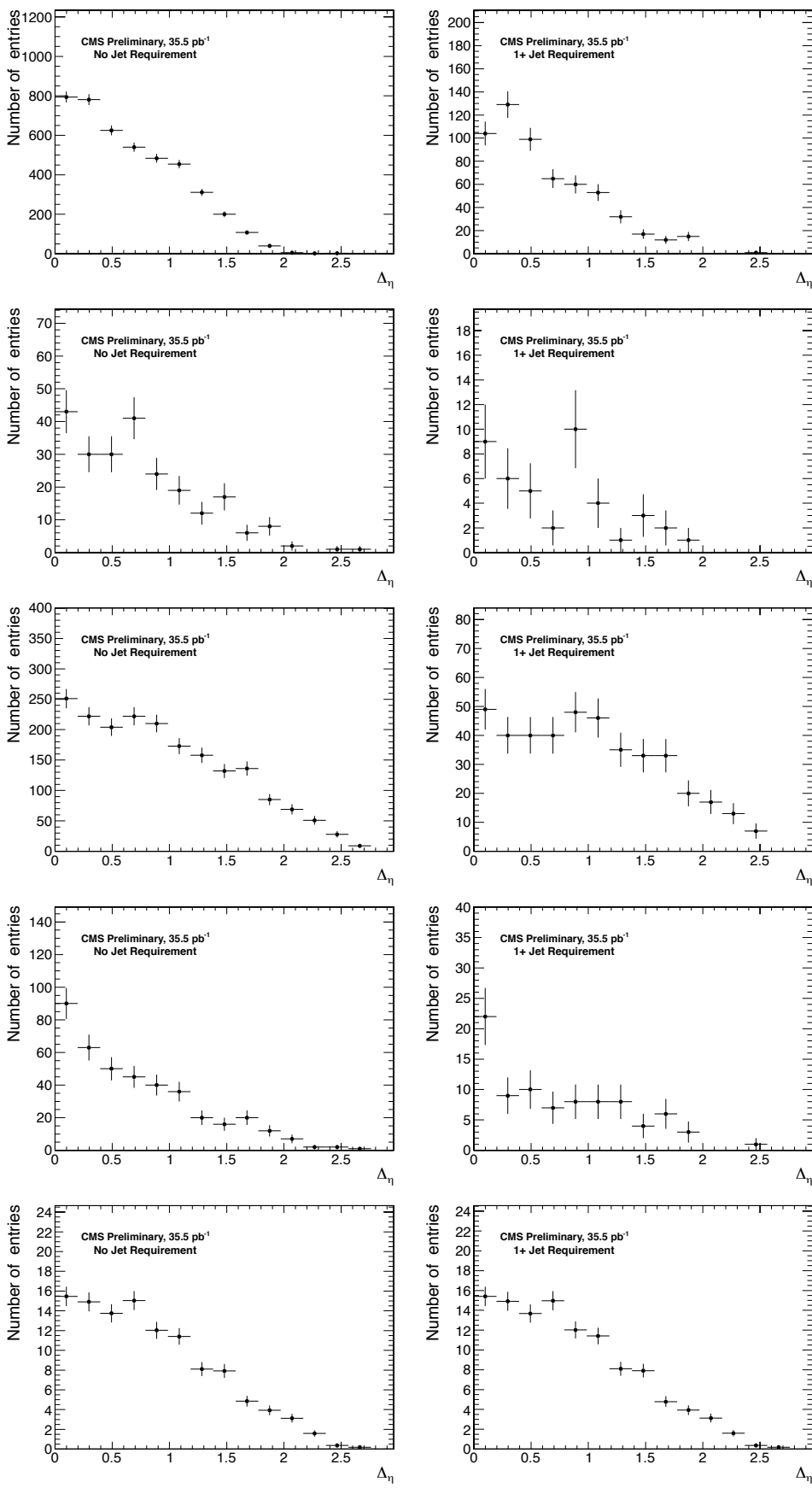


Figure 59: left plots: deltaeta for ee, e γ , ff, $\gamma\gamma$ and GGM events with no jet requirement; right plots: same sequence except with ≥ 1 jet requirement

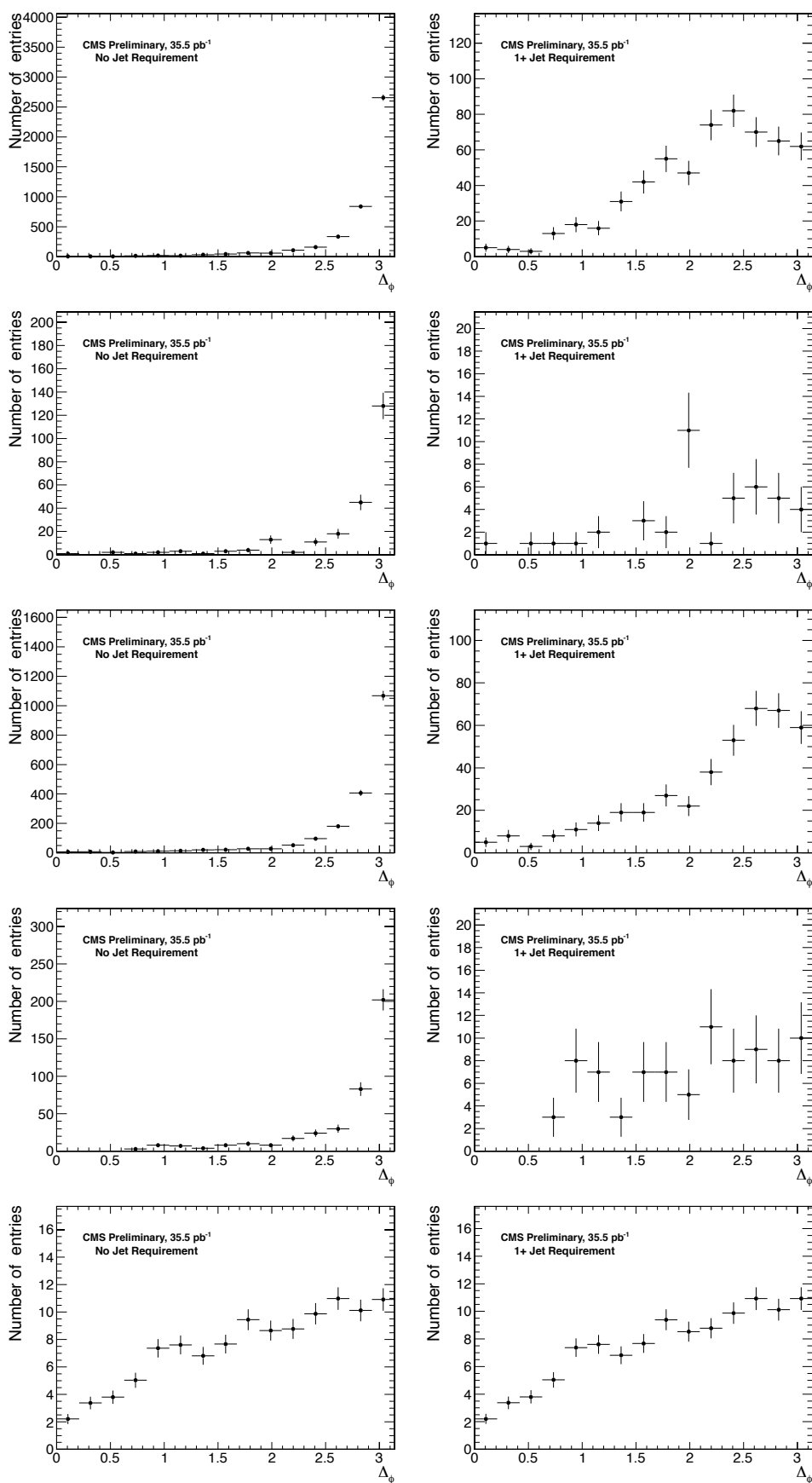


Figure 60: left plots: deltaphi for ee, $e\gamma$, ff, $\gamma\gamma$ and GGM events with no jet requirement; right plots: same sequence except with ≥ 1 jet requirement

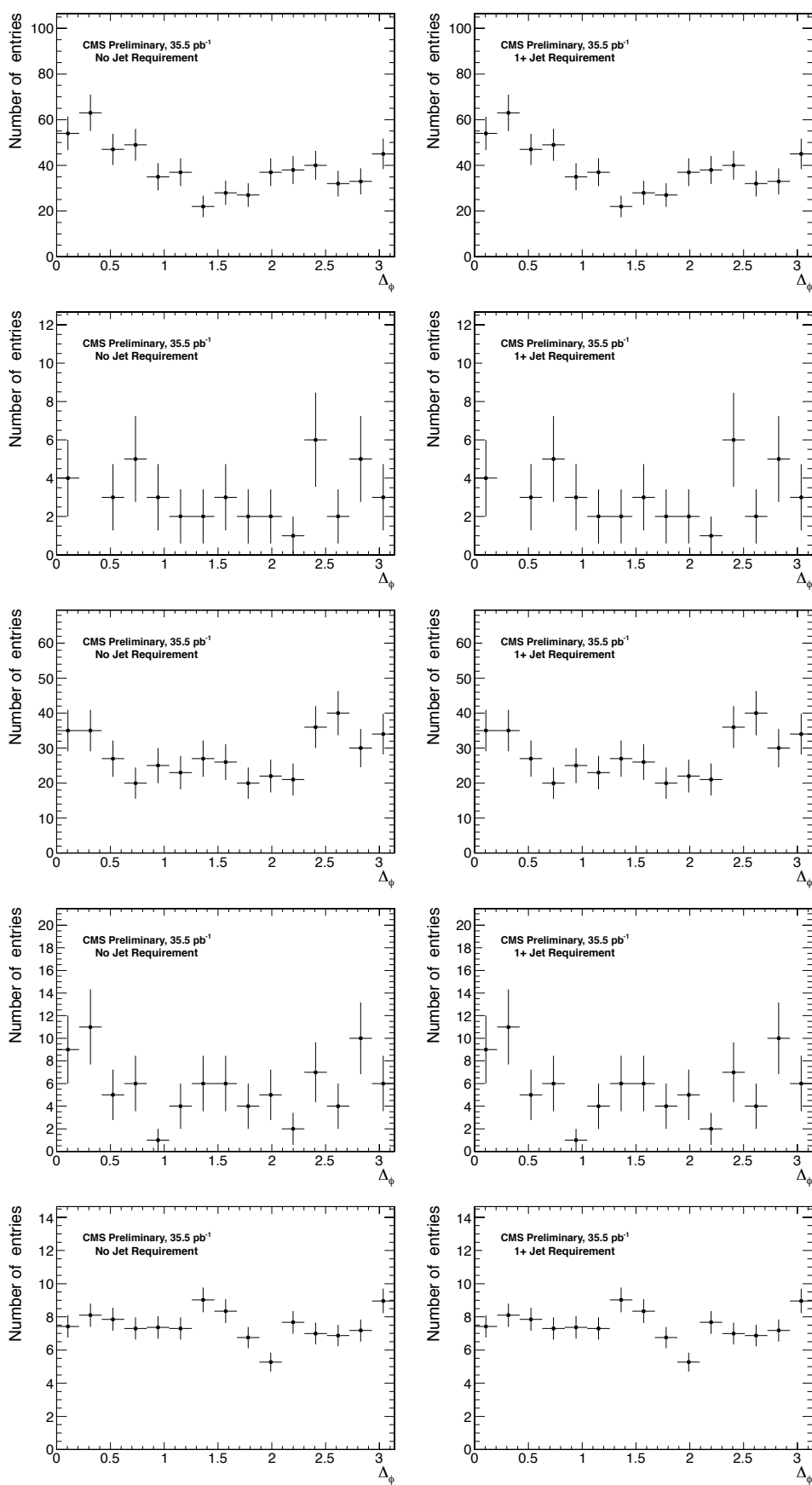


Figure 61: left plots: $\Delta\phi$ between leading jet and MET for ee, e γ , ff, $\gamma\gamma$ and GGM events with no jet requirement; right plots: same sequence except with ≥ 1 jet requirement

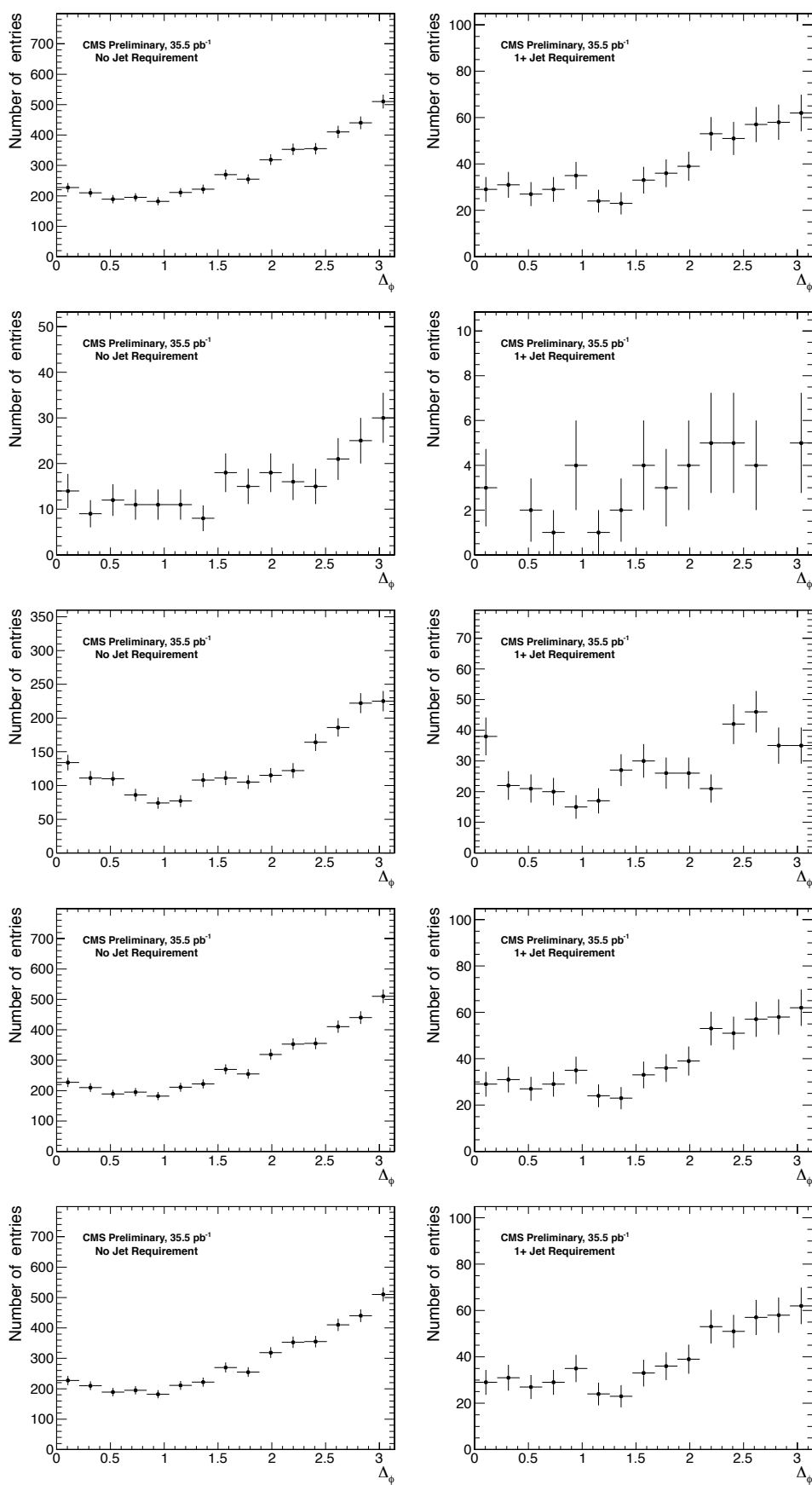


Figure 62: left plots: delta phi between leading photon and MET for ee, e γ , ff, $\gamma\gamma$ and GGM events with no jet requirement; right plots: same sequence except with ≥ 1 jet requirement

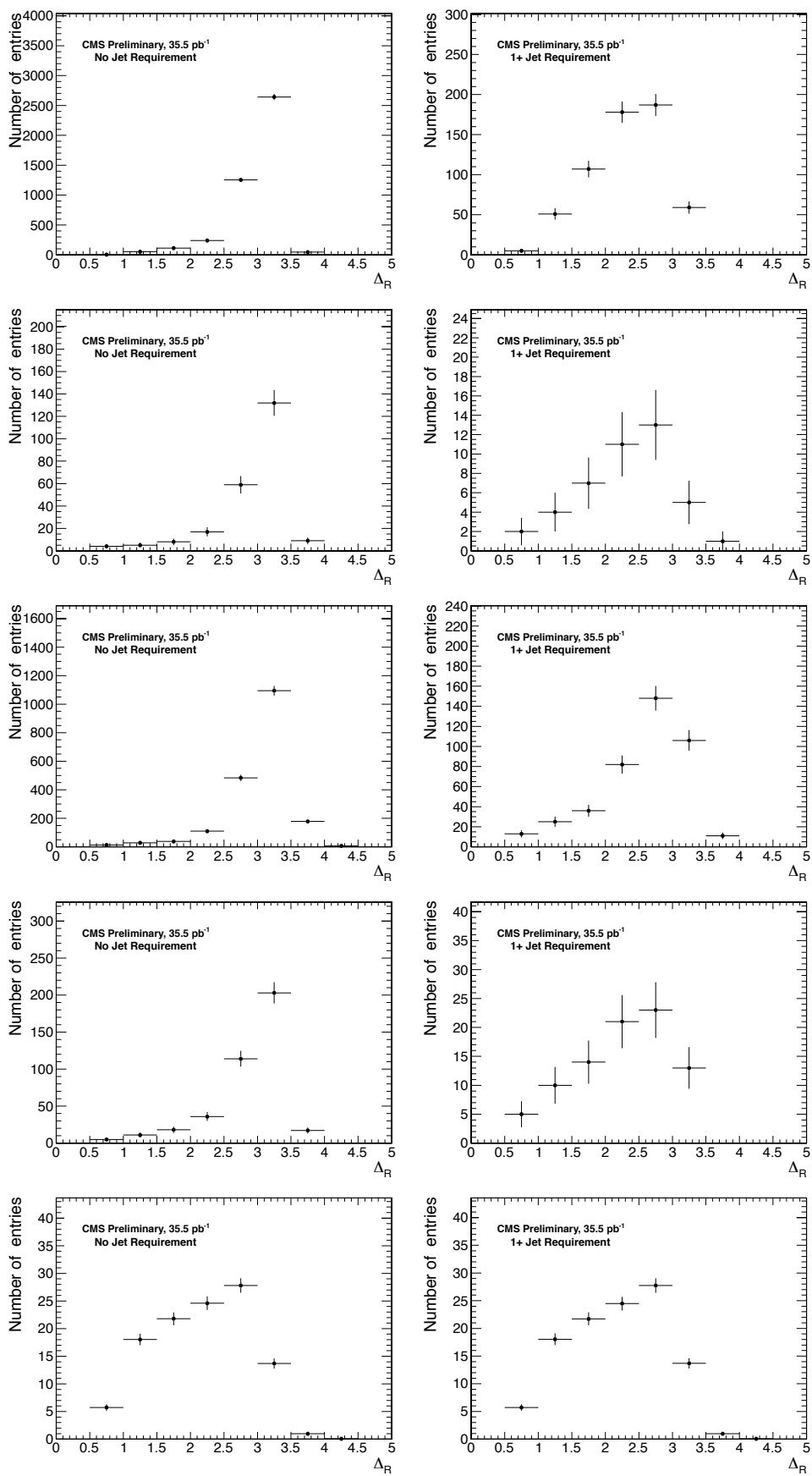


Figure 63: left plots: delta R for ee, e γ , ff, $\gamma\gamma$ and GGM events with no jet requirement; right plots: same sequence except with ≥ 1 jet requirement

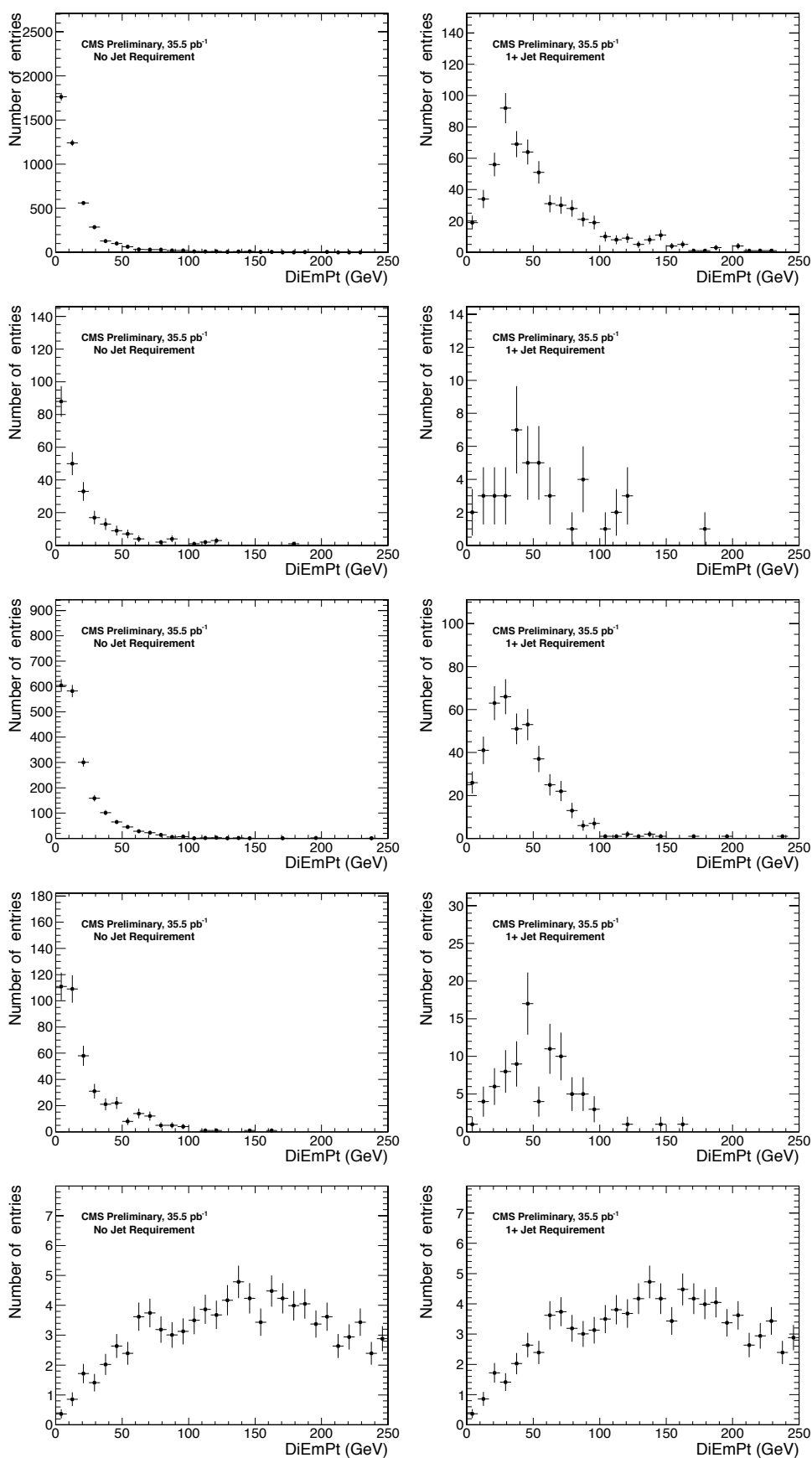


Figure 64: left plots: diEmPt for ee, e γ , ff, $\gamma\gamma$ and GGM events with no jet requirement; right plots: same sequence except with ≥ 1 jet requirement

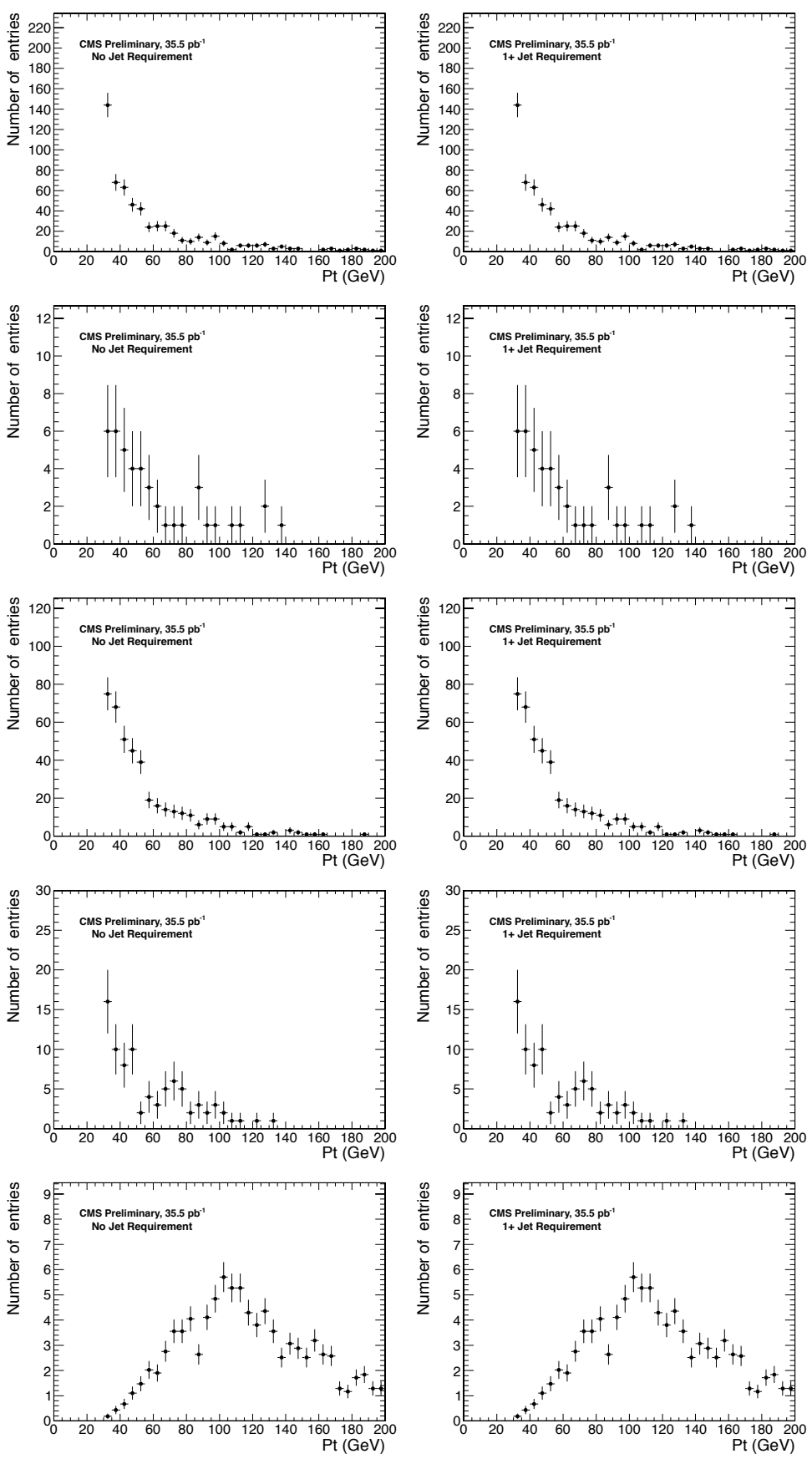


Figure 65: left plots: p_T of the leading jet for ee, e γ , ff, $\gamma\gamma$ and GGM events with no jet requirement; right plots: same sequence except with ≥ 1 jet requirement

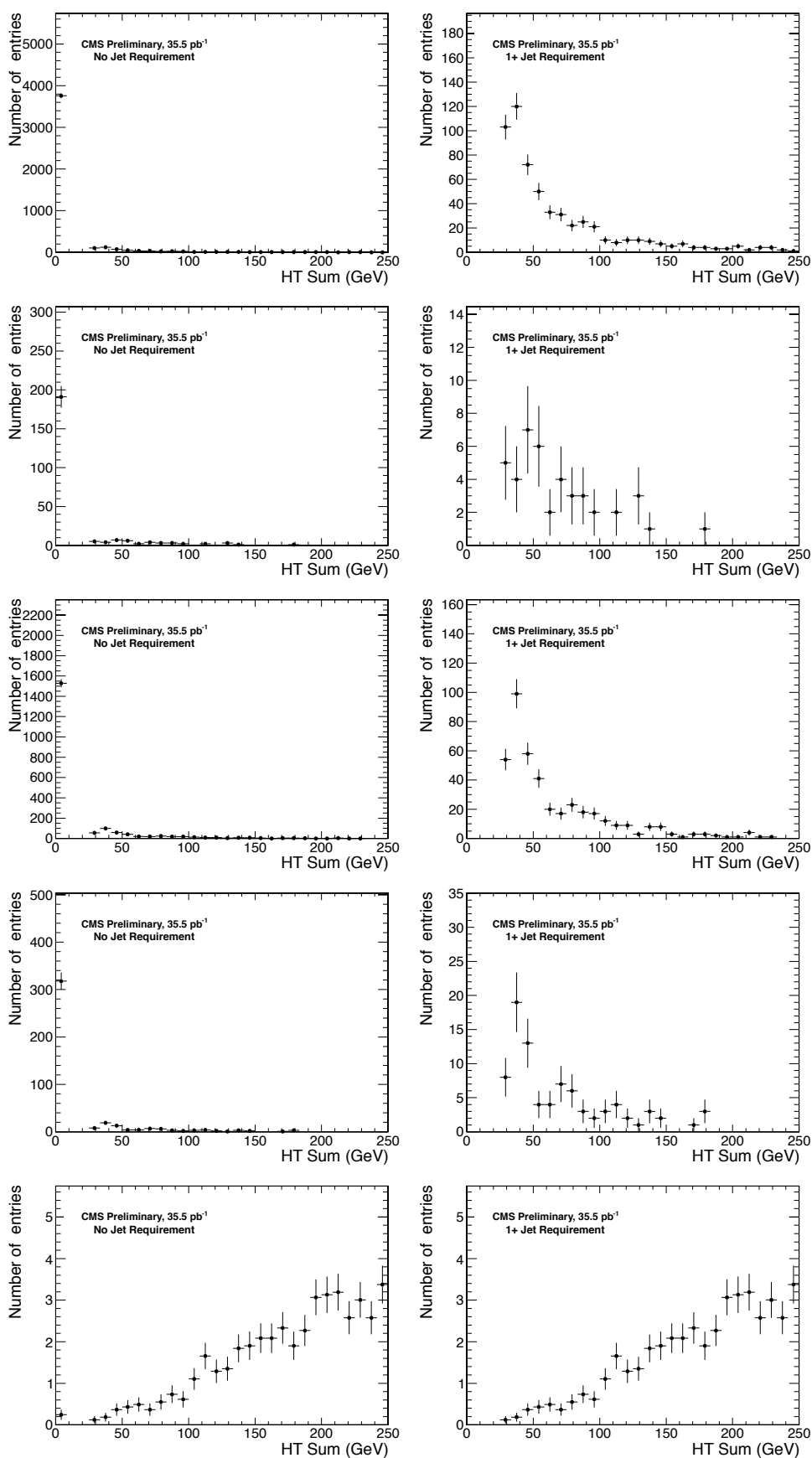


Figure 66: left plots: jet HT sum for ee, e γ , ff, $\gamma\gamma$ and GGM events with no jet requirement; right plots: same sequence except with ≥ 1 jet requirement

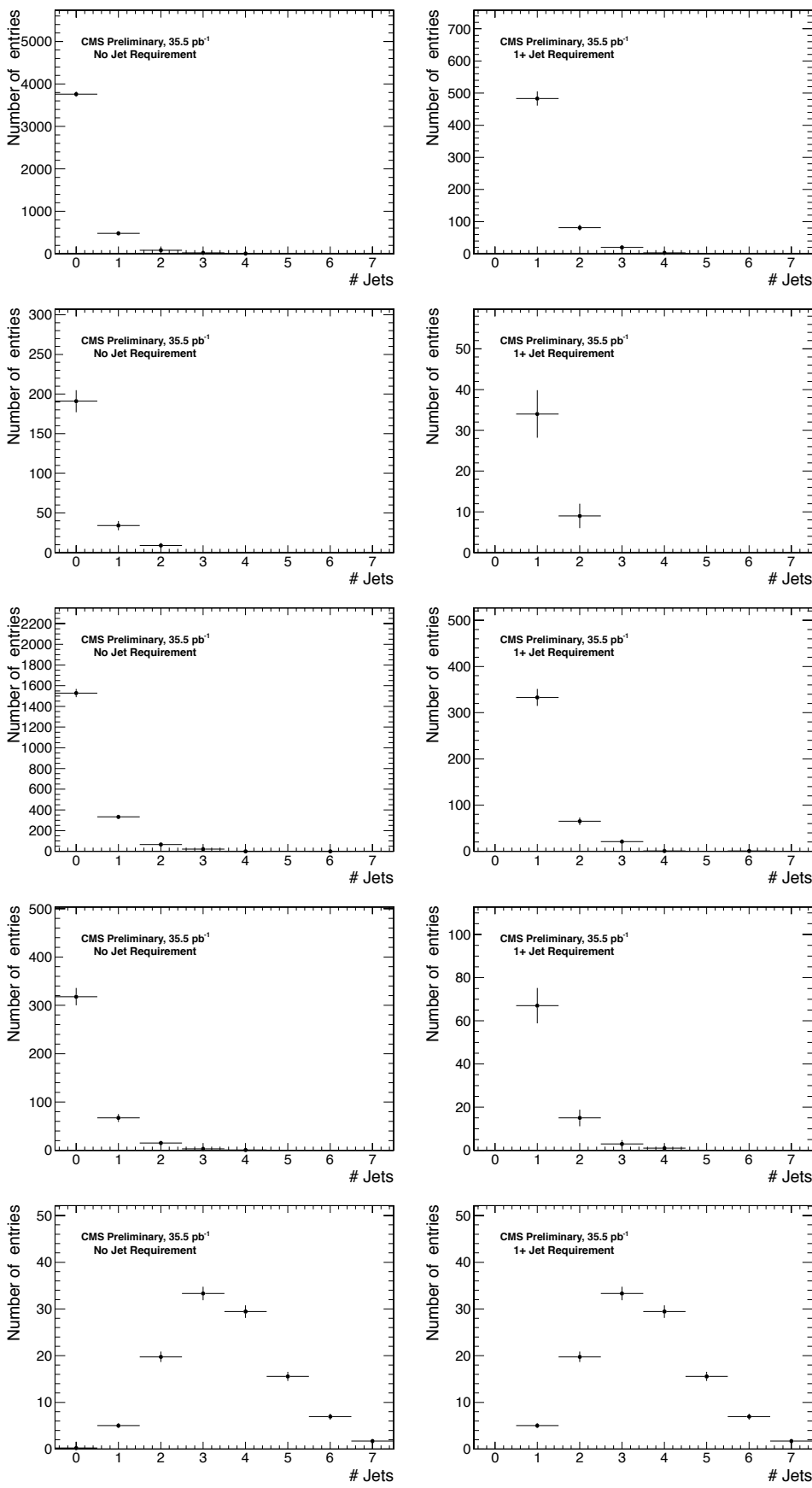


Figure 67: 1st row-left plot: ee events- number of jets with no jet requirement; right plot: same except with ≥ 1 jet requirement; 2nd row-left plot: e γ events- number of jets with no jet requirement; right plot: same except with ≥ 1 jet requirement; 3rd row-left plot: ff events- number of jets with no jet requirement; right plot: same except with ≥ 1 jet requirement; 4th row-left plot: $\gamma\gamma$ events- number of jets with no jet requirement; right plot: same except with ≥ 1 jet requirement; 5th row-left plot: GGM events-number of jets with no jet requirement; right plot: same except with ≥ 1 jet requirement

928 References

- 929 [1] P. Fayet, Phys. Lett. **B70**, 461 (1977); *ibid.* **B86**, 272 (1979); *ibid.* **175**, 471 (1986); G. F. Giudice and
930 R. Rattazzi, “Gauge-Mediated Supersymmetry Breaking” in G. L. Kane: *Perspectives on Supersymmetry*,
931 World Scientific, Singapore (1998), p. 355-377 and references therein; P. Meade, N. Seiberg, and D. Shih,
932 arXiv:0801.3278v3[hep-ph] 8 Mar 2008; M. Buican, P. Meade, N. Seiberg, and D. Shih, arXiv:0812.3668v4
933 [hep-ph] 10 Dec 2009; S. Abel et al. arXiv:0910.267v2 hep-ph] 26 Oct. 2009.
- 934 [2] A. Askew et al., ”Understanding Missing Transverse Energy in Di-Photon Events for SUSY Searches”, CMS
935 AN-2009/094.
- 936 [3] A. Askew et al., ”Understanding Missing Transverse Energy in Di-Photon Events with 7 TeV Data”, CMS
937 AN-2010/168.
- 938 [4] V.M. Abazov *et al.* (D0 Collaboration), Phys. Lett. B **659**, 856 (2008); D. Acosta *et al.*, Phys. Rev. D **71**,
939 031104(R) (2005).
- 940 [5] Particle Data Group Collaboration, “Review of Particle Physics, Section 32.3.1: The Bayesian approach”,
941 Phys. Lett. B667 (2008) 1. doi:10.1016/j.physletb.2008.07.018.
- 942 [6] NNPDF JHEP 1005:075,2010.

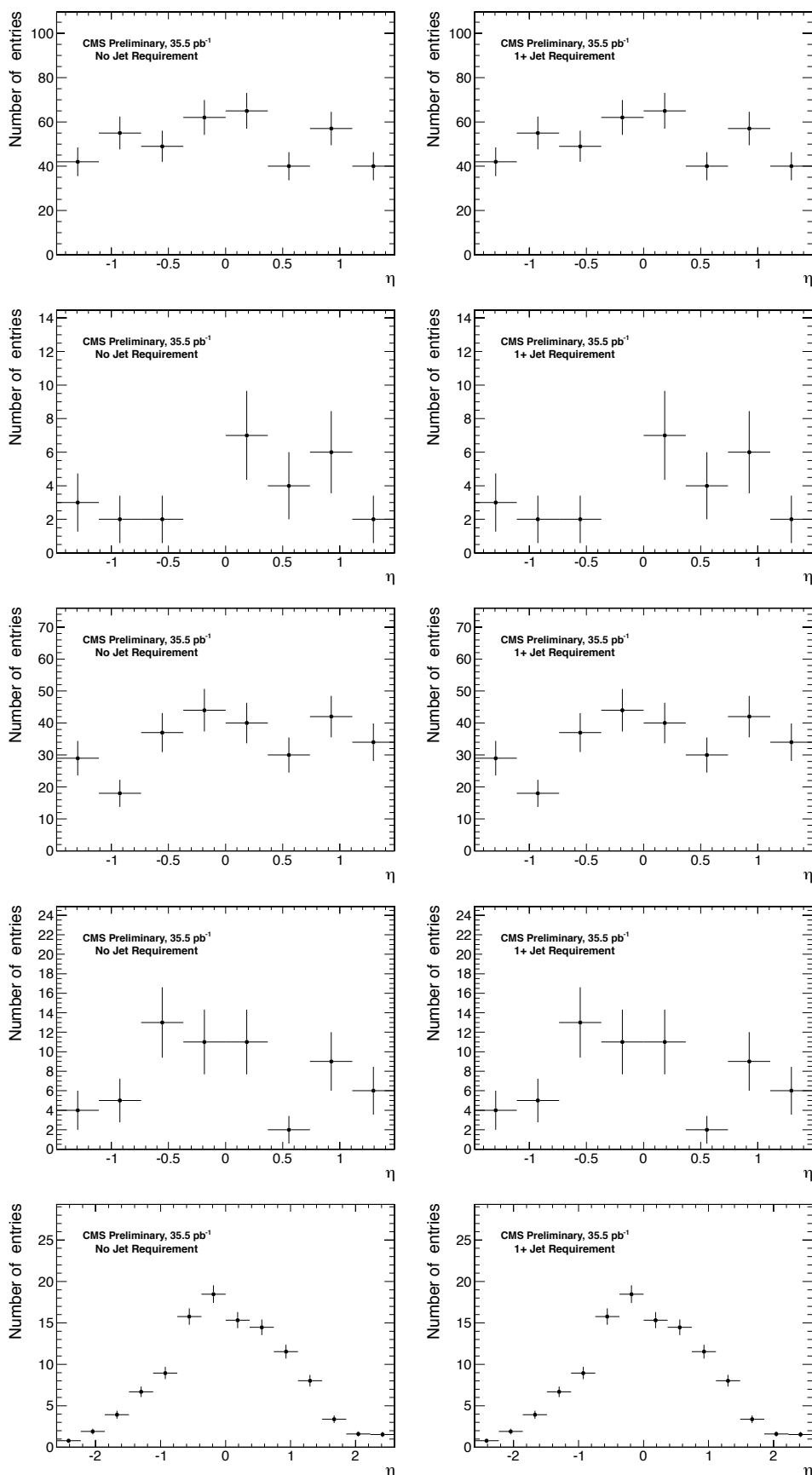


Figure 68: 1st row-left plot: ee events jet η with no jet requirement; right plot: same except with ≥ 1 jet requirement; 2nd row-left plot: $e\gamma$ events jet η with no jet requirement; right plot: same except with ≥ 1 jet requirement; 3rd row-left plot: ff events jet η with no jet requirement; right plot: same except with ≥ 1 jet requirement; 4th row-left plot: $\gamma\gamma$ events jet η with no jet requirement; right plot: same except with ≥ 1 jet requirement; 5th row-left plot: GGM events jet η with no jet requirement; right plot: same except with ≥ 1 jet requirement

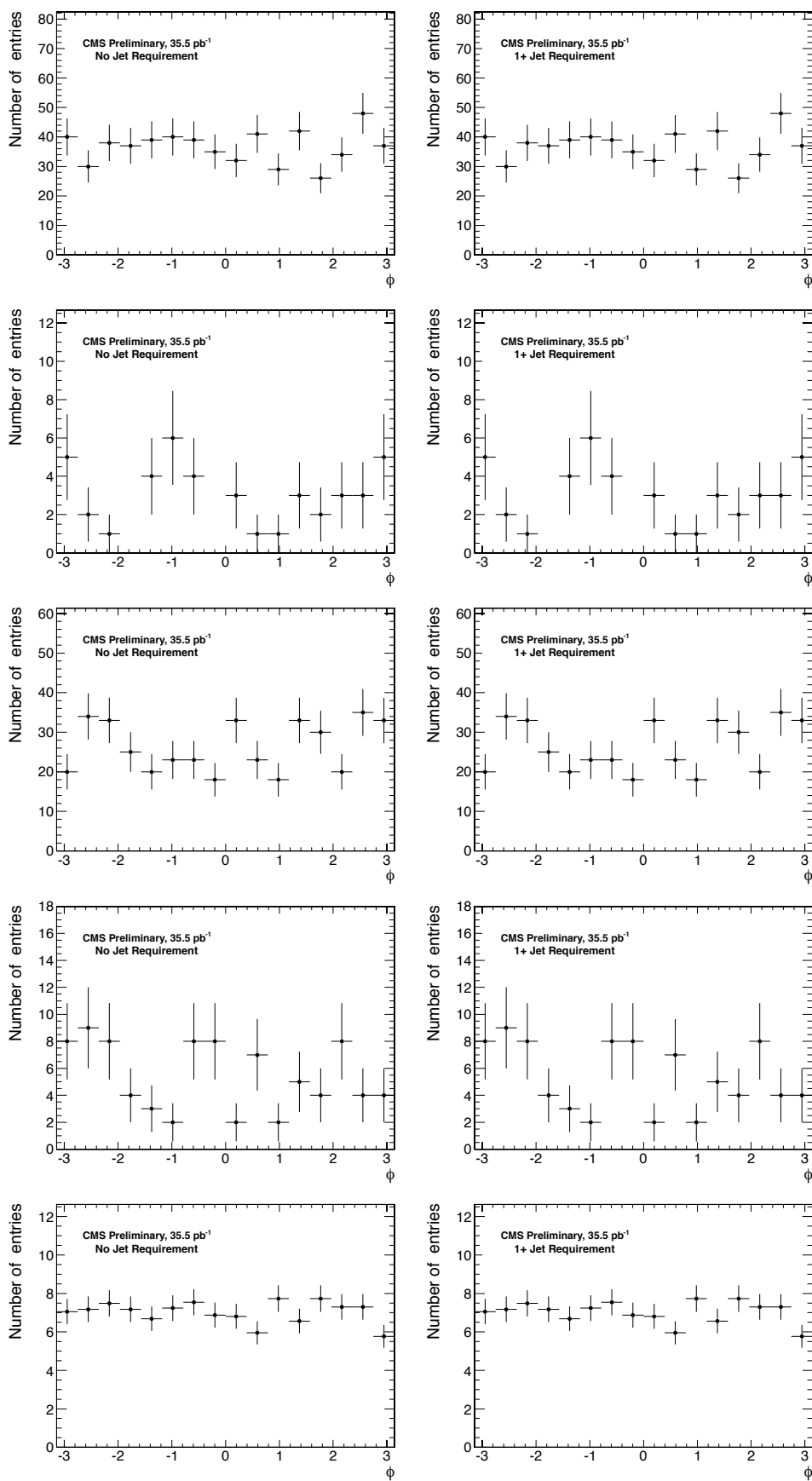


Figure 69: 1st row-left plot: ee events jet ϕ with no jet requirement; right plot: same except with ≥ 1 jet requirement; 2nd row-left plot: $e\gamma$ events jet ϕ with no jet requirement; right plot: same except with ≥ 1 jet requirement; 3rd row-left plot: ff events jet ϕ with no jet requirement; right plot: same except with ≥ 1 jet requirement; 4th row-left plot: $\gamma\gamma$ events jet ϕ with no jet requirement; right plot: same except with ≥ 1 jet requirement; 5th row-left plot: GGM events jet ϕ with no jet requirement; right plot: same except with ≥ 1 jet requirement